

https://dspace.org/

# Optically stimulated luminescence dating of Kalundu and Urewe tradition ceramics

**Haupt, Rachel Xenia**

**2024-03**

University of the Witwatersrand, Johannesburg

https://hdl.handle.net/10539/45234

Haupt, Rachel Xenia. (2024). Optically stimulated luminescence dating of Kalundu and Urewe tradition ceramics. [Master's dissertation, University of the Witwatersrand, Johannesburg]. WIReDSpace.

Downloaded from a DSpace repository. https://dspace.org/



UNIVERSITY OF THE
WITWATERSRAND,
JOHANNESBURG

# Optically stimulated luminescence dating of Kalundu and Urewe tradition ceramics.

**Rachel Haupt**
**(1619250)**

Submitted in fulfilment of the requirements for the degree

**Master of Science (by dissertation)**

in
**Geography**
in the Faculty of Science, University of the Witwatersrand, Johannesburg, South Africa

Supervisor: Prof. Mary Evans
Co-supervisor: Prof. Maria Schoeman

March 2024

# Plagiarism declaration

I, Rachel Xenia Haupt (Student number: 1619250), declare this dissertation is my own, unaided work. It is being submitted for the degree of Master of Science at the University of the Witwatersrand, Johannesburg. It has not been submitted before for any degree or examination at any other University.



20/08/2024

(Signature of candidate) (Date)

# Abstract

Optically stimulated luminescence (OSL) dating is a method of providing the direct age of artefacts. While radiocarbon and seriation dating provide indispensable insight into archaeological sites, the direct dating of artefacts is beneficial in entangled contexts. The Lydenburg Heads Site is significant to the beginning of the Early Farming Communities (EFCs) sequence within the Mpumalanga province. The site has been occupied multiple times, as can be seen from the presence of the two major ceramic traditions of the age, Urewe and Kalundu. The site was originally excavated and analysed by Evers (1982) in the 1970s, with a reanalysis of the ceramic assemblage by Whitelaw (1996) and organic residue analysis on the ceramics by Becher (2021). The use of OSL dating on twelve ceramic sherds allowed for new insights into the chronological intricacies within the study site.

To determine the age of the ceramics, the OSL quartz dating technique was used. The adjustments to the technique involved the use of a less destructive means of sample extraction. A slightly altered version of the standard means of sample extraction was used to create a comparison and allow the dating of the ceramics to be reliable. The minimal destruction technique (MET) combined with the bulk sampling proved useful to the dating of the ceramics.

The use of previously excavated ceramics meant that some aspects of age determination required estimation and analysis. The major obstacles from such were the water content, the depth of burial, and the lack of in situ soil samples. In light of the elements of ambiguity for the site, the OSL dating considered these variations and how they affected the age.

The Urewe tradition ceramics were determined to be in 6$^{th}$ and 8$^{th}$ century AD. The finding creates the alignment with the range of the radiocarbon ages done within previous work and the assumptions made by Evers (1982) and Whitelaw (1996). The Kalundu tradition ceramics ages were determined to be between the 7$^{th}$ and 10$^{th}$ century AD, conflicting with previous assumptions on the occupation. The result is the possibility the ceramic assemblages could be considered to be contemporaneous.

The work in this thesis has, in part, been presented at the Luminescence and Electron Spin Resonance Dating conference in Copenhagen (LED2023) and at the Association of Southern African Professional Archaeologists 2024 Biennial Meeting (ASAPA 2024).

To Janicé, Shelly, Amy, and Kevin.

# Acknowledgements

The most important thanks need to go to my incredible supervisors. Prof. Mary Evans, thank you for allowing and trusting me to work in the OSL laboratory. Working and being mentored by you has shown me that science is not a straight line but requires thinking and rethinking. You have allowed me to experiment and see passions and opportunities I did not know existed. Prof. Alex Schoeman, thank you for showing me the extended world of archaeology and listening to my questions that felt silly at times. You have provided insight into topics I had yet to tackle, allowing me to get to the conclusions on my own but still pushing me back on track throughout. The advice and support from both of you allowed this project to be completed.

Thank you to Dr Ragna Redelstorff and Phillip Hine from SAHRA for processing my application and allowing me to perform the dating on the ceramics (permitID: 4105). I would like to thank Dr Julia Becher, whose work on the pottery before me made my life a lot easier. Subsequently making a deeper analysis of the ceramics possible.

Daria, thank you for helping me in the lab and answering my questions regarding OSL dating. Han, thank you for allowing me a space outside of all this, in which reality existed and an afternoon could feel relaxed.

My family provided me with constant motivation, mainly through the aim of completing my master's faster than Connie and making Celia the least qualified member of the Grosfam group. Mom, thank you for taking my calls and telling me I can do this. Dad, for helping get the technical aspects down and making me wear the U2-esque glasses. Bobbe, for offering me every book you found that ended in 'ology'. Con for being willing to reply to no context messages with sound advice. Abs for working beside me and listening to tears or excitement with equal care.

Finally, I want to thank my household. Amy, Kevin, and Shelly, thank you for annoying me at 3 pm every single day to get up and play. Janicé, you were the most constant and important support for me. Having you as my partner allowed me to feel safe within all the scary. I love you.

# Table of Contents

Plagiarism declaration ..... i

Abstract ..... ii

Acknowledgements ..... v

Table of Contents ..... vi

LIST OF FIGURES ..... ix

LIST OF TABLES ..... xiii

LIST OF ABBREVIATIONS, ACRONYMS AND SYMBOLS ..... xv

Chapter 1 - INTRODUCTION ..... 1

1.1 Background ..... 1

1.2 Rationale ..... 2

1.3 Aims ..... 2

1.4 Objectives ..... 3

1.5 Study site ..... 3

1.6 Outline of dissertation ..... 5

Chapter 2 - LITERATURE REVIEW ..... 7

2.1 Introduction ..... 7

2.2 Ceramic analysis, function, and style in South Africa ..... 7

2.3 Chronological significance of the Lydenburg Heads Site ..... 15

2.3.1 Evers' Excavation ..... 16

2.3.2 Early farming communities ..... 22

2.4 Principles of luminescence dating ..... 25

2.4.1 The equivalent dose ..... 27

2.4.2 The dose rate ..... 30

2.4.3 Age calculations ..... 33

2.5 Chronology in archaeology ..... 34

2.5.1 Modification of mineral extraction ..... 39
2.6 Summary ..... 41
Chapter 3 - METHODOLOGY ..... 42
3.1 Introduction ..... 42
3.2 Excavation of ceramic samples ..... 42
3.3 Sample extraction ..... 49
3.3.1 Quartz extraction using minimal extraction technique ..... 50
3.3.2 Quartz extraction for bulk samples ..... 53
3.4 Sample preparation ..... 53
3.4.1 Bulk sample preparation ..... 54
3.4.2 Minimal extraction technique sample preparation ..... 56
3.4.3 $D_R$ sample preparation ..... 57
3.5 Instrumentation ..... 57
3.6 Dose recovery and preheat test ..... 58
3.7 Equivalent dose ($D_e$) measurements ..... 60
3.8 Dosimetry measurement ($D_R$) ..... 61
3.9 Age calculations ..... 63
3.10 Permission process ..... 63
3.11 Summary ..... 64
Chapter 4 - RESULTS ..... 65
4.1 Introduction ..... 65
4.2 Radiocarbon ages recalibration ..... 65
4.3 $D_e$ Sample extraction ..... 66
4.4 Dose recovery and preheat temperature tests ..... 68
4.5 Equivalent dose ($D_e$) results ..... 71
4.6 Dose rate ($D_R$) results ..... 83
4.7 Age calculations ..... 85
4.7.1 Age variations from depth and water content ..... 94
4.8 Summary ..... 99

Chapter 5 - DISCUSSION .....100
5.1 Introduction .....100
5.2 Chronology of the ceramic tradition .....100
5.3 Occupation phases of the ceramic tradition.....109
Chapter 6 – CONCLUSIONS .....112
6.1 Summary of findings .....112
6.2 Limitations of study and recommendation for future research .....113
REFERENCE LIST .....115
Chapter 7 - APPENDIX .....134
Appendix A Recalibration of $^{14}C$ .....134
Appendix B Calculations of Dose Rate.....141
Appendix C Post analysis photographs .....146
Appendix D Dose rates for variations in water content and depth.....150

# LIST OF FIGURES

Figure 1.1. Location of the study site: Lydenburg Heads Site. ..... 4

Figure 1.2. Map showing the locations of the pits, archaeological material and geological features (Evers, 1982a, p. 17). ..... 5

Figure 2.1. Ceramic terminology with visual representation and definition (Modified after Huffman, 2007, p. 117). ..... 12

Figure 2.2. Timeline of relevant traditions and facies for the Lydenburg Heads Site, subsequent facies refers to the continuation of various branches not shown in the figure (After Huffman, 2007, p. 118). ..... 13

Figure 2.3. Map showing the locations of the pits, archaeological material and geological features (Modified after Evers, 1982a). The location of the charcoal samples that were radiocarbon dated are marked with green (star), and the pits that were identified by Becher (2021) as containing Kalundu pottery are marked in red (square), and those containing Urewe pottery are marked in blue (circle). The map is showing the grid lines and grid O XI is further subdivided into smaller 2x2 m grid. ..... 17

Figure 2.4. Sections of pits 3, 7, 9, 10 and 12 (Evers, 1982a, pp. 18–19) ..... 18

Figure 2.5. Examples of information available on sherds. Red indicates the site; blue indicates the location based on the grid system; and yellow indicates further details such as depth or layer. ..... 20

Figure 2.6. Map of the EFC archaeological sites near the Lydenburg Heads Site (after Evers, 1975). ..... 23

Figure 2.7. Diagram showing the concept of luminescence dating. Upon burial or removal from heat the signal within the mineral increases (A to B). Once exposed to heat or light the signal is ‘zeroed’ or reset (B to C). The signal once reset will begin to accumulate charge immediately (C to D). The burial or production age is in relation to the signal accumulated within the mineral (A to C or C to E). (Modified after Feathers, 2003) ..... 26

Figure 2.8. Trap saturation versus time graph. The graph begins with showing the signal increase over time, then at ‘A’ a resetting event occurs (heating of pottery). The amount of radiation required to get from ‘B’ to ‘A’ is representative of the $D_e$. From ‘C’ to ‘D’ the charge increases again with a subsequent resetting event at ‘D.’ The

lines ‘A’ to ‘Ct’ and ‘Ct’ to ‘E’ shows how the age is affected when a material has been partially reset, with the material retaining charge and the result being this signal released not being proportional to the time of deposition or since heating. (Modified after Feathers, 2003) ..... 28

Figure 3.1. Example of information provided for database creation for the samples. A: One of the three boxes received; B: a bag which was located within the boxes with multiple individually bagged sherds. C: an example of how each sample was received, including a smaller bag with details written about the sherd and a yellow card produced by Becher (2021) with details about the sherd. ..... 43

Figure 3.2. Image showing the technique of bulk and MET sample extraction. The MET sampling is shown to enter from the broken side of the ceramic. The diameter of the drill location is 2mm, with the two drilling locations closely spaced together. The bulk sampling technique is shown to punch out a cylinder using an 8/10mm tile diamond core drill bit. ..... 51

Figure 3.3. Location of drill points in LHS40. ..... 52

Figure 3.4. Workflow diagram showing the process of $D_e$ sample preparation of the ceramics. ..... 56

Figure 4.1. Recalibrated radiocarbon results for Pta-328 and Pta-1634. ..... 65

Figure 4.2. Recalibrated radiocarbon results for the sites Lydenburg Heads Site (purple - pit 1, blue – near pit 8), Doornkop (light grey) and Klingbeil (dark grey). ..... 66

Figure 4.3. Weight of sample extracted using the MET against the thickness of the ceramics at drill site. ..... 68

Figure 4.4 Dose recovery vs preheat temperature (a) samples were irradiated in the reader (b) samples were exposed to solar irradiation for 30 minutes. The viable temperatures are outlined in red. ..... 70

Figure 4.5. OSL curves for selected samples and discs; blue is the signal and yellow is the background (column 1). Dose response curves selected samples and discs; blue is the given and measured known doses and red is the natural OSL signal interpolated onto the dose response curve to determine the $D_e$ (column 2). ..... 75

Figure 4.6. Abanico plots for all samples (Plot design by Dietze *et al.*, 2016). The z-axis is equivalent dose (Gy). ..... 79

Figure 4.7. Abanico plots showing comparison of LHS40a, LHS40b, LHS40c, and LHS40d. ..... 81

Figure 4.8. Ages for the Urewe samples, including the CAM and ADM determined $D_e$. 86

Figure 4.9. Ages for the Kalundu sample, including the CAM and ADM determined $D_e$. ..... 89

Figure 4.10. All ceramic ages calculated using the CAM and ADM $D_e$. ..... 91

Figure 4.11. Showing the variation in the age with variation in depth for the selected Kalundu ceramics. The deeper the sample, the younger the age; however, at depths below 0.3 m the age experiences slight increases and decreases. ..... 95

Figure 4.12. Showing the variation in the age with alteration to the depth for the selected Urewe ceramics. The deeper the sample, the younger the age; however, at depths below 0.3 m the age experiences slight increases and decreases. ..... 96

Figure 4.13 Changes in water content and the variations in age of the samples, using a depth of 0.3 m or maximum possible depth. ..... 98

Figure 5.1. All OSL ages including the CAM and ADM ages. Demarcation of the general range of the different facies for the Kalundu and Urewe traditions, and the radiocarbon recalibrated ages for LHS. ..... 105

Figure 5.2. LHS40 ages in comparison to location on ceramic. The ages are shown as the CAM age with the ADM age in brackets below. ..... 108

Figure 5.3. Timeline of occupation compared to other OSL ages and $^{14}C$ ages. ..... 110

Appendix figure A.1. OxCal calibration of Pta-1634 and Pta-328 using Hogg *et al.* (2020) calibration curve. The samples are from the Lydenburg Heads Site (Inskeep, 1971; Evers, 1982a) ..... 134

Appendix figure A.2. OxCal calibration of Pta-2944, Pta-2535, and Pta-2536 using Hogg *et al.* (2020) calibration curve. The samples are from the Doornkop site in the Mashishing region (Evers, 1988). ..... 135

Appendix figure A.3. OxCal calibration of Pta-1663, Pta-2160, and Pta-1747 using Hogg *et al.* (2020) calibration curve. The samples are from the Klingbeil site in the Mashishing region (Evers, 1980). ..... 136

Appendix figure A.4. OxCal calibration of radiocarbon samples from Tshokwane (TSH1) and Skukuza (SK17) (Jordaan, 2016). ..... 137

Appendix figure A.5. OxCal calibration curve of radiocarbon samples from Skukuza (SK17) (Jordaan, 2016). ..... 138

Appendix figure A.6. OxCal calibration curve of radiocarbon samples from Tshokwane (TSH1) (Jordaan, 2016). ..... 140

# LIST OF TABLES

Table 2.1. Ceramic characteristics in relation to research objectives. The Prehistoric Ceramics Research Group's (2010) table with focus on aspects that highlight 'Chronology' and 'Function and Use', to reflect the patterns in South African first millennium pottery. ..... 10

Table 2.2. Description of pits 1, 2, 5, 6, 7, and 9. The pits of interest to the project are highlighted in grey (Evers, 1982a). ..... 19

Table 2.3. Description of pits 4, 8, and 10. The pits of interest to the project are highlighted in grey (Evers, 1982a). ..... 19

Table 2.4. Description of pits 3, 11, and 12. The pits of interest to the project are highlighted in grey (Evers, 1982a). ..... 20

Table 2.5. Luminescence and radiocarbon dating sites of interest worldwide. ..... 36

Table 2.6. Luminescence and radiocarbon dating sites of interest in South Africa. ..... 37

Table 3.1. List of Kalundu pottery sherds from the Lydenburg Heads Site including box and bag number, original pit and grid code, and photographs of the outside (left) and inside (right). ..... 44

Table 3.2. List of Urewe pottery sherds from the Lydenburg Heads Site including details of how they were received (box and bag), original locations (pit, spit, and code), and photographs of the outside (left) and inside (right). ..... 46

Table 3.3. Sample list including the ceramic tradition and the method of quartz extraction: bulk sampling ($D_e$ bulk) or MET ($D_e$ MET). ..... 49

Table 3.4 Dose recovery protocol for the OSL samples, including the steps to produce the dose response curve. ..... 59

Table 3.5. SARs protocol for the OSL samples, including the steps followed for individual samples. ..... 60

Table 3.6. Conversion rates for thorium, uranium, and potassium (Cresswell *et al.*, 2018) ..... 62

Table 4.1. Weight of extracted sample for MET and bulk sampling, and thickness of location of sampling for MET samples. For the samples LHS40, four samples were extracted and as a result there is no 2$^{nd}$ hole for those MET samples. ..... 67

Table 4.2. Preheat temperatures at which the samples were measured. For samples LHS02 and LHS29, the tests were performed twice and at both temperatures. ..... 70

Table 4.3. Rejection rate, including the total discs tested and rejected per sample. ..... 72

Table 4.4. The $D_e$ determined using the central age model (CAM), additive dose model (ADM) and pure arithmetic mean (AM) and overdispersion (OD) ..... 82

Table 4.5. Potassium, thorium, and uranium concentrations obtained through XRF and ICP-MS testing..... 83

Table 4.6. Final annual dose rate ($D_R$) for each ceramic, including the depth, water content (WC), and the cosmic (Dc), beta (Dβ) and gamma (Dγ) dose rates. ..... 84

Table 4.7. Urewe ceramics OSL ages, showing the pit, CAM, and ADM ages. ..... 85

Table 4.8. Kalundu ceramics OSL ages, showing the pit, CAM and ADM ages. ..... 88

Table 4.9. Full details of all samples, including: the final depth; thorium, uranium and potassium concentration; water content (WC); cosmic dose rate (Dc); environmental dose rate ($D_R$); the overdispersion (OD) including error; the CAM equivalent dose and age including errors; the ADM equivalent dose and age including errors. The errors that are not shown are uniform and as follows: Th: ± 0.15, U: ± 0.03, K: ± 0.02, WC: ± 1, and Dc: ± 0.02. ..... 92

Table 4.10. Estimated depths based on the pit. ..... 94

Appendix table C.1. Post analysis photographs Kalundu ceramics. ..... 146

Appendix table C.2 Post analysis photographs Urewe ceramics. ..... 148

Appendix table D.1. Dose rates for all samples with changes to water content and depth. ..... 150

# LIST OF ABBREVIATIONS, ACRONYMS AND SYMBOLS

| | |
|---|---|
| $^{14}C$ | Carbon -14 |
| AD | Anno domini |
| ADM | Average Dose Model |
| Amsl | Above mean sea level |
| BCE | Before common era |
| BP | Before present |
| CAM | Central age model |
| $CO_2$ | Carbon dioxide |
| $D_e$ | Equivalent dose (Gy=J/kg) |
| $D_R$ | Dose rate |
| EFC | Early farming community |
| EIA | Early iron age |
| FMM | Finite Mixture Model |
| Gy | Gray, SI unit for radiation dose (1 Gy = 1 J/kg) |
| $H_2O_2$ | Hydrogen peroxide |
| HCl | Hydrochloric acid |
| HF | Hydrofluoric acid |
| ICP-MS | Inductively coupled plasma mass spectrometry |
| IR | Infrared |
| IRSL | Infrared stimulated luminescence |
| K | Potassium |
| ka | Kiloannum (1 ka = 1,000 a) |
| LED | Light emitting diode |

| | |
|---|---|
| LHS | Lydenburg Heads Site |
| Ln | Natural signal |
| Lx | Regenerative dose |
| MAM | Minimum age model |
| MET | Minimal Extraction Technique |
| N | Nitrogen |
| OD or σ | Overdispersion |
| ORA | Organic Residue Analysis |
| OSL | Optically stimulated luminescence |
| ppm | Parts per million |
| RPM | Revolutions per minute |
| SAR | Single aliquot regenerative (protocol) |
| $SiO_2$ | Quartz |
| SPT | Sodium polytungstate |
| Th | Thorium |
| TL | Thermoluminescence |
| Tn | Test dose for natural signal |
| Tx | Test dose for regenerative dose |
| U | Uranium |
| WC | Water content |
| XRF | X-ray fluorescence |
| α | Alpha |
| β | Beta |
| γ | Gamma |
| μm | Micrometre (1mm =1000 μm) |

# CHAPTER 1 - INTRODUCTION

## 1.1 Background

In 1956/1957 Dr K. L. von Bezing noticed fragments of terracotta heads, ceramic vessels and other artefacts eroding out of the north facing slopes of the Sterkspruit valley, southeast of Lydenburg (von Bezing and Inskeep, 1966; Evers, 1982a; Whitelaw, 1996). Seven hollow terracotta head sculptures were reconstructed from the fragments, and the site was named the Lydenburg Heads Site for these rare finds (Maggs and Davison, 1981; Whitelaw, 1996). The terracotta heads are considered ceremonial objects, deeply imbued with symbolism and might have played a pedagogical role in child initiation schools (Inskeep and Maggs, 1975; Maggs and Davison, 1981; Hall, 2015; also see Loubser, 1993).

The children being initiated lived in a well-established, sedentary agricultural community that practiced crop farming and pastoralism (Maggs and Davison, 1981; Evers, 1982a; Huffman *et al.*, 2020). Their food was cooked in ceramic vessels (Becher *et al.*, 2024), which were discarded in pits and then found by von Bezing and excavated by Evers (1982a) in the mid 1970's. Evers interpreted the ceramic assemblage as representing one occupation. With the increase in knowledge and research on the first millennium communities, Whitelaw (1996) revisited the original observations made by Evers (1982a). He (Whitelaw, 1996) identified ceramics from multiple facies of two different traditions at the site: Kalundu and Urewe. Consequently, he argued that the site was occupied by two different communities, since the two traditions reflected the origins of communities that moved into the region through different pathways. It is unclear from the archaeology if the occupations overlapped, which highlights the significance of obtaining the temporal relationship between the traditions and thereby the occupation of the site.

Previous attempts to establish when the site was occupied used radiocarbon dating performed on charcoal and typological seriation. The proposed occupation dates are that of the late 5th and early 6th AD (Inskeep, 1971, p. 493; Evers, 1975, p. 76; Evers and Vogel, 1980, p. 231), 7th AD (Whitelaw, 1996, p. 76), 9th and 11th centuries AD (Whitelaw, 1996, p. 82). The varied dates are a result of an increase in knowledge of the ceramic sequence overtime and the revisiting of the site with said knowledge. The ages allow an insight into the depth of use of the region, but do not completely resolve the relationship between the two (or more) occupations of the Lydenburg Heads Site. Consequently, the need to provide absolute dates for artefacts, such as ceramics, remains.

## 1.2 Rationale

Whitelaw (1996, p. 82) correctly claimed that his untangling of the ceramic sequence at the Lydenburg Heads Site means that "…archaeologists will be better able to estimate more accurately the date and length of occupation of Mpumalanga EIA sites on the basis of ceramic style." To date, however, there are no high-resolution ages that establish the timing of these occupations. Luminescence dating can assist in this, because it determines the firing or last usage ages of the pottery to be determined. This absolute dating technique is therefore a suitable tool to identify the temporal context of Kalundu and Urewe traditions at the Lydenburg Heads Site and refine understandings of the occupation sequence.

## 1.3 Aims

This project aims to constrain the timing and age of the ceramics ascribed to the Urewe and Kalundu traditions excavated from the Lydenburg Heads Site to establish if the occupations were contemporaneous or sequential.

## 1.4 Objectives

1) To determine the ages for the Kalundu and the Urewe Tradition ceramics using optically stimulated luminescence (OSL) dating techniques
2) Compare the ages derived from traditional quartz extraction methods to that of the minimal extraction techniques.
3) Establish whether the two traditions were contemporaneous or sequential by evaluating the luminescence ages of Kalundu and Urewe Tradition ceramics.

## 1.5 Study site

The Lydenburg Heads Site (LHS) is in the Mpumalanga Province of South Africa, approximately 6 km southeast of the town of Mashishing (formerly Lydenburg) (Figure 1.1). The LHS was previously referred to as Sterkspruit 66/72, and it is located in the present-day Sterkspruit Nature Reserve (Evers, 1975, 1982a). Within the Sterkspruit Valley the site is bordered by rivers on the eastern and northern sides (Evers, 1982a). Located on the Drakensberg Escarpment with the Lowveld region less than 50 km away, the site can be considered a transition from the high lying escarpment towards the central plateau of South Africa (Evers, 1974; Inskeep and Maggs, 1975). Mashishing is within the summer rainfall zone of South Africa and considered to be in the Lydenburg Montane Grassland and Lydenburg Thornveld biome (Mucina *et al.*, 2006; Truc *et al.*, 2013; Hahn *et al.*, 2016). The region is located within the rain shadow of the Drakensberg Mountains, which reduces the amount of rainfall (Sjöström *et al.*, 2017; Schoeman *et al.*, 2019; Olatoyan *et al.*, 2023).

In climate reconstructions, the area has been shown to fluctuate in conditions from mesic to dry conditions (Sjöström *et al.*, 2017; Schoeman *et al.*, 2019; Olatoyan *et al.*, 2023). During the latter half of the first millennium, conditions were dry, with a shift occurring around 1000 AD for a period of 250 years of mesic environment

(Sjöström *et al.*, 2017). It is during the mesic periods where Early Farming Communities (EFCs) experienced the largest expansion (Sjöström *et al.*, 2017). The shifts between dry and mesic do not inherently mean the fluctuations were extreme but instead that the environment cannot be considered stable or homogeneous.

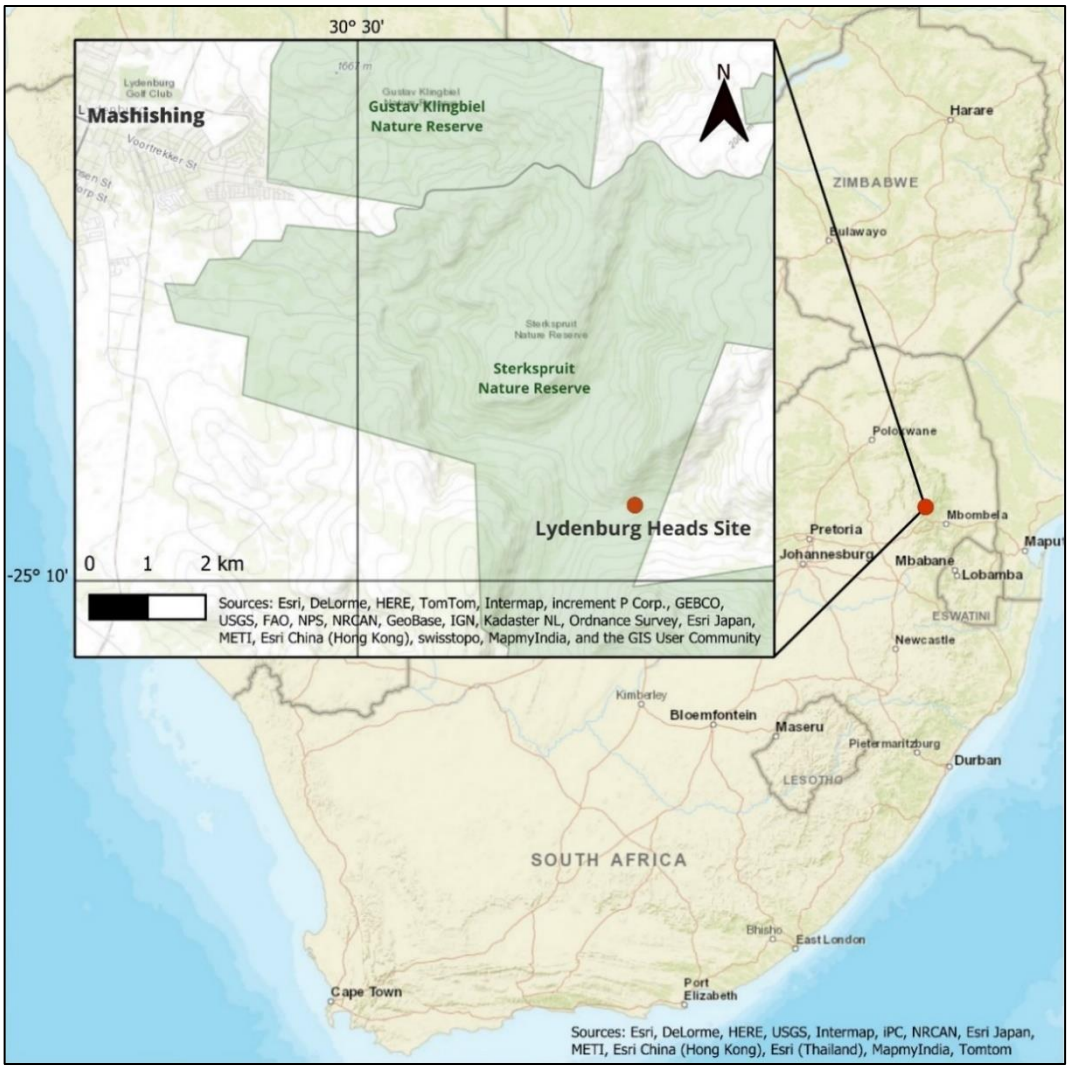


Figure 1.1. Location of the study site: Lydenburg Heads Site.

Sheetwash and gully erosion had removed the site's surface, which allowed the chance identification of the site by von Bezing in the 1950s (von Bezing and Inskeep, 1966; Evers, 1982a). However, the erosion caused enough damage to complicate the reconstruction of the layout of the settlement significantly (Evers, 1982a). This is not a special feature of this site, since the whole Lydenburg Valley

is prone to sheetwash, and the formation of gullies often impact archaeological sites (Marker and Evers, 1976).

Despite the erosion, the extent of the LHS could be established; it was 270 m in diameter and contained twelve pits (Evers, 1982a). The pits were numbered, and the site was plotted using a grid system of roman numerals and alphabetical sequences (see Figure 1.2). Evers' (1982a) excavation trenches were located at N IX, L IX, and M VII.

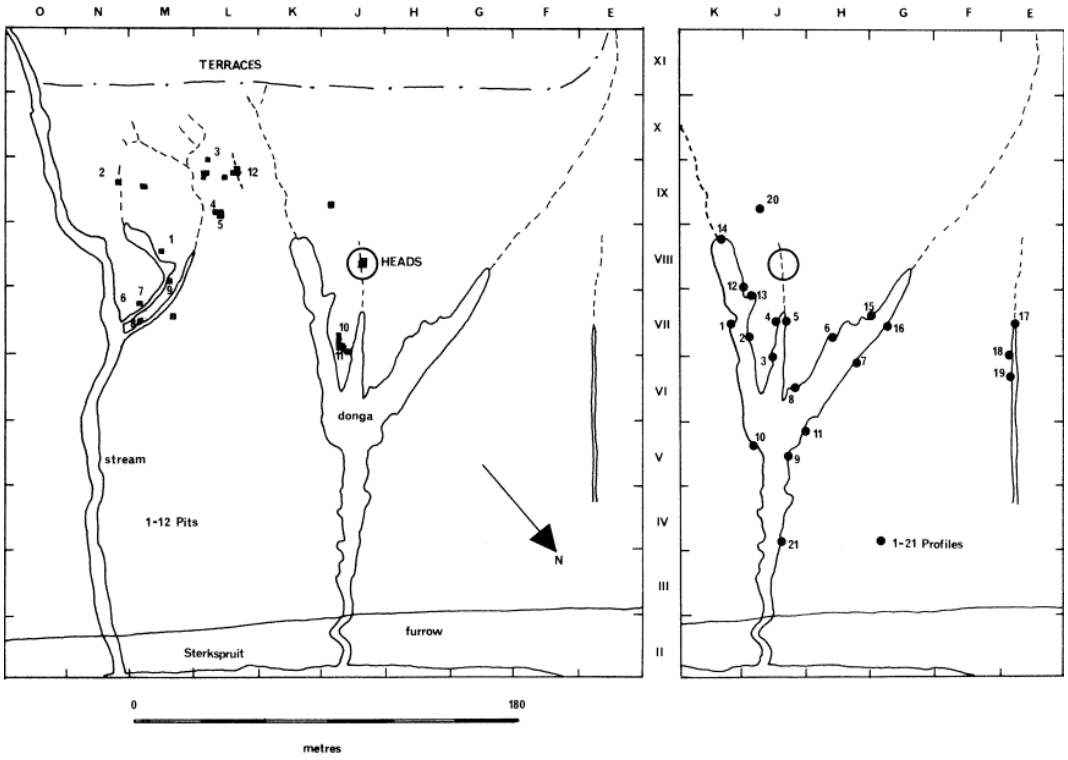


Figure 1.2. Map showing the locations of the pits, archaeological material and geological features (Evers, 1982a, p. 17).

## 1.6 Outline of dissertation

Chapter 1 provides the background to the study, the aims, objectives, and rationale of the research. In addition, a description of the study site and its characteristics are provided.

In Chapter 2 the relevant literature, including research on EFCs within southern Africa, ceramic function and style, and research done at the study site is presented. I also explain the process of OSL dating of pottery, as well as case studies on the use of luminescence dating of museum artefacts and previously excavated artefacts.

The research methodology is described in Chapter 3, which outlines the processes and techniques followed to obtain the results, including sample collection, preparation, testing and OSL dating for the traditional and minimal quartz extraction techniques.

The results of the luminescence dating are presented in Chapter 4. This is followed by a discussion of the significance of the results in Chapter 5.

The main conclusions of the findings are summarised in Chapter 6.

The reference list and Appendices follow the main chapters.

# CHAPTER 2 - LITERATURE REVIEW

## 2.1 Introduction

The pertinent literature can be considered in three sections of interest: the archaeological context, the methodologies of luminescence dating, and the interplay of these two facets within the production of chronologies in archaeology. The interpretation of the first-millennium ceramic style is at the core of understanding the origins, interactions, and societal formation of the early farming communities (EFCs). Thus, it is important to review the history of ceramic classification. Next, Lydenburg Heads ceramics are contextualised by discussing the first millennium of South African ceramic sequences. After this, I summarise what is known about the Lydenburg Heads Site (LHS), focusing on previous work done and identifying gaps in the data and understanding. The section on luminescence dating follows, with focus on the means of obtaining ages for sites. I explain how luminescence dating can be used to date archaeological material directly by exploring the development and application of the technique and its use to date archaeological sites globally and locally, highlighting the application of the dating of ceramics.

## 2.2 Ceramic analysis, function, and style in South Africa

Research into the archaeology of farming communities in southern Africa has flourished since the 1960s. An occupation period that, after the initial intense focus on Great Zimbabwe (e.g. Randall-Maciver, 1906; Caton-Thompson, 1931) and Mapungubwe (e.g. Fouché, 1937; Gardner, 1963), had been neglected. This changed after the work of Mason (1951, 1952, 1954, 1981) began to expose the number and expanse of 'Iron Age[1]' archaeological sites in the region north of the Vaal River. After the development of radiocarbon dating in the 1940's by Arnold

[1] The term 'Iron Age' is not unproblematic as was clearly argued by Maggs (1992) and Hall (1992); also see Mitchell (2013) and Schoeman (2020). Consequently, I avoided the use of the term in this dissertation as far as possible.

and Libby (1949), archaeologists started to draw a distinction between first- and second-millennium sites, which were called Early and Late Iron Age sites, respectively (see Maggs, 1993). With this distinction in place, research began to focus on understanding the chronology of movements and settlements rather than proving the pre-colonial existence of these peoples (see Kuper, 1980; Huffman, 1982; Evers, 1988). The most numerous material culture they left behind - ceramics - is used by archaeologists as both cultural and temporal indicators for these persons (Evers, 1977, 1988).

The earliest evidence for the presence of EFCs in southern Africa dates to the 4$^{th}$ century AD (Huffman, 1970; Antonites, 2016; Lander and Russell, 2018, 2020; Schoeman, 2020; Fredriksen, 2023; Grollemund *et al.*, 2023). The following years were marked by an increase in the number of settlements and their expansion throughout the summer rainfall region of southern Africa (Mitchell and Whitelaw, 2005; Antonites, 2016; Schoeman, 2020; Grollemund *et al.*, 2023). Unlike the autochthonous hunter-gatherer population, the early farming communities favoured sedentism, agriculture and, where the conditions allowed, animal husbandry (Antonites, 2016; Fredriksen, 2023; Grollemund *et al.*, 2023). However, it is important to note that the spread of the EFCs was not the first example of pastoralism within southern Africa (Grollemund *et al.*, 2023), since cattle- and sheep-keeping pastoralists were present at Toteng in Botswana by 2070 ± 40 BP (Beta-190488), and there is direct evidence for sheep farming at Spoegriver in the Northern Cape by 2105 ± 65 BP (OxA-3862) (Sealy and Yates, 1994; Coutu *et al.*, 2021).

There also are two distinct ceramic groupings in eastern and western South Africa, thin- and thick-ware. The earlier thin-ware (made by hunter-gathers and hunter-gatherers with sheep or pastoralists) is present in the Western and Northern Cape from the first millennium BC, while thick-ware appears in northeastern South Africa with the arrival of farming communities (Sadr and Sampson, 2006; Sadr, 2008; Lander and Russell, 2020; Fredriksen, 2023). A study by Fewlass *et al.*

(2020) used Organic Residue Analysis (ORA) on one agriculturalist and two hunter-gatherer sites from the first millennium in the Lesotho Highlands. This showed the presence of dairy within the hunter-gatherer ceramics and, thus, their knowledge and practice of livestock domestication (Fewlass *et al.*, 2020).

The manufacturing techniques, ceramic style, and uses of these ceramics evolved over time. Although not within the frame of the first millennium, Fowler's (2006) classification of Zulu ceramics is a useful guide when considering vessel function. He highlighted that the shape and size of ceramics are linked to their use. The focus is on the capacity, availability of items and transportation of the ceramics (Fowler, 2006). Clearly, vessels were put to many uses, including storage, cooking, consuming food, and ritual. The variables such as dimensions, shape, and stylisation hint towards the function of the vessel as well as the chronology (see Table 2.1).

Storage vessels, created to store or transport goods or food (Huffman, 1970, 1982, 1989; Ashley, 2010; Klatzow, 2010; Dunne *et al.*, 2019; Lander and Russell, 2020; Denbow and Wilmsen, 2023), can be for wet or dry storage, with liquid storage vessels often being necked, thus providing use through shape and size (Fowler, 2006). This storage might be long or short-term (Ashley, 2010; Ashley and Grillo, 2015).

Table 2.1. Ceramic characteristics in relation to research objectives. The Prehistoric Ceramics Research Group's (2010) table with focus on aspects that highlight 'Chronology' and 'Function and Use', to reflect the patterns in South African first millennium pottery.

| **Variables** | **Chronology** | **Function and use** |
|---|---|---|
| Fabric type | * | * |
| Form type | * | * |
| Vessel Type | * | * |
| Extent of form | * | * |
| No. of sherds | * | * |
| Weight of sherds | * | * |
| Diameter of rim | | * |
| Diameter of base | * | * |
| Wall thickness | | * |
| Height | | * |
| Girth/shoulder | | * |
| Surface treatment | * | * |
| Decoration | * | * |
| Manufacturing technique | * | |
| Residues | | * |
| Perforation type | | * |
| Condition | * | * |
| Colour | | * |
| Re-use | | * |

Cooking vessels are very common artefacts to find but can be used uniquely for different foods or cooking purposes. Cooking vessels provide possible insight into prior cooking and food consumption practices (Dunne *et al.*, 2019). With the increased population in communities the need for food increases. The sizes of cooking pots can suggest possible population increase, while Inskeep and Maggs (1975) argue that the lack of larger cooking vessels in a site implies the lack of presence within an assemblage and not entirely meaning a smaller population. Cooking vessels are useful to archaeologists, as the cooking residue can be used to determine possible dietary practices (Copley *et al.*, 2004; Degano *et al.*, 2019; Dunne *et al.*, 2019; Becher, 2021). In addition the soot can be used for radiocarbon dating (Miller, 1991). Bowls such as Evers' (1982a) mode 2 bowls, were probably

used to serve food. Other vessels include drinking cups, such as those Huffman (1970) found in Zambia.

Ceremonial and ritual ceramics are evident in many regions. The decorative patterns coupled with the shaping and stylisation of certain ceramics, such as masks or ceramic heads, are obvious examples (Mitchell and Whitelaw, 2005; Thebe and Sadr, 2017). The terracotta heads from the LHS exemplify these likely ceremonial objects (Maggs and Davison, 1981; Hall, 2015; Huffman *et al.*, 2020; Schoeman, 2020). In addition to the ceramics made with ritual use in mind, others used in ritual might have been reconfigured mundane objects. This category of ceramic vessel includes vessels used in burials at first-millennium sites such as Broederstroom (Mason, 1986), Nanda (Whitelaw, 1993) and KwaGandaganda (Whitelaw, 1994; Whitelaw and Moon, 1996), as well as the bottomless pots found in pits on first-millennium sites, which Whitelaw (1993) linked to female initiation.

While ceramic vessels have many specific functions, Evers (1988) noted the overall similarity of the ceramic styles within southern Africa, with smaller regions of stylistic alterations (Evers, 1988; Evers *et al.*, 1988; also see Whitelaw, 2012). He concluded that the smaller regions of different styles were geographically distinguishable and unique facies within the larger region (Evers, 1988; Evers *et al.*, 1988; also see Whitelaw, 2012). The similarity is due to first-millennium farming community ceramic styles within southern Africa being part of the Chifumbaze Complex (Evers, 1982b; Whitelaw, 1996; Huffman *et al.*, 2020).

The terminology used to describe the ceramics and the aspects surrounding them are important as the terms can have alternative meanings in different fields. In order to reduce the possible confusion, the terminology used is based on common practice of the EFC archaeological literature and described in Figure 2.1. The pertinent terms are that of ‘Tradition’ and ‘Facies.’ ‘Tradition’ refers not to generation customs but instead a grouping of related ceramic units. Although the ceramic styling is evidently a product of cultural practices, the distinction is important.

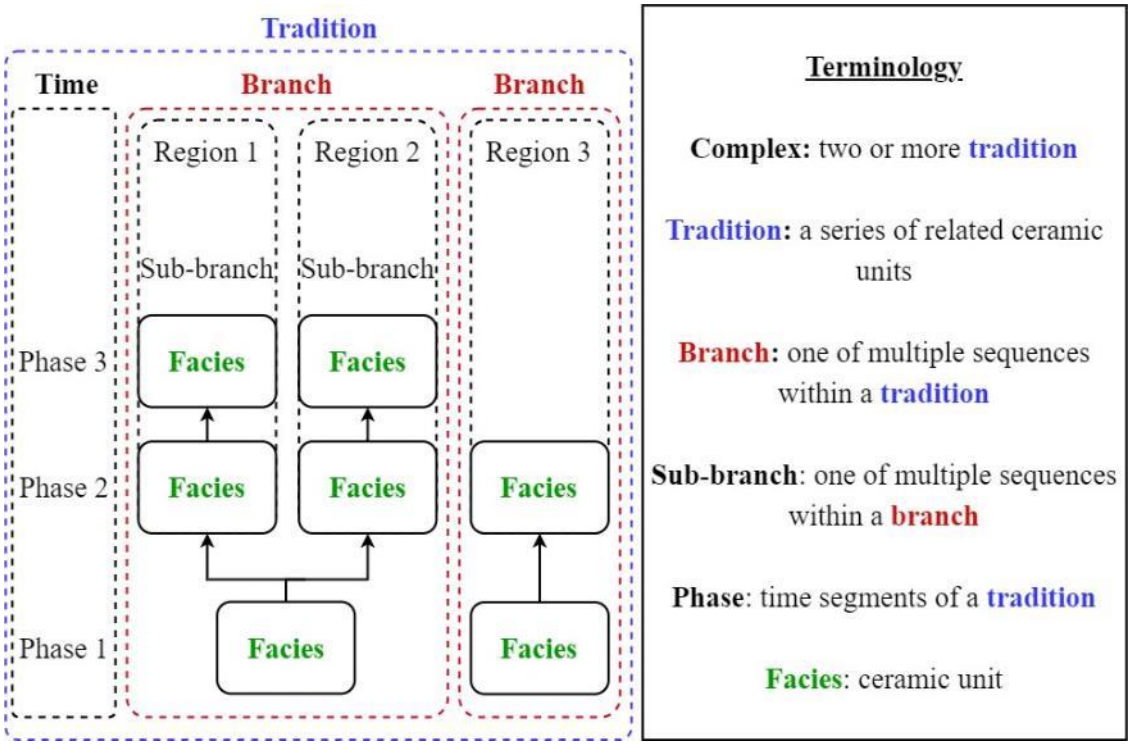


Figure 2.1. Ceramic terminology with visual representation and definition (Modified after Huffman, 2007, p. 117).

The Chifumbaze Complex comprises two traditions Urewe (also referred to as the Western Stream) and Kalundu (also referred to as the Eastern Stream) (Evers, 1982a; Huffman, 1989; Whitelaw, 1996; Huffman *et al.*, 2020; Huffman, 2021; Fredriksen, 2023). Although the two ceramic traditions are comparable in basic stylistic aspects, their profiles, motifs and combinations of those are different (Huffman *et al.*, 2020). These traditions evolved separately over time, such as the Garonga facies of the Urewe tradition, and the Happy Rest facies of the Kalundu tradition (see Figure 2.2). However, sometimes the traditions merged forming distinct facies such as the Doornkop facies from the Mzonjani and Happy Rest facies (Huffman, 2007; Figure 2.2).

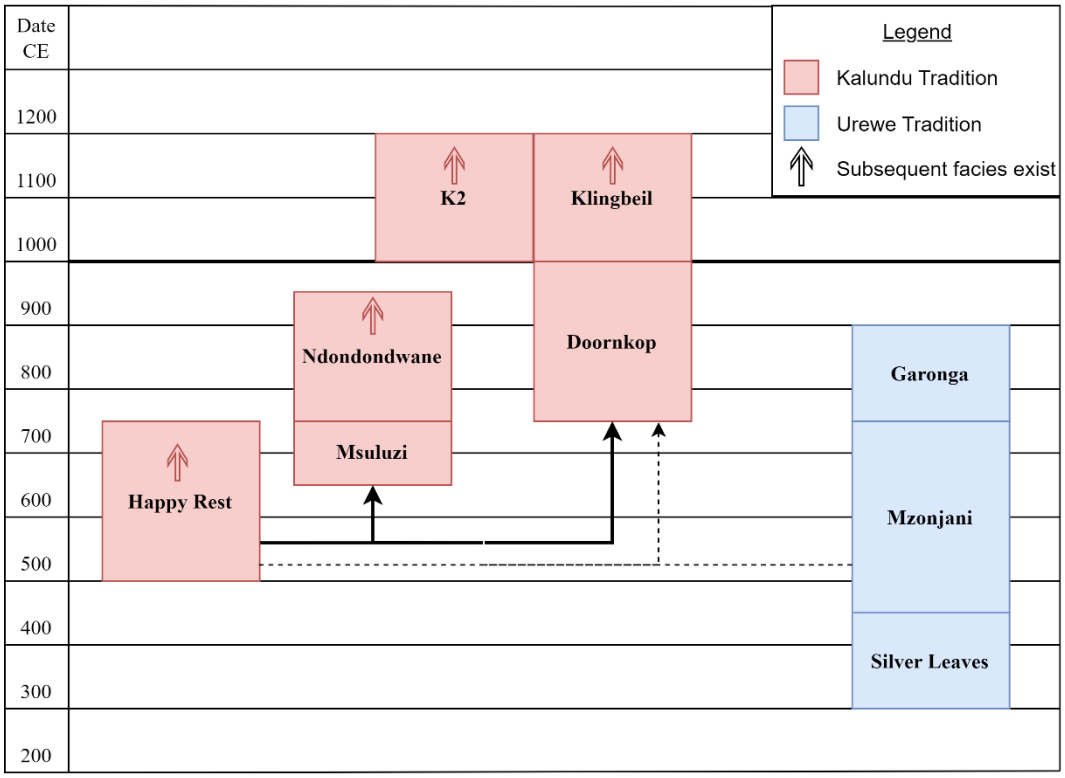


Figure 2.2. Timeline of relevant traditions and facies for the Lydenburg Heads Site, subsequent facies refers to the continuation of various branches not shown in the figure (After Huffman, 2007, p. 118).

In South Africa, the Urewe tradition consists of two unrelated first-millennium branches, the central Nkope branch and the eastern Kwale branch (Huffman, 1989; Huffman *et al.*, 2020; Huffman, 2021; Fredriksen, 2023). The other branches within the Urewe tradition, the Moloko and Blackburn branches, will not be discussed as they occur in the second millennium (Whitelaw, 2012; Fredriksen, 2023). The Nkope and the Kwale branch are similar in stylistic designs, such as profile combinations, decoration layout and motifs (Huffman *et al.*, 2020). The difference is mostly in the amount of motifs and the position of decorations on the ceramics (Huffman *et al.*, 2020).

In South Africa, the Urewe tradition (in particular the Kwale branch) begins with Silver Leaves, the earliest facie within South Africa made by a farming community (Whitelaw, 2012). Originally, this assemblage was grouped with the subsequent

Mzonjani phase, named the Matola phase (Whitelaw, 1996; Antonites, 2013; Whitelaw and van Rensburg, 2020; Fredriksen, 2023). The Silver Leaves assemblage is characterised by horizontal incisions and bevelled aspects (Antonites, 2013). Silver Leaves is present in Mozambique, Eswatini, KwaZulu-Natal and Limpopo in South Africa (Whitelaw and van Rensburg, 2020; Fredriksen, 2023).

Mzonjani assemblages are characterised by everted and not bevelled rims (Antonites, 2013). The spatial distribution of Mzonjani is larger than that of Silver Leaves and includes Limpopo, Mpumalanga and KwaZulu-Natal, showing the expansion of the EFC in the northeast of South Africa (Antonites, 2013; Fredriksen, 2023). The ages of these ceramic assemblages' rest on a few dates, so interpretations vary. For Antonites (2013, 2016) Silver Leaves ranges from 200 – 350 CE, with Mzonjani being the following 300 years. Whitelaw and van Rensburg (2020) put Silver Leaves 280 – 450 CE and Mzonjani 450 – 600 CE. The following facie is Garonga/Goronga, with even more ambiguous ages from the 8$^{th}$ to the 10$^{th}$ century AD (Burrett, 2007; Antonites, 2013).

The Kalundu tradition in South Africa, begins with Happy Rest (previously known as Matakoma) and developed into the Msuluzi facie (Mitchell and Whitelaw, 2005; Sadr, 2008; Schoeman, 2020; Fredriksen, 2023). The Happy Rest facie is dated to between the 6$^{th}$ and 8$^{th}$ centuries AD (Whitelaw, 1996; Mitchell, 2013; Huffman *et al.*, 2020; Fredriksen, 2023). Happy Rest vessels have curved necks, decorated rim bands and multiple bands of decoration (Whitelaw, 1996). Msuluzi decoration involves crosshatched rims, with distinctive necks and inverted vessels only (Maggs, 1980; Whitelaw, 1996; Huffman, 2007).

Although the Urewe and Kalundu traditions exhibit distinct characteristics, the identification of facies is not always accurate owing to similarities within and between ceramic branches. Furthermore, the fluidity of interaction cannot be ignored. The interaction between peoples allowed the production of subsequent facies, for example the interaction of the people making Mzonjani (Urewe tradition)

and Happy Rest (Kalundu tradition) ceramics resulted in the Doornkop facie, which is probably the Kalundu ceramics present at the LHS, but further research is needed (Whitelaw, 1996). The ceramics from Skukuza (SK17) show the interaction and merging of Mzonjani (Urewe tradition) and Msuluzi and Ndondonwane (Kalundu) pottery assemblages (Jordaan, 2016).

The conflation of the ceramic traditions shows important interaction between peoples. The partial analysis of ceramics and other artefacts from original excavations has been attributed to overlooking sites of interaction between ceramic assemblages (Jordaan, 2016). The connection between Tshokwane (TSH1) and a SK17 cluster provides evidence of interaction in two EFC sites in the Kruger National Park (Jordaan, 2016). The Mpumalanga sequences are not discrete assemblages, but instead non-parallel interaction and development. Understanding sites in isolation and within the sequence provides the complexities needed to produce the most accurate chronology.

## 2.3 Chronological significance of the Lydenburg Heads Site

The LHS was initially identified as an archaeological site in 1956/1957 by Dr K. L. von Bezing (von Bezing and Inskeep, 1966; Inskeep and Maggs, 1975; Evers, 1982a; Whitelaw, 1996). The site gained interest owing to the unique material culture found there, such as small terracotta heads likely with a ceremonial significance (von Bezing and Inskeep, 1966). Von Bezing collected sherds between 1962 and 1964 (von Bezing and Inskeep, 1966; Inskeep and Maggs, 1975; Evers, 1982b; Whitelaw, 1996). The site contained pottery, terracotta heads, iron, copper, and ostrich eggshells, indicating an extensive archaeological settlement (von Bezing and Inskeep, 1966). All the collections during this period were from shallow trenches exposed when sheet erosion removed the topsoil (von Bezing and Inskeep, 1966, p. 102). Charcoal was also collected to perform radiocarbon dating, and the sample Pta-328 was processed at the CSIR Physical Research Laboratory (Inskeep, 1971, p. 493). Pta-328 was taken from near pit 8 at surface level, with the

uncalibrated age being determined as 1460 ± 50 BP (490 ± 50 AD) (Inskeep, 1971; Evers, 1982a).

### 2.3.1 Evers' Excavation

The first scientific archaeological excavation of LHS only occurred between 1974 and 1978, with all previous finds being surface or exploratory trips (Evers, 1982a). The first formal excavation's main goal was to locate the findspot for the Lydenburg Heads and thus gain insight into their internment (Evers, 1982a). The site was seen as being important to understanding the broader Natal region EFC expansion and occupations (Evers, 1982a). The site grid was set up as shown in Figure 2.3, with the area where the heads were found being located at J VIII. The grid system used involved 30 by 30 m blocks, with capital letters and Roman numerals (Figure 2.3) (Evers, 1982a). The smaller 2 x 2 m excavation grids were labelled with lowercase letters and numbers in a similar fashion (Evers, 1982a). In order to grapple with the erosional, depositional and occupation history, twenty-one soil profiles were excavated from the donga (erosion gully) and surrounding area and documented (Evers, 1982a, see Figure 1.2 for soil profile locations). The site had experienced extensive erosion, making determining the settlement layout impossible (Evers, 1982a). The excavation also included 12 pits and surface collections.

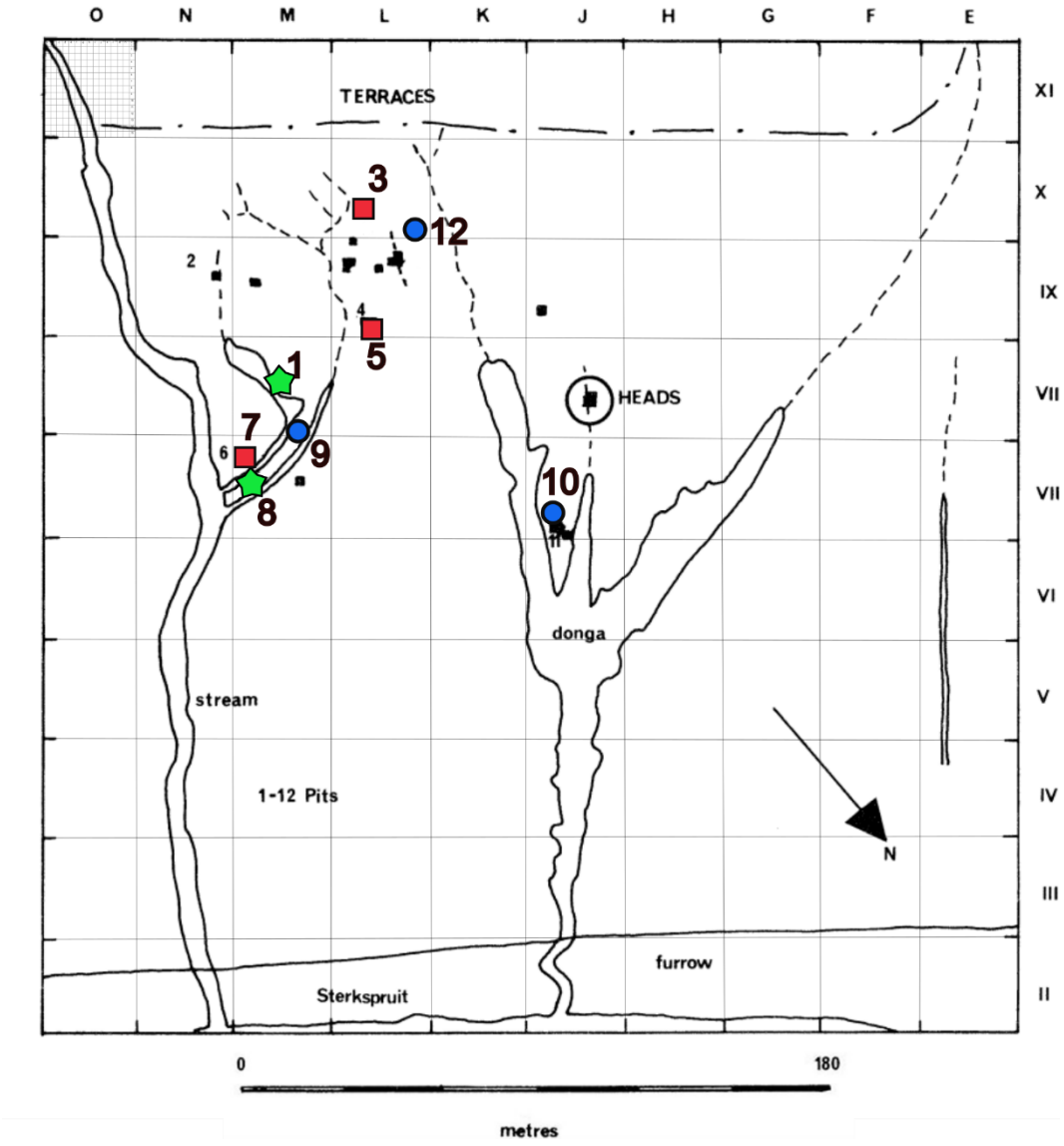


Figure 2.3. Map showing the locations of the pits, archaeological material and geological features (Modified after Evers, 1982a). The location of the charcoal samples that were radiocarbon dated are marked with green (star), and the pits that were identified by Becher (2021) as containing Kalundu pottery are marked in red (square), and those containing Urewe pottery are marked in blue (circle). The map is showing the grid lines and grid O XI is further subdivided into smaller 2x2 m grid.

Excavation showed that the pits ranged from well-defined pits filled with ash (see pit 10 in Figure 2.4 and Table 2.3), to pits that were only able to be defined through distribution of finds (see pit 3 and 12 in Figure 2.4 and Table 2.4) (Evers, 1982a). Ceramics were found in all of the pits, with variations in size and quantity (Evers,

1982a). Similarly, charcoal was present in many pits although only two pits were dated through radiocarbon dating (see pit 1 and 8 in Table 2.2 and Table 2.3) (Evers, 1982a). Evidence of metalworking was found in multiple pits throughout the site, with the slag found to be likely from a single occupation (Evers, 1982a). The metal working also was substantiated through the find of copper and iron beads (Evers, 1982a).

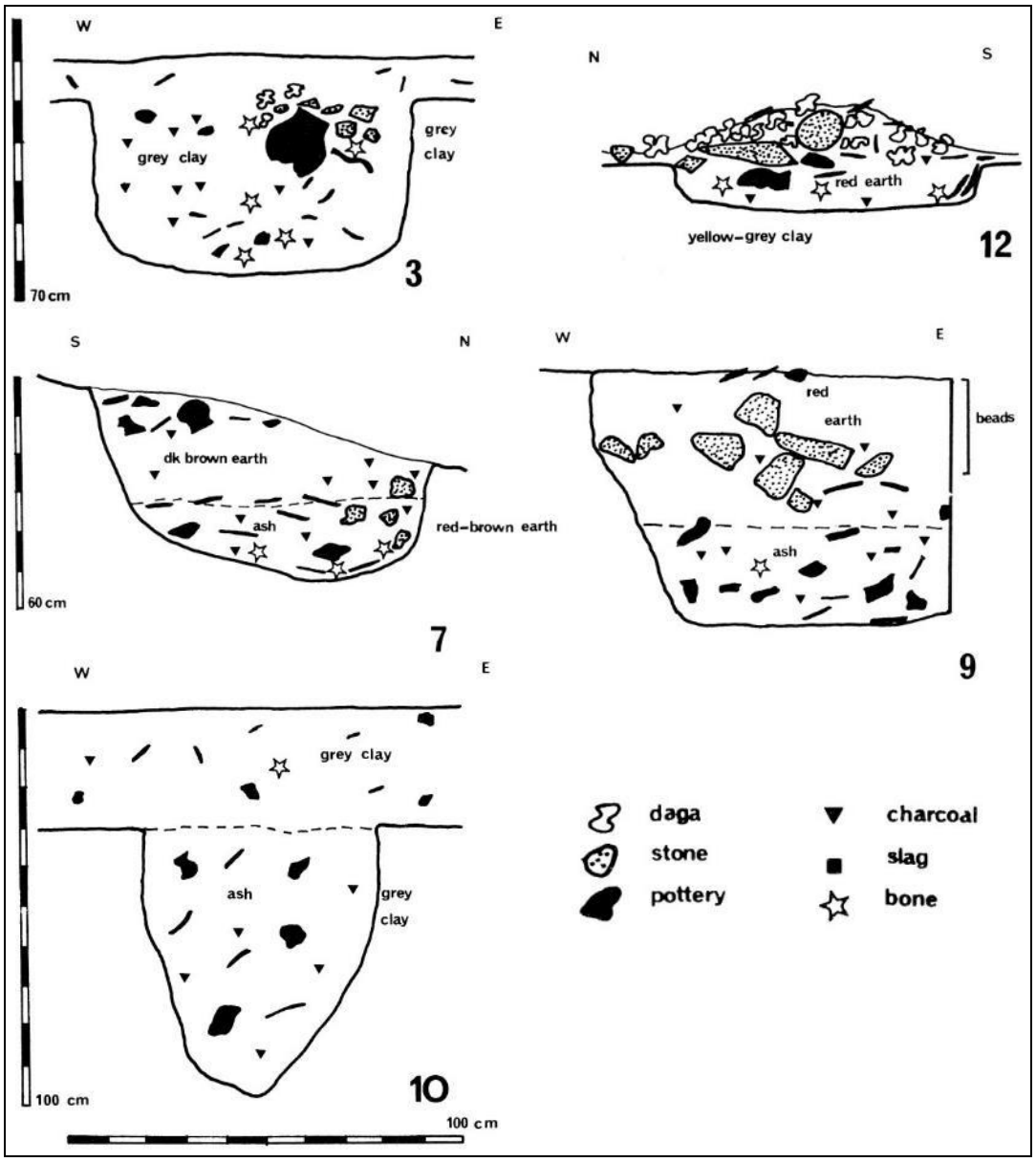


Figure 2.4. Sections of pits 3, 7, 9, 10 and 12 (Evers, 1982a, pp. 18–19)

Table 2.2. Description of pits 1, 2, 5, 6, 7, and 9. The pits of interest to the project are highlighted in grey (Evers, 1982a).

| Pit | Max diameter | Preserved depth | Finds | |
|---|---|---|---|---|
| Pit fill type 1: red-brown loam top layer, with a red loam fill and khaki ash basal deposit | | | | |
| 1 | 120 cm | 80 cm | Pta-1634 (at 45-65cm depth), ceramics and slag | |
| 2 | 130 cm | 83 cm | Dagha, charcoal, ceramics, and bones | |
| 5 | 69 cm | 70 cm | Possibly truncated | Variably distributed |
| 6 | 96 cm | 41 cm | | Variably distributed, ceramics between ash and loam |
| 7 | 90 cm | 50 cm | | Variably distributed, ceramics between ash and loam |
| 9 | 90 cm | 66 cm | | Variably distributed, ceramics, bone, charcoal, Achatina, iron (slag), copper beads |

Table 2.3. Description of pits 4, 8, and 10. The pits of interest to the project are highlighted in grey (Evers, 1982a).

| Pit | Max diameter | Preserved depth | Finds |
|---|---|---|---|
| Pit fill type 2: Khaki ash fill | | | |
| 4 | 46 cm | 68 cm | Evenly distributed |
| 8 | 107 cm | 51 cm | Evenly distributed ceramic, slag, charcoal and Pta-328 found near on surface, assumed to have eroded out of the pit |
| 10 | 65 cm | 83 cm | Evenly distributed ceramic, charcoal, and bone near surface. |

Table 2.4. Description of pits 3, 11, and 12. The pits of interest to the project are highlighted in grey (Evers, 1982a).

| Pit | Max diameter | Preserved depth | Finds |
|---|---|---|---|
| Pit fill type 3: Difficult to distinguish pit fill, finds determined the pit extent | | | |
| 3 | 80 cm | 43 cm | Grey clay with ceramics, bones, and charcoal |
| 11 | 50 cm | 35 cm | Ceramics |
| Unidentified pit fill: gulley through pit had eroded it heavily | | | |
| 12 | 76 cm | 10 cm | Dagha, bones, charcoal, and ceramics |

Evers' team labelled the sherds from these pits with information, although not consistently with all information (Figure 2.5). The information included the site name and the find location based on the grid system, pit numbers, and find depth.

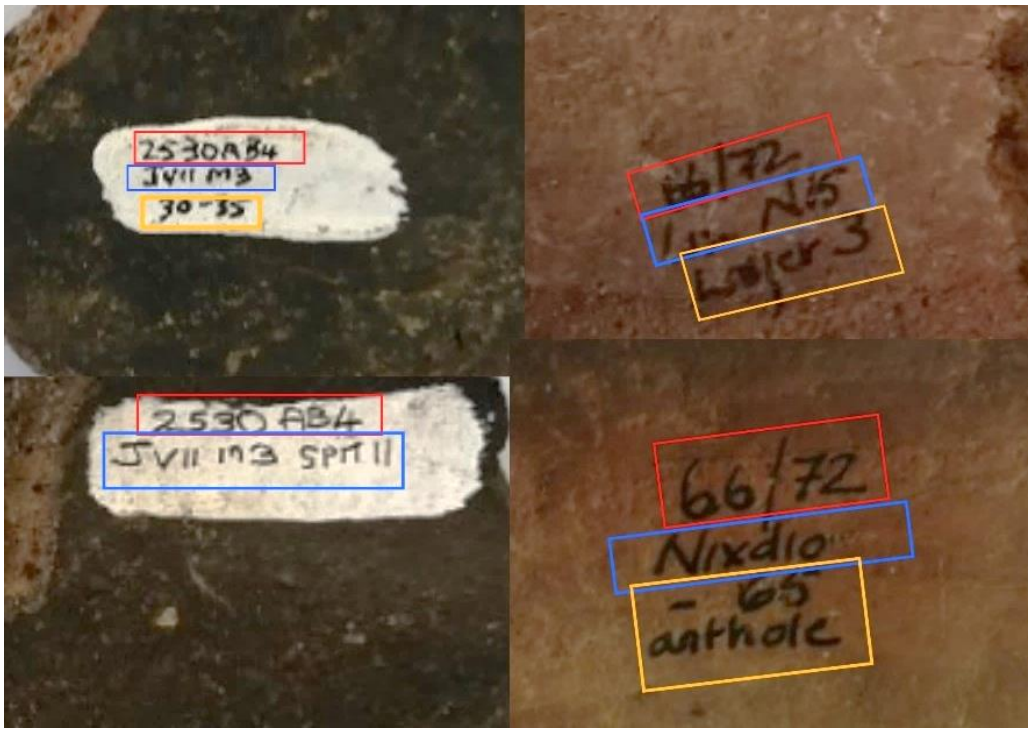


Figure 2.5. Examples of information available on sherds. Red indicates the site; blue indicates the location based on the grid system; and yellow indicates further details such as depth or layer.

During this excavation, Evers (1982a) found 158 reconstructable vessels, which he classified into pottery classes (Evers, 1982a, p. 21). He suggested these formed part of a single assemblage, as was originally hypothesised by Inskeep and Maggs (1975). Thus, placing the Heads and all ceramics (vessels and sherds) in a single occupation in the 6$^{th}$ century AD. However, Whitelaw's (1996) reanalyses of the ceramic assemblage suggested that there were two distinct non-contemporaneous ceramic traditions and multiple facies present. This challenged previous approaches to the Mpumalanga occupation, which suggested that the sequence lacked evidence for change over time (Evers, 1988; Whitelaw, 1996).

A study by Becher (2021) on 40 pottery samples from the LHS tried to establish if the Urewe and Kalundu tradition pottery from the site had different uses. She used lipid biomarkers (Gas Chromatography-Mass Spectrometry) and compound-specific isotopic (Gas Chromatography-combustion-Isotope Ratio Mass Spectrometry) analysis. This analysis marked the first use of organic residue analysis (ORA) in the context of southern Africa early farming ceramics (Becher *et al.*, 2024). The samples included 20 samples from both the Doornkop and Mzonjani facies, allowing a comparative analysis of the facies of assumed differing ages (Becher, 2021; Becher *et al.*, 2024). The ceramics were shown to be multifaceted with both facies presenting animal fat and plant oils (Becher, 2021; Becher *et al.*, 2024). The presence of ruminant carcass fat on both facies implies the possibility of domestication of animals such as cattle, goats and sheep (Becher, 2021; Becher *et al.*, 2024). The presence of non-ruminant adipose (fat) implies the processing of wild animals such as pigs (Fewlass *et al.*, 2020; Becher, 2021). The Mzonjani pottery displayed a presence of non-ruminant adipose, while the Doornkop pottery showed two examples of ricinoleic acid (a component of seed oil) (Becher, 2021; Becher *et al.*, 2024). The two examples of ricinoleic acid on the ceramics support the possibility of the medicinal use or plant processing (Becher, 2021; Becher *et al.*, 2024).

Evers submitted charcoal from a depth of between 450 and 650 mm in Pit 1 (Figure 1.2) for radiocarbon dating. The sample age was determined to be 1410 ± 50 BP (540 ± 50 AD, Pta-1634) (Evers and Vogel, 1980; Evers, 1982a). Consequently, Evers (1982a) suggested the occupation of the LHS started in the 6th century and lasted until the 7th century AD (Evers, 1982a). Whitelaw suggested that these dates only related to part of the Urewe tradition occupation (Whitelaw, 1996). The second occupation postulated by Whitelaw (1996) to be by the Kalundu tradition, is not reflected in this sample and he argued that it took place between the 9th and 11th century AD.

Whitelaw recalibrated the radiocarbon ages, using the Pretoria Calibration Programme (Talma and Vogel, 1993), to 615 - **644** - 663 AD (Pta-328) and 644 - **663** - 683 AD (Pta-1634) (Whitelaw, 1996; central intercept in bold). The Southern African Radiocarbon Database (SARD) recalibrated these ages to 537 - 760 AD (Pta-328) and 592 - 769 AD (Pta-1634) (see Loftus *et al.* (2019) and https://c14.arch.ox.ac.uk/sadb/db.php; the ranges are shown for 2 sigma). The radiocarbon ages are significant for chronologies of not just a site but also for a ceramic sequence. In this light it is important to see the LHS contextually, by reviewing other sites of a similar nature and within the Mpumalanga sequence.

### 2.3.2 Early farming communities

There are three EFC sites close to the LHS (Figure 2.6). These are Klingbeil 2530AB1 and Klingbeil 2530AB2 (formally Lydenburg 57/73 and Lydenburg 58-59/73, respectively) to the north of the LHS (Evers, 1980; Figure 2.6). Both Klingbeil 2530AB1 and Klingbeil 2530AB2 are part of the Kalundu tradition (Evers, 1980). The Klingbeil facies, which follows Doornkop, is named after the site (Evers, 1980; Huffman, 2007; Schoeman, 2020; Fredriksen, 2023). There are three radiocarbon dates for Klingbeil 2530AB1. These are 970 ± 50 BP (Pta-1747), 1120 ± 50 BP (Pta-2160) and 1160 ± 50 BP (Pta-1663) (Evers, 1980). The calibrated ages, using the Hogg *et al.* (2013) curve, were 1026-1200 AD (Pta-1747),

862-1131 AD (Pta-2160) and 777-1021 AD (Pta-1663) (Schoeman, 2020). Klingbeil 2530AB2 remains undated (Evers, 1980).

The Doornkop site is located further south than the Klingbeil and LHS (Figure 2.6). The site was the first in the Mashishing region to be theorised to have multiple occupations (Evers, 1988). The three radiocarbon ages for the Doornkop site are 1270 ± 60 BP (Pta-2944), 1210 ± 50 BP (Pta-2535) and 1140 ± 50 BP (Pta-2536). The calibrated ages, using the Hogg *et al.* (2013) curve, were 674 - 967 AD (Pta-2944) and 693 – 992 AD (Pta-2535) (Antonites *et al.*, 2014).

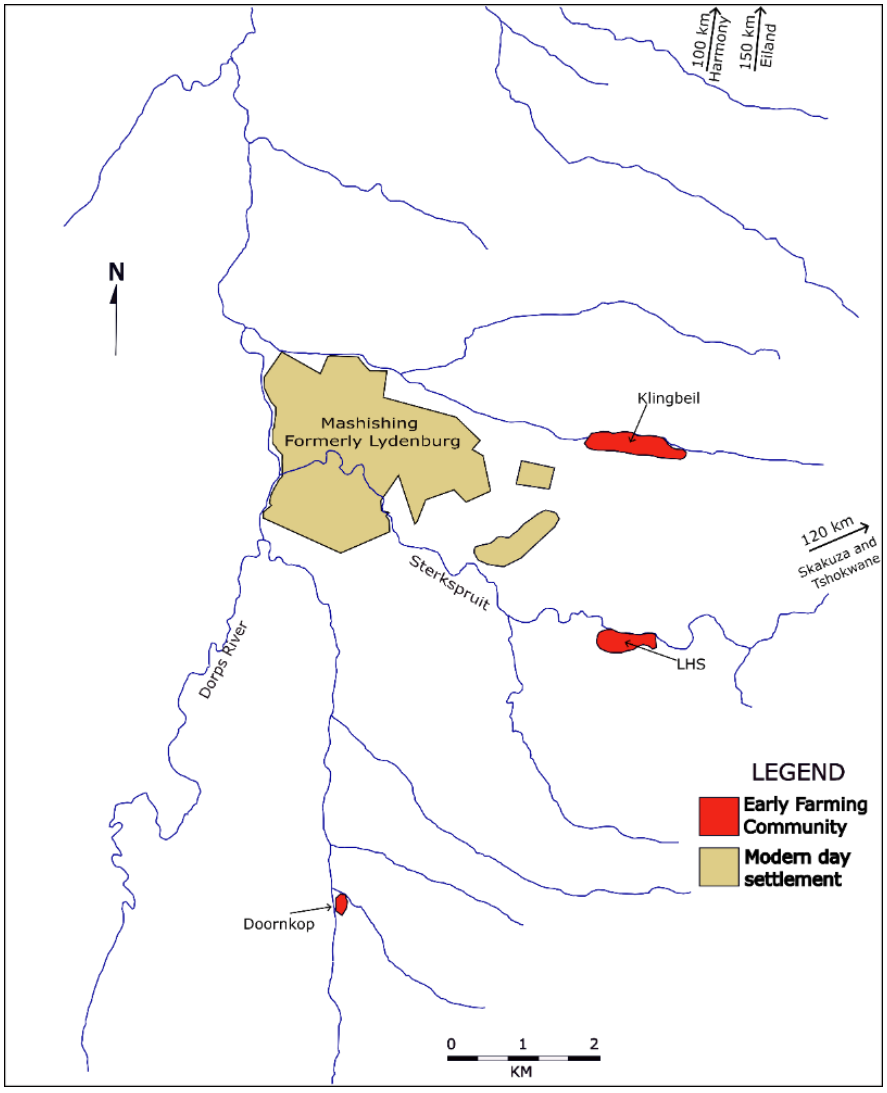


Figure 2.6. Map of the EFC archaeological sites near the Lydenburg Heads Site (after Evers, 1975).

The distinction between facies in ceramic assemblages can be difficult to establish at multiple occupation sites, which are common in the first millennium; for example, excavations at Harmony and Eiland have shown three occupations, firstly in the 4th to 6th century AD, then in the 11th to the 14th century AD and lastly in the 16th/17th century AD (Evers, 1974, 1975, 1977, 1982b; Antonites, 2013; Schoeman, 2020). Harmony and Eiland are salt producing EFC sites located in the Limpopo province (see Figure 2.6 for reference to LHS). The stages of occupation all include different ceramic facies, with the first phase being Silver Leaves then Eiland and then Letaba (Evers, 1974, 1975, 1977, 1982b; Antonites, 2013).

Sites of a comparable nature are important in understanding the sequence of events and the connections between ceramics of multiple sites and timelines. These include the site of Tshokwane (TSH1) and Skukuza (SK17) located just over 120 km to the east of the LHS, that were excavated in the 1980's (see Figure 2.6 for reference to LHS) (Jordaan, 2016). TSH1 has four radiocarbon ages associated with the site, one from the original excavation by Meyer (1986) and three from the reanalysis by Jordaan (2016). The ages range from 545 to 764 AD (Jordaan, 2016; Schoeman, 2020). The ages and ceramic style typology place it within a similar period to the first hypothesised occupation of the LHS (Jordaan, 2016; Schoeman, 2020).

The Skukuza (SK17) site's radiocarbon ages, from Meyer's 1986 excavation and Jordaan (2016), were between 660 and 992 AD (Jordaan, 2016; Schoeman, 2020). This means this site is contemporaneous with Lydenburg and two other sites named Lebalelo and Mototolong (Huffman and Schoeman, 2011; Jordaan, 2016; Schoeman, 2020). All the sites had multicomponent assemblages. SK17 had multiple occupations with ambiguous demarcation, similar to the LHS (Jordaan, 2016). The assemblages were deemed to be Mzonjani, Msuluzi and Ndondondwane (Jordaan, 2016; Schoeman, 2020). Mototolong was also a multi occupation site and had Mzonjani and Doornkop ceramics (Huffman and Schoeman, 2011; Jordaan, 2016; Schoeman, 2020). Clearly, the LHS formed part of a much larger network of Early Farmer Communities in northeastern South Africa.

The EFC sequence, particularly in sites of multiple occupations, is difficult to disentangle. Although the use of radiocarbon dating and seriation have proved indispensable, the need for a robust absolute dating technique for the complex sites is shown. The processes of direct dating of ceramics are important when other artefacts, such as charcoal, cannot be conclusively connected to the sherds or vessels.

## 2.4 Principles of luminescence dating

The radiometric technique of luminescence dating allows the direct dating of archaeological artefacts (see Aitken, 1985; Bøtter-Jensen and Mejdahl, 1988; Bøtter-Jensen *et al.*, 2000; Murray and Wintle, 2000). Although usages have extended into geochronology, the technique and concepts of thermoluminescence were improved by Aitken (1985) as an archaeological dating technique on pottery and ceramic artefacts. The principles of luminescence dating are in the accumulation of charge within the crystalline structure of mineral such as quartz and feldspar (Aitken, 1985; Murray and Wintle, 2000; Mahan *et al.*, 2022). The impurities in the crystal lattice allows electrons to be trapped within the mineral, which owing to natural ionising radiation increases over time (Figure 2.7) (Aitken, 1985; Murray and Wintle, 2000; Mahan *et al.*, 2022). The result is that through measuring the signal released, upon zeroing or resetting the grain, a relation can be made to the age of the material.

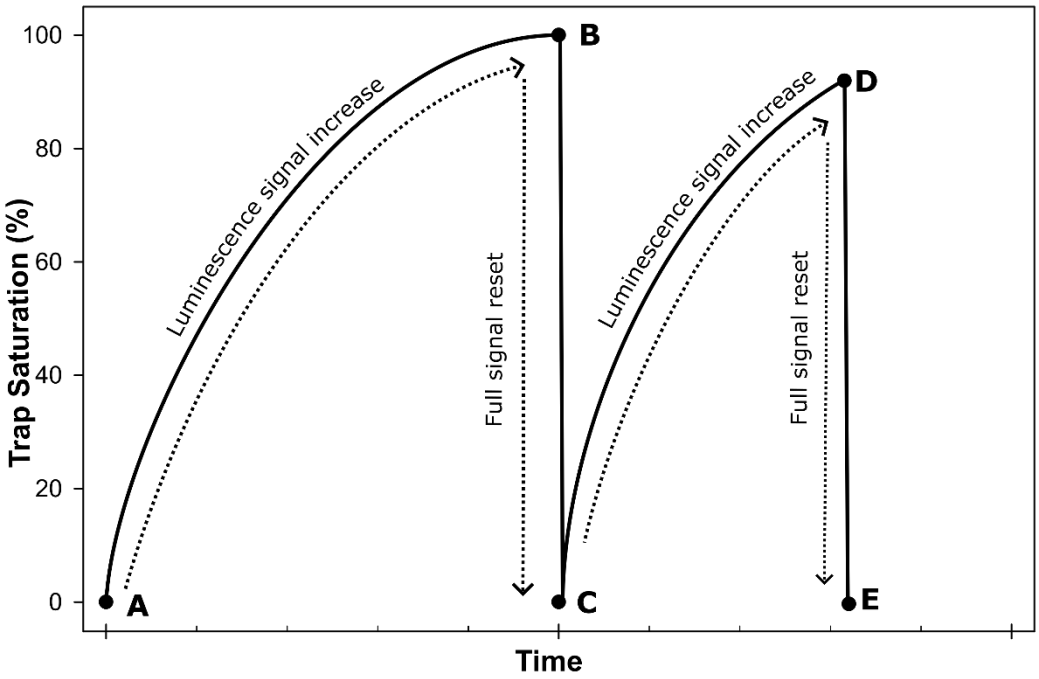


Figure 2.7. Diagram showing the concept of luminescence dating. Upon burial or removal from heat the signal within the mineral increases (A to B). Once exposed to heat or light the signal is 'zeroed' or reset (B to C). The signal once reset will begin to accumulate charge immediately (C to D). The burial or production age is in relation to the signal accumulated within the mineral (A to C or C to E). (Modified after Feathers, 2003)

Luminescence dating allows one to determine the age of burial for sediment and firing for ceramics (Figure 2.7: point A and C) (Aitken, 1985; Feathers, 2003; Fuchs and Lang, 2009; Mahan *et al.*, 2022; Moska *et al.*, 2021; Reimann *et al.*, 2011). The luminescence dating of pottery is thus dated to the moment of firing or last exposure to extreme heat (Feathers, 2003). This holds significance to dating the artefacts to a likely anthropogenically stimulated event (production or use of artefact) and thus creates a link between an activity and an absolute age. The anthropogenically stimulated events are more likely within the case of pottery or ceramics as the naturally occurring heat will not reach a threshold high enough to reset the signal. The trap saturation is the point at which the charge can no longer increase. Although, based on the likely ages of ceramics and the range of luminescence dating, this is highly unlikely for ceramics. This technique requires the artefact to contain feldspar or quartz grains, while no organic materials are needed (Aitken,

1998, 1985; Arnold *et al.*, 2015; Feathers, 2003; Moska *et al.*, 2021; Rhodes, 2011; Wallinga, 2002)

The requirement to reset the signal (the partial or full removal of energy in the crystalline structure of the pottery) in ceramics is heating from 300°C for extended periods. However, 500°C is considered the actual required temperature for signal resetting (Feathers, 2003; Mahan *et al.*, 2022). The resetting or zeroing temperature is often only reached when the pottery is fired, although can be reached during use if extreme heats are obtained (Feathers, 2003). Thus, the age is determined to be since creation or (less likely) active use of an archaeological artefact.

To determine the age of a sample the following equation is used:

$$Age = \frac{D_e}{D_R} \qquad \text{Equation 1}$$

$D_e$: equivalent dose in grays (Gy); $D_R$: Dose Rate in grays per kiloannum ($\frac{Gy}{ka}$)
(Aitken, 1985; Wallinga, 2002; Duller, 2004; Lamothe, 2016; Mahan *et al.*, 2022)

### 2.4.1 The equivalent dose

The equivalent dose ($D_e$) is a fundamental measurement for determining the age of sediment or artefacts using OSL dating. The $D_e$ is the laboratory dose that is equivalent to the originally trapped signal in the artefact or sediment (Murray and Wintle, 2000; Lamothe, 2016; Murray *et al.*, 2021; Mahan *et al.*, 2022). Original techniques of TL to determine the $D_e$ have largely shifted towards OSL techniques and protocols (Mahan *et al.*, 2022). The shift is in large due to creation of techniques with fewer errors, such as interpolated $D_e$ instead of extrapolated $D_e$ in TL (Hood and Schwenniger, 2016). The $D_e$ relates to the dose absorbed and thus should be considered equivalent to the palaeodose (Feathers, 2003; Guérin *et al.*, 2017).

To understand the $D_e$, it is important to be aware of the effects of partial resetting or bleaching. When zeroing or resetting the signal in artefacts or sediments, external factors can make it that the signal is not fully released, a process called partial resetting or bleaching. The results are that the signal measured for the $D_e$ includes the residual signal (see Figure 2.8). Partial bleaching in sediment can be the result of sediment mixing, transportation of grains in water, anthropogenic alterations, and shielding of grains. While the partial bleaching of ceramics can come about through anomalous heating events, manufacturing processes, and exposure of grains through damage. To produce ages, the consideration needs to be made to possible partial bleaching events and errors to the $D_e$ values.

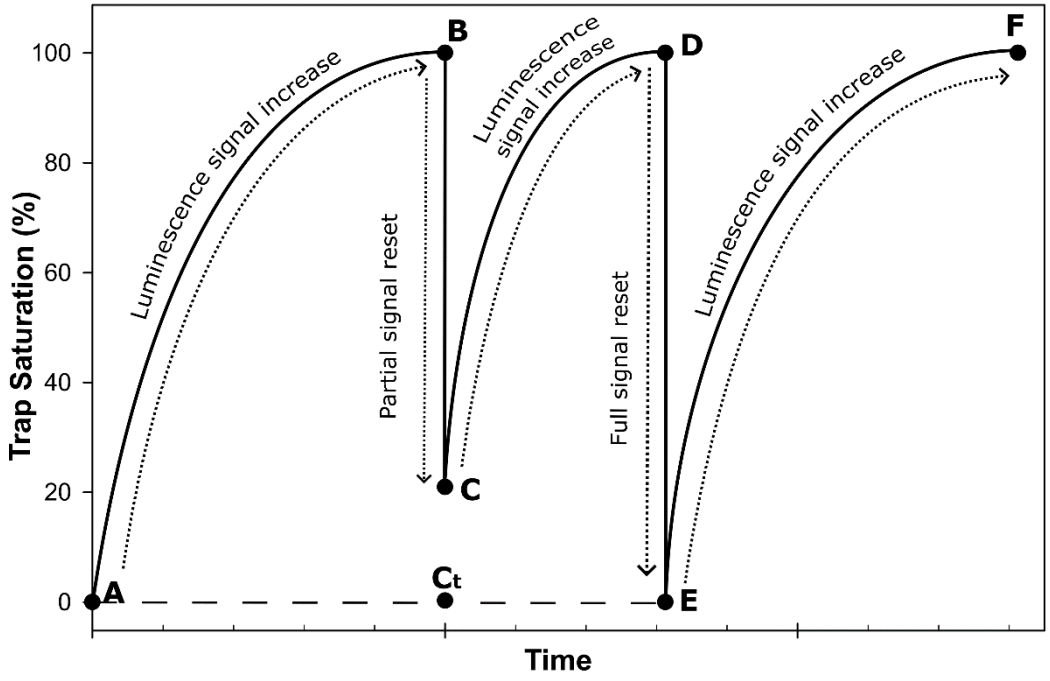


Figure 2.8. Trap saturation versus time graph. The graph begins with showing the signal increase over time, then at 'A' a resetting event occurs (heating of pottery). The amount of radiation required to get from 'B' to 'A' is representative of the $D_e$. From 'C' to 'D' the charge increases again with a subsequent resetting event at 'D.' The lines 'A' to 'Ct' and 'Ct' to 'E' shows how the age is affected when a material has been partially reset, with the material retaining charge and the result being this signal released not being proportional to the time of deposition or since heating. (Modified after Feathers, 2003)

The overdispersion (OD) parameter defines the variation/scatter in $D_e$ measurements which fall outside the assumed statistical analysis and is often used to assess the extent of incomplete bleaching (Galbraith and Roberts, 2012). This results in inaccurate measurements of the $D_e$ and thus needs to be taken into account when reviewing data (Murray *et al.*, 2021; Mahan *et al.*, 2022). Numerous protocols have been developed to measure the De, which associate the laboratory measured signal to known irradiation doses. A major protocol developed for OSL dating is the Single Aliquot Regenerative Dose (SAR) Protocol (Murray and Wintle, 2000; Wintle and Murray, 2006). The SAR protocol is considerably popular because it includes data interpolation, monitoring tests, and corrections for sensitivity changes (Murray and Wintle, 2000; Hood and Schwenniger, 2016; Murray *et al.*, 2021).

The SAR protocol involves a series of cycles of which progressively larger beta doses are monitored by a fixed test dose. The cycle begins with the measurement of the natural signal (Ln). The sample is then exposed to a known radiation (beta doses), the response of the sample to the radiation is measured (L1, L2, etc). The regenerative dose (Lx) is a function of the OSL signal measured from the increasing beta doses (L1, L2, etc). The sample is then given a fixed and known test dose of which the response is measured (Tn, T1, T2, etc). The regenerative test dose (Tx) is a function of the OSL signal measured from the fixed test dose (T1, T2, etc). The changes in sensitivity are correct with the inclusion of the regenerative test doses (Ln/Tn, L1/T1, L2/T2, etc). The dose response curve is the regenerative doses divided by the test doses (Lx/Tx). While the interpolation of the natural signal and the test dose (natural) (Ln/Tn) provide the $D_e$.

The recycling test involves comparison of the first and last regenerative dose measurements, allowing review of the reproducibility results within the laboratory setting. The ratio of the two measurements should be 1, although common practice allows ratios between 0.9 and 1.1 (Murray and Wintle, 2000). The recuperation test involves the addition of a zero dose within the regenerative dose cycle. The result should be little to no change in the signal (Murray and Wintle, 2000). Finally, the

dose recovery test reviews that the given and measured doses are in unity, thus allows ratios between 0.9 and 1.1 (Murray and Wintle, 2000). The monitoring tests (Recycling ratio, recuperation tests and test dose error) are used for acceptance criteria.

### 2.4.2 The dose rate

The second element in Equation 1 is that of the dose rate. The $D_R$ is the radioactivity of the sample and surrounding environment. The $D_R$ comprises the rate of accumulation due to exposure to cosmic radiation (c), gamma (γ) radiation, alpha (α) radiation, and beta (β) radiation, which incorporates the ionising radioactivity within the environment (Bailiff, 1997; Aitken, 1998; Duller, 2004; DeWerd, 2020; Mahan *et al.*, 2022).

The dose rate equals the summation of the alpha, beta, gamma, and cosmic dose rates (Aitken, 1985, 1998):

$$\mathrm{D_R} = \mathrm{D}\alpha + D\beta + \mathrm{D}\gamma + \mathrm{Dc} \qquad \text{Equation 2}$$

$$\mathrm{D_R} = \text{Dose rate}\left(\frac{\mathrm{Gy}}{\mathrm{ka}}\right);\ \ \mathrm{D}\alpha = \text{alpha dose rate};\ D\beta = \text{beta dose rate};$$

$$\mathrm{D}\gamma = \text{gamma dose rate};\ \mathrm{Dc} = \text{ cosmic dose rate}$$

The alpha, beta, gamma, and cosmic dose rates in Equation 2, are determined through radionuclide dosimetry, water content, geographic location, depth of sample and grain size (Aitken, 1998; Mahan *et al.*, 2022). The radionuclide dosimetry involves the measurement of the uranium (U), thorium (Th) and potassium (K) concentration. The presence of these elements allows the environment and the grains to absorb ionising radiation over time. The U and Th affect the alpha, beta, and gamma dose rates, while the K affects the gamma and beta dose rates.

The alpha attenuation (Bell, 1980; Aitken, 1985; Grün, 1987) and beta attenuation (Aitken, 1985; Bell, 1979; Mejdahl, 1979; Fain *et al.*, 1999; Preusser, 1999; Brennan, 2003) are affected by grain size and energy emission from uranium, thorium and potassium. Alpha particles are larger and thus have a limited range, resulting in increased alpha attenuation with an increase in grain size. In contrast beta particles are smaller and have a larger range, allowing decreased beta attenuation with grain size. As a result, consideration must be made to the dosimetry and grain size for accurately determining the $D_R$. The depth of the sample is affected by longer ranged radiation and thus affects the gamma and cosmic dose rates (Aitken and Xie, 1990; Prescott and Clay, 2000; Mahan *et al.*, 2022). Finally, the effects of geographic location (longitude, latitude, and altitude) influence the cosmic dose rate (see Prescott and Hutton, 1994).

The major issues surrounding the $D_R$ are the assumptions made to produce the dose rate. The first assumption is that there is equilibrium in the decay chain (Feathers, 2003; Rhodes, 2011; Moska *et al.*, 2021; Mahan *et al.*, 2022). The decay chain of $^{238}U$, $^{235}U$ and $^{232}Th$ are assumed to be in secular equilibrium, which means the decay rates and accumulation of each are essentially identical (Moska *et al.*, 2021; Murray *et al.*, 2021; Mahan *et al.*, 2022). If the decay chains were in disequilibrium the U and Th dose rates would change through time.

The second assumption is that of an infinite matrix, in which the dosimeter or sample is located within a homogeneous sediment (evenly distributed radioisotopes) with a radius larger that the of the range of a relevant radioactive ray (Aitken, 1985; Adamiec and Aitken, 1998, Guérin *et al.*, 2012). The assumption is important in allowing the conversion of the concentrations of radioisotopes to alpha, beta and gamma dose rates, which is done using conversion factors (see Adamiec and Aitken, 1998; Guérin *et al.*, 2017; Cresswell *et al.*, 2018)

The third assumption is surrounding the water content, which has been shown to affect the $D_R$ (Aitken, 1998; Wallinga, 2002; Rhodes, 2011; Murray *et al.*, 2021;

Mahan *et al.*, 2022). Water content is important owing to the solubility of U (as uranyl ion $(UO_2)^{+2}$) (Preusser *et al.*, 2008; Feathers *et al.*, 2020; Mahan *et al.*, 2022). Water absorbs radiation and, as a result, reduces the amount of radiation absorbed by the dosemeter/sample (Wallinga, 2002; Rhodes, 2011; Murray *et al.*, 2021; Mahan *et al.*, 2022). In certain contexts, the water content can be assumed stable or without extreme fluctuations. Hood and Schwenniger (2016) used the minimal extraction technique of quartz grains to date Egyptian ceramics. In concept, the Egyptian environment would pose little variability to water content as the area is generally hot and dry (Hood and Schwenniger, 2016). The association with material cultures and the environmental setting need to be considered, with settlements or sites being located in alluvial fans, deltas, at level with the water table or close to a water source (Hood and Schwenniger, 2016).

$$Water\ content\ (\%) = \frac{weight_{\ wet}\ (g) - weight_{\ dry}\ (g)}{weight_{\ wet}\ (g)} \times 100 \qquad \text{Equation 3}$$

(Aitken, 1998; Wallinga, 2002; Jacobs, 2010; Han *et al.*, 2021)

Water content estimates can be influenced by measuring the actual water content of an artefact. This involves weighing an artefact before and after drying in an oven (Equation 3). In previously excavated and stored material, the weighing of the sherds or sediment will hold no information as the water content would have changed since excavation. Considering the water contents clear uncertainty, it is important to review the natural environment and make situational and educated guesses on likely ranges for water content. The Dγ and Dβ were corrected for water content using the following equations (Aitken and Xie, 1990):

$$D_{\beta\ wet} = \frac{D_{\beta\ dry}}{1 + (1.25 \times WC)} \qquad \text{Equation 4}$$

$$D_{\gamma\ wet} = \frac{D_{\gamma\ dry}}{1 + (1.25 \times WC)} \qquad \text{Equation 5}$$

### 2.4.3 Age calculations

To calculate the OSL age, statistical methods must be used to determine a single representative $D_e$ value. The age models produce the representative $D_e$ value, from which the age can be determined by dividing it by the dose rate. Although called age models, the statistical measurements are done on the $D_e$ only, as the $D_R$ is a single value per sample. Numerous age models have been developed for use in OSL dating. The central age model (CAM, Galbraith *et al.*, 1999) involves the assumption that the ages are normally distributed and allows the calculation of OD (Guérin *et al.*, 2017; Mahan *et al.*, 2022). In contrast the minimum age model (MAM) is not reliant on the $D_e$ values being normally distributed and instead uses statistical analysis to determine the minimum age possible (Galbraith *et al.*, 1999; Lian and Roberts, 2006; Mahan *et al.*, 2022). Furthermore, the Average Dose Model (ADM) (Guérin *et al.*, 2017), is similar to CAM with the addition of alterations for the microdosimetry and is considered well suited to heterogeneous samples (Mahan *et al.*, 2022). Both Guérin *et al.* (2017) and Murray *et al.* (2021), speak of a determination of the $D_e$ for multi-grained aliquots as being best suited to simple arithmetic means.

Each model includes inherent errors, and as a result, the observations of the OD (overdispersion) are made to help review the sample and the spread of data between aliquots. In cases of well-bleached samples, the CAM, ADM, or arithmetic mean will be the most applicable (Olley *et al.*, 2004; Galbraith *et al.*, 2005, Guérin *et al.*, 2017). In terms of the best suited for the well-bleached samples would be firstly the arithmetic mean followed by the ADM and finally CAM. While for samples that are not well-bleached, MAM is preferable to prioritise the lowest dosed aliquots. The production of the CAM age allows the OD to be determined allowing further analysis in the cases of assumed partial bleaching or other ages skewing elements. As result CAM ages are often produced even when the model is not the best fit for a sample. The choice of age model needs to consider the individual samples or site for the accuracy of the age.

## 2.5 Chronology in archaeology

The method of producing chronologies within the context of archaeology is important for constraining timing and producing comparative analysis. With dating sciences being a broad field, one can define them as relative or absolute dating techniques (Sherwood *et al.*, 1994; Botha and Porat, 2007). Relative dating techniques relevant to archaeology are seriation and stratigraphy-based dating. Stratigraphy reviews the object in relation to the surrounding strata to determine the comparative age (Botha and Porat, 2007; Avery *et al.*, 2008). Seriation is the technique of reviewing the artefacts in terms of stylisation over time. The seriation technique is prominent in the relative dating of the EFC within South Africa (see Huffman, 2007).

In terms of absolute dating of archaeology within South Africa, the prominent method is radiocarbon dating. Radiocarbon ages have been shown to be substantial within the section 2.3.2: Early farming communities. This dating technique is reliant on the presence of organic material with a measurable carbon content in the site (Arnold and Libby, 1949, Hua, 2009, Feathers, 2003; Murray *et al.*, 2021; Mahan *et al.*, 2022). Radiocarbon ages are related to the time of death of the organism; for example, dated charcoal will be associated with the time of the tree being felled.

Although this technique is very helpful in constraining timing, in some cases, the ability to associate the artefact with other organic finds is difficult. The use of OSL dating can thus be used in situations where radiocarbon dating is not applicable (lacking organic material) or insufficient (complex occupations). It is important to note that when reviewing younger ages, both techniques hold benefits and can provide ages where appropriate. In older samples, one needs to consider that OSL dating can derive ages over 500,000 years while radiocarbon dating has a limit of ~50,000 years. The limit to ~50,000 years for radiocarbon dating is owing to the half-life of $^{14}C$, which in older samples is less distinguishable from background

radiation owing to the small quantities of $^{14}C$ (Taylor, 2018; Murray *et al.*, 2021). Although, the age limit of radiocarbon dating does not pose a risk in studies of the EFC.

Within the context of chronology in archaeology, the techniques of combined radiocarbon and OSL dating is evident (see Table 2.5 for international examples and Table 2.6 for South African examples) (Aitken, 1985, 1989; Pienaar *et al.*, 2008; Sánchez *et al.*, 2008; Zink *et al.*, 2012; al Khasawneh *et al.*, 2019; Anderson and Feathers, 2019; Tribolo *et al.*, 2022a, 2022b; Pacompia *et al.*, 2023). Since radiocarbon dating is a more common field and was practised for many years before the applications of OSL dating, sites often have original radiocarbon ages and subsequent OSL ages.

Table 2.5. Luminescence and radiocarbon dating sites of interest worldwide.

| **Site** | **Luminescence age (ka)** | **Luminescence technique** | **$^{14}$C ages** | **Source** |
|---|---|---|---|---|
| **Tell Damiyah, Jordan** | Youngest: 2.4 ± 0.14<br>Oldest: 2.96 ± 0.23<br>(sediment) (not all shown) | OSL<br>Quartz<br>SAR protocol | Between:<br>809 and 745 BC;<br>380 and 203 BC | (al Khasawneh *et al.*, 2019) |
| **Tunata-hill site, Peru** | 0.49 ± 0.02 (ceramics) | OSL and TL<br>Quartz<br>SAR protocol | 540 ± 70 cal BP<br>570 ± 100 cal BP | (Kigoshi *et al.*, 1962; Pacompia *et al.*, 2023) |
| **Tall Abu Fahd (TAF) and Tall Qsubi (TG), Syria** | 2.64 ± 0.64 (TAF pottery)<br>2.88 ± 0.52 (TQ pottery)<br>2.64 ± 0.24; 2.68±0.24 (TAF sediment)<br>2.78 ± 0.16; 3.05±0.28 (TQ sediment) | Quartz and feldspar<br>OSL and TL<br>Double SAR protocol | 3220 ± 35 cal BP (Ua-34233) | (Sánchez *et al.*, 2008) |
| **Ahteut, Alaska** | 0.78 ± 0.07 (1230 ± 70 AD)<br>0.27 ± 0.10 (1740 ± 100 AD)<br>1.05 ± 0.35 (960 ± 350 AD)<br>1.37 ± 0.26 (640 ± 260 AD) | OSL and TL<br>Quartz and feldspar<br>Double SAR protocol<br>Ceramics | 900 - 680 cal BP (1060 -1270 cal AD)<br>Tree ring data: 750 - 700 cal BP (1200 -1250 AD) | (Anderson and Feathers, 2019) |

Table 2.6. Luminescence and radiocarbon dating sites of interest in South Africa.

| **Site** | **Luminescence age (ka)** | **Luminescence technique** | **$^{14}$C ages** | **Source** |
|---|---|---|---|---|
| **Hoedjiespunt 1, South Africa** | 96 ± 8 (CAM), 101 ± 8 (ADM)<br>116 ± 10 (CAM), 128 ± 12 (ADM)<br>104 ± 9 (CAM), 111 ± 9 (ADM)<br>99 ± 8 (CAM), 104 ± 9 (ADM)<br>(not all shown) | OSL and TL<br>Quartz<br>SAR protocol<br>Shell midden | - | (Tribolo *et al.*, 2022a, 2022b) |
| **Rose Cottage, South Africa** | 8.60 ± 0. 60<br>13.6 ± 1.40<br>13.00 ± 1.200<br>(Not all shown) | OSL<br>Quartz<br>SAR protocol<br>Sediment | 8 614 ± 38 (Pta-5560)<br>12 690 ± 120 (Pta-5593)<br>13 360 ± 150 (Pta-5601)<br>(Not all shown) | (Pienaar *et al.*, 2008) |
| **Limpopo, South Africa** | 1.370 ± 0.22 (Mzonjani)<br>1.550 ± 0.21 (Happy Rest)<br>(ceramics)<br>(not all shown) | OSL<br>Quartz and feldspar<br>Double SAR protocol | 675 – 780 AD (Mzonjani) (Pta-8949)<br>440 – 640 AD (Happy Rest) (Pta-9546)<br>(not all shown) | (Zink *et al.*, 2012) |

When reviewing ages produced through radiometric techniques, it is important to consider what was measured and information that can be associated with the ages. The technique of sediment dating is used in archaeological contexts to date the stratigraphy and assumes the associated artefacts found within maintain the same age. In producing a stratigraphic chronology for an archaeological site, bulk $^{14}C$ dating is useful. Bulk radiocarbon dating is the dating of a bulk sample, such as an organic-rich sediment layer or peat (Strunk *et al.*, 2020). OSL ages can also be produced from sediment where the site contains feldspar or quartz.

Although the use of bulk $^{14}C$ is extensive, the focus was on literature of $^{14}C$ dating of artefacts. The $^{14}C$ dating of artefacts can be charcoal (Evers and Vogel, 1980; Pienaar *et al.*, 2008; Shirar, 2011; Zink *et al.*, 2012), bone (Pienaar *et al.*, 2008; Shirar, 2011), shells (Tribolo *et al.*, 2022a, 2022b) or any item containing sufficient organic material. Critical analysis is needed for all forms of dating when comparing the ages. The ages provided by $^{14}C$ dating are not always directly related to the site or occupation in question. Works by Anderson and Feathers (2019) and al Khasawneh *et al.* (2019) showed combined usage of $^{14}C$, OSL ages and typological dating. While the OSL ages from al Khasawneh *et al.* (2019) line up well with the $^{14}C$, the uncertainty of the OSL ages brings their reliability into question. Although the ages between the OSL and $^{14}C$ showed a variation, the possibilities of the outlying OSL ages for the Alaskan site being related to a possible more recent occupation needs to be considered (see Table 2.5) (Anderson and Feathers, 2019). In contrast the connections between ceramics OSL dating and $^{14}C$ dating of Limpopo, South Africa and Tunata-hill Site, Peru placed the ceramics and $^{14}C$ in the same time-period (Zink *et al.*, 2012; Pacompia *et al.*, 2023).

In Table 2.5 and Table 2.6, the use of OSL quartz dating can be seen in multiple countries and environments. The issue of feldspar contamination needs to be considered when reviewing a pure quartz targeted OSL ages. The studies by Zink *et al.* (2012), Sánchez *et al.* (2008), and Anderson and Feathers (2019), dated using the double SAR protocol, which measured the emitted signal from the IRSL

(infrared stimulated luminescence) and OSL stimulations (Banerjee *et al.*, 2001; Lamothe *et al.*, 2018). In contrast Pienaar *et al.* (2008) used etching from HF during sample preparation to remove the feldspar contamination, although possible errors are attributed to feldspar contamination.

The choice of age model used needs to be considered in accordance with the data available and the environment/sample characteristics. Tribolo *et al.* (2022b), dated the archaeological site of Hoedjiespunt 1 in South Africa using multiple age models for analysis. The age differences between the CAM and ADM ages are shown to be considerably different owing to the larger distribution of the $D_e$ (Tribolo *et al.*, 2022b). The justification of the choice in age model must be considered, such as the use of the CAM age owing to low overdispersion and/or Gaussian distribution of the $D_e$ by Pienaar *et al.* (2008) and Sánchez *et al.* (2008).

Overall, the extensive use of OSL dating shows not only success worldwide but locally for dating archaeological sites. The dating of ceramics by Sánchez *et al.* (2008), Zink *et al.* (2012), Anderson and Feathers (2019), and Pacompia *et al.* (2023), all successfully produced chronologies using quartz OSL dating and the SAR (or variation of) protocol. While the success of dating the ceramics is important, the destructive nature of OSL dating cannot be ignored.

### 2.5.1 Modification of mineral extraction

Luminescence dating needs the presence of mineral such as quartz or feldspar in the sediment or artefact. The result is that the target minerals need to be extracted from the excavated sample or ceramic. The conventional process of obtaining the mineral from ceramics is destructive, with the removal of the contaminated edges and the subsequent crushing of the sherd (Zimmerman, 1971; Aitken, 1985; Murray and Wintle, 2000). Although OSL dating is a valuable direct dating technique, the destructive nature makes it unsuitable for museum pieces or artefacts unique or wanting preservation.

Hood and Schwenninger (2015) developed a minimum extraction technique (MET) that allows for the extraction of quartz or feldspar grains without visible destruction of the artefact. The MET technique was created to date Egyptian museum artefacts (Hood and Schwenninger, 2015; Hood and Schwenniger, 2016; Hood *et al.*, 2019; Hood, 2022). The technique involves using diamond drill bits to drill small holes within artefacts. The result is the small blemishes on the artefacts without complete or widely visible markings.

The technique was performed on seven wavy-handled ceramics and three wine jars from the Turah and Hierakonpolis Egyptian sites (Hood *et al.*, 2019). Although three of the vessels produced insufficient luminescence signal, the seven successful vessels yielded promising relative ages (Hood *et al.*, 2019). The technique was used as a relative age, thus rejecting the need for environmental dose rate measurements. The relative ages were realistic and consideration for the limited dataset encouraged the use of the technique in a situation involving more vessels (Hood *et al.*, 2019). The limitation to the technique is in the smaller data size for any vessel. Owing to the small amount of sample, internal variations within a vessel will heavily skew the results.

The samples are prepared similarly to the normal samples, with consideration of the reduced size of the grains and quantity of the samples. The smaller grain size and quantity of sample is owing to the drilling technique grinding the grains and the smaller sampling location. The heavily reduced HF (to etch the sample and remove feldspar contribution) and HCl (to remove carbonates) wash time and cycles result in the sample size not being as reduced, although this results in contamination from possible feldspar material (Hood and Schwenninger, 2015). Thus, in the testing of the material, this was taken into consideration (Hood and Schwenninger, 2015).

## 2.6 Summary

Ceramics are the most common material culture for EFC of southern Africa. Through reviewing the ceramic functionality and stylisation, one can see the significance of this cultural material for understanding past societies. The Urewe and Kalundu traditions form the foundation of the South African agropastoralists in the first millennium. By placing the Lydenburg Heads Site (LHS) within context of the Mpumalanga sequence, the ceramic assemblages are shown to be intermingled and blurred. The direct dating of the ceramics from the LHS will provide a chronology from which the ceramic sequence may be better understood.

# CHAPTER 3 - METHODOLOGY

## 3.1 Introduction

The ages of archaeological material are fundamental to establishing context and occupation, movement, and societal timescales. Relative dating, such as ceramic style, can provide useful information when sufficient contextual information is available. The use of absolute dating techniques, however, is essential to disentangling complex or blurred archaeological settings such as the Lydenburg Heads Site (LHS). I used optically stimulated luminescence (OSL) to establish the ages of ceramics, excavated from the LHS. Here, I describe the processes followed, beginning with the sample collection and preparation and then the testing. The OSL technique methods follow an equivalent dose sample preparation, dose recovery tests, equivalent dose tests, dosimetry, and age calculations. The quartz grains were extracted using the traditional methods (see Aitken, 1985) and the minimal extraction technique (MET) (Hood and Schwenninger, 2015). It is important to note that the information on the bags and boxes was taken as correct, as I had no means of checking accuracy. Prior to sampling, a permit was obtained from the South African Heritage Resource Agency (SARHA) to alter the ceramics from the LHS (permitID: 4105).

## 3.2 Excavation of ceramic samples

The ceramics used in Becher's (2021) research had assumed ages based on radiocarbon ages and ceramic style. While radiocarbon dating and typology seriation are useful techniques, the direct dating of the ceramics remained unknown. Consequently, the pots she sampled will be used in this research and dated using OSL dating. The sherds, as stated in previous chapters, were excavated between 1976 and 1978 (Evers, 1982a). They were received in three cardboard boxes (Figure 3.1 A). Each box contained multiple bags of samples from similar localities (Figure 3.1 B). I noted the sample name, box, bag, code, and tradition for each sherd and

photographed each sherd. The photographs included an overview photograph (the sherd, bag, and sample card from previous research - Figure 3.1 C) and close-up photographs of the front and back. The previous sample names were used to allow me to link my data to previous work and to determine the origin pit.




Figure 3.1. Example of information provided for database creation for the samples. A: One of the three boxes received; B: a bag which was located within the boxes with multiple individually bagged sherds. C: an example of how each sample was received, including a smaller bag with details written about the sherd and a yellow card produced by Becher (2021) with details about the sherd.

The samples selected for this project included both Kalundu and Urewe tradition ceramics as identified by Becher (2021) in consultation with Gavin Whitelaw (also see Whitelaw, 1996) as well as the size and shape of the pottery. All the sherds had sections removed for Organic Residue Analysis (ORA) (Becher, 2021; Becher *et*

*al.*, 2024). I photographed the sherds after the removal of OSL samples, and these photographs are included in Appendix C (these photographs will be submitted to SAHRA as part of the permit report).

Considering the samples were excavated and had testing performed on them before this research, the sample collection involves the details and state in which the samples were provided to the researcher. Table 3.1 shows the details and photographs of the Kalundu ceramics and Table 3.2 for the details and photographs of the Urewe ceramics used within the research. The photographs have altered contrast to allow greater viewing capacity of the details, although the written descriptions are shown in the pit and code columns as well. Other details of importance are how the sherds were received, 'Box' and 'Bag,' which allows the cross checking of details as bags contained sherds of similar locality and boxes were split by ceramic tradition. The samples include seven Urewe tradition ceramics from pits 9, 10, and 12 and five Kalundu tradition ceramics from pits 3, 5, and 7.

Table 3.1. List of Kalundu pottery sherds from the Lydenburg Heads Site including box and bag number, original pit and grid code, and photographs of the outside (left) and inside (right).

| Sample | Box | Bag | Pit | Code |
|---|---|---|---|---|
| LHS10 | 3 | 6 | 5 | LIX / k2 / pit 5 |
|   | | | | |
| Sample | Box | Bag | Pit | Code |
| LHS23 | 1 | 9 | 3 | LIX / n15 |




| LHS24 | 3 | 6 | 5 | LIX / k2 / pit 5 |
|---|---|---|---|---|




| LHS29 | 3 | 5 | 7 | MVII / o12 / ii |
|---|---|---|---|---|

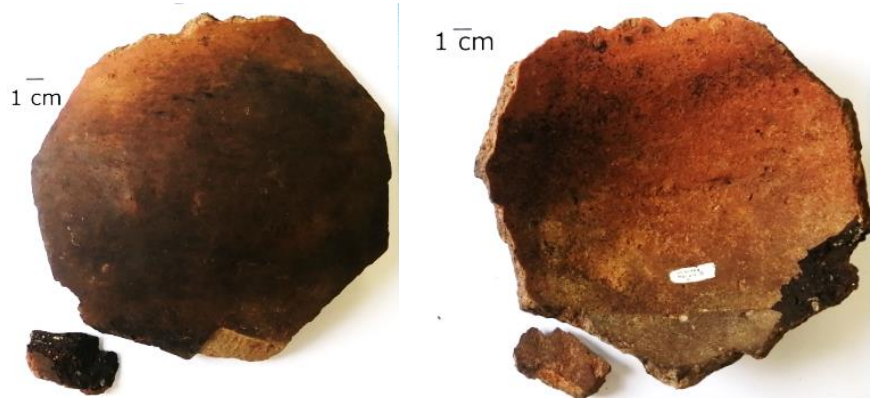


| Sample | Box | Bag | Pit | Code |
|---|---|---|---|---|
| LHS40 | 3 | 6 | 5 | LIX / k2 / pit 5 |




Table 3.2. List of Urewe pottery sherds from the Lydenburg Heads Site including details of how they were received (box and bag), original locations (pit, spit, and code), and photographs of the outside (left) and inside (right).

| Sample | Box | Bag | Pit | Code |
|---|---|---|---|---|
| LHS02 | 1 | 8 | 10 | JVII / m3 |




| Sample | Box | Bag | Pit | Code |
|---|---|---|---|---|
| LHS07 | 2 | 1 | 9 | MVII / f2 / g2 |




| | | | | |
|---|---|---|---|---|
| LHS11 | 2 | 2 | 12 | LIX / f12 / g12 / f13 / g13 |




| | | | | |
|---|---|---|---|---|
| LHS12 | 2 | 2 | 12 | LIX / f12 / g12 / f13 / g13 |




| Sample | Box | Bag | Pit | Code |
|---|---|---|---|---|
| LHS18 | 2 | 1 | 9 | MVII / f2 / g2 |




| | | | | |
|---|---|---|---|---|
| LHS25 | 1 | 8 | 10 | JVII / m3 |

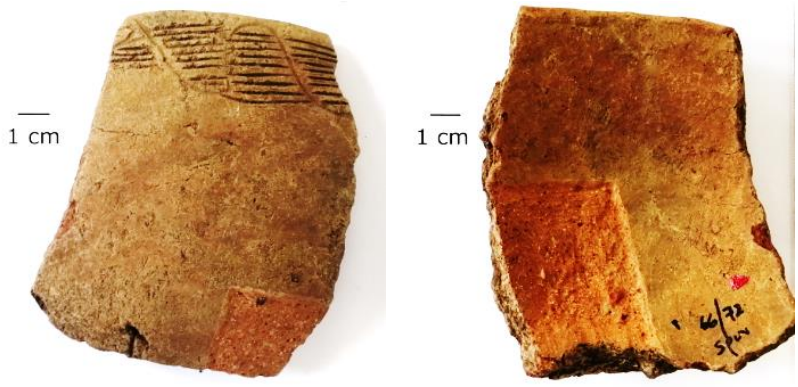


| | | | | |
|---|---|---|---|---|
| LHS35 | 1 | 8 | 10 | JVII / m3 / 30-35 |



## 3.3 Sample extraction

Separate samples were collected for the dose rate ($D_{R)}$ and equivalent dose ($D_e$) measurements. The sampling began with determining which quartz extraction method would be used on each sample (see Table 3.3). Sample size, shape, and tradition determined whether they would be considered a bulk sample[2], MET sample or both. For the Kalundu ceramics there were a total of five pot sherds, with a sampling of seven MET samples and four bulk samples. The Urewe ceramics contained a total of seven pot sherds, with a sampling of five MET samples and five bulk samples. In Table 3.3 the sample name and the testing performed can be reviewed. The result was that an almost even distribution of MET and bulk sampling occurred on the Urewe and Kalundu ceramics. All work was performed in the Luminescence Laboratory at the University of Witwatersrand, unless otherwise stated.

Table 3.3. Sample list including the ceramic tradition and the method of quartz extraction: bulk sampling ($D_e$ bulk) or MET ($D_e$ MET).

| CODE | Pit | Tradition | $D_e$ MET | $D_e$ Bulk |
|---|---|---|---|---|
| **LHS10** | 5 | Kalundu | Y | Y |
| **LHS23** | 3 | Kalundu | N | Y |
| **LHS24** | 5 | Kalundu | Y | Y |
| **LHS29** | 7 | Kalundu | Y | Y |
| **sLHS40a** | 5 | Kalundu | Y | N |
| **LHS40b** | 5 | Kalundu | Y | N |
| **LHS40c** | 5 | Kalundu | Y | N |
| **LHS40d** | 5 | Kalundu | Y | N |
| | Kalundu | 5 | 7 | 4 |

[2] The term "bulk sample" was used as a description of the samples prepared using a modified version of the standard quartz extraction technique described by Aitken (1985). The use of the term "bulk" is not owing to the large quantity of sample taken but instead the larger sample size compared to the MET samples. All reference to bulk samples hereafter is exclusively defined in this manner and are not to be confused with bulk radiocarbon.

| CODE | Pit | Tradition | $D_e$ MET | $D_e$ Bulk |
|---|---|---|---|---|
| **LHS02** | 10 | Urewe | Y | Y |
| **LHS07** | 9 | Urewe | Y | Y |
| **LHS11** | 12 | Urewe | N | Y |
| **LHS12** | 12 | Urewe | N | Y |
| **LHS18** | 9 | Urewe | Y | N |
| **LHS25** | 10 | Urewe | Y | N |
| **LHS35** | 10 | Urewe | Y | Y |
| | Urewe | 7 | 5 | 5 |
| | Total | 12 | 12 | 9 |

### 3.3.1 Quartz extraction using minimal extraction technique

In the case of museum material that cannot experience the destructive techniques of OSL sample preparation, the minimal extraction technique (MET) was created to tackle this need (Hood *et al.*, 2019; Hood and Schwenninger, 2015). To test the applicability of this technique, quartz were extracted from the LHS ceramics using MET. The samples were prepared under safe-light conditions with only red-light present. The selected samples for the MET all began with basic observations based on sizing, thickness, and likely orientation (location of rim and base) of the pottery. Drilling site selection allowed consideration for uneven heating of the pot, thickness of sherd, fragility, and lack of contamination from previous research. All locations where the drilling would cause breakage, were immediately rejected.

Furthermore, the sites closer to a possible base of the ceramic, thicker sites and sites that were accessible for drilling were considered. In cases where one condition was not met, the site best fitting the most criteria were selected. All sherds were drilled from a broken edge of the vessel to allow depth of drilling (see Figure 3.2).

The sherd was placed in a handheld grip with Styrofoam cushioning the sherd on both sides, protecting it and allowing stability during drilling. The drilling involved

the use of a 2 mm ball burr diamond drill bit and a 1.5 mm cylinder burr diamond drill bit. The original MET method called for a 1.5 mm core diamond drill bit (Hood and Schwenninger, 2015), but owing to the inability to locate one of that size and type, a cylinder drill bit was used as a substitute. Both drill bits are diamond-coated to avoid contamination.

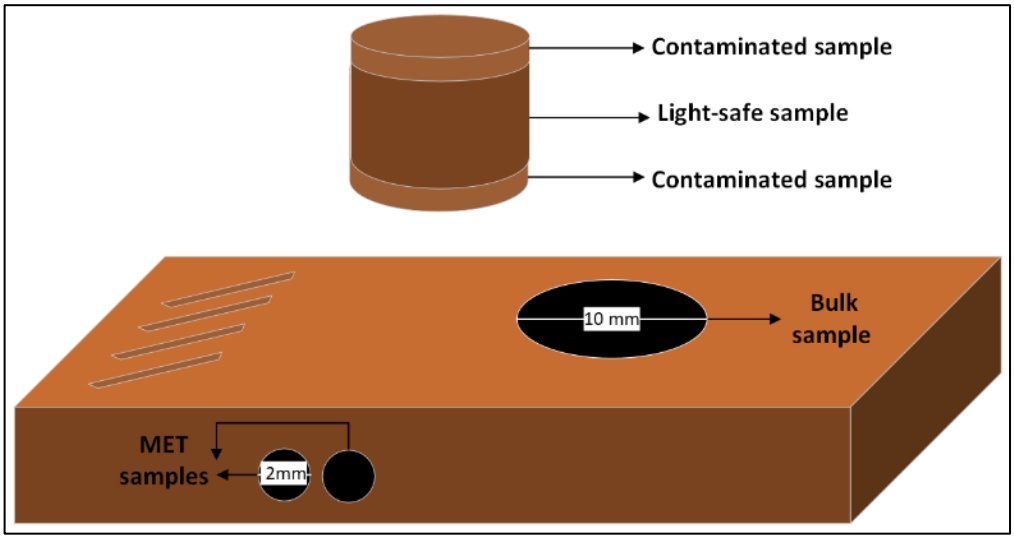


Figure 3.2. Image showing the technique of bulk and MET sample extraction. The MET sampling is shown to enter from the broken side of the ceramic. The diameter of the drill location is 2mm, with the two drilling locations closely spaced together. The bulk sampling technique is shown to punch out a cylinder using an 8/10mm tile diamond core drill bit.

The drilling was done with a handheld Dremel. The 2 mm ball drill bit was used on each sample to mark the location of the drilling site, and drill ~ 2 mm into the sherd. The method of determining the depth to stop was by reviewing the ball drill bit's protrusion out of the sherd. The lack of an accurate method of measuring the depth means that samples will differ slightly. The original sample removed from this process is not suitable for $D_e$ measurements as there was a likelihood of light contamination. The hole was then dusted clean of all material and the extracted fraction was bagged.

The subsequent drilling was done with the 1.5 mm cylinder burr drill bit. The drill bit was inserted into the hole and slowly moved to drill deeper. Owing to the smaller diameter of the drill bit than the hole, one needs to be careful not to contaminate the collected sample by touching the edges of the first 2 mm of the hole. The depth of drilling was determined by the fragility of the ceramics and the hardness of the material and typically ranged from 4 – 4.5 mm. The extracted material was collected and weighed to be used in the $D_e$ measurements. Owing to the small amount of material collected, each ceramic had two drilled locations to increase the sample yield. The two drill locations were placed within 5 mm of each other and considered a single sample. Owing to the variations in drilling location and the possibility of differential heating, the ages of sample were hypothesised to differ based on drilling location. As a result, sample LHS40 was used as a comparative sampling method, with four samples taken from the pot at different locations (Figure 3.3). In this sample, the drilled holes were covered to avoid contamination from other drill locations.

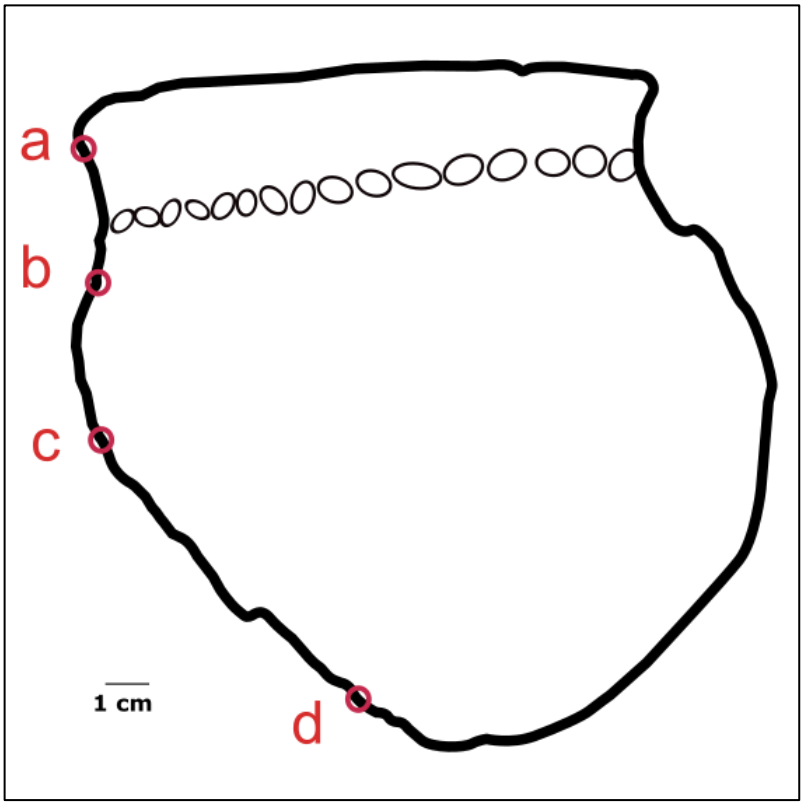


Figure 3.3. Location of drill points in LHS40.

### 3.3.2 Quartz extraction for bulk samples

The bulk samples were extracted using a Ryobi bench drill press. The drill press allows the uniform and controlled drilling action that is impossible from handheld drills. The sherds were secured onto the base of the drill using different-sized vices. Owing to the fragility and lack of straight edges on the sherds, foam was used to help support and prevent the vice from damaging the sherds. Considering the diverse shaping of the sherds, many adjustments were needed between samples to provide correct support and location of drilling.

The drill bits used were 10 mm diamond core tile drill bits. Diamond drill bits were used to avoid contamination and provide easier drilling. The drilling was done slowly to avoid breaking of the sherds. Water was sprayed on the drill site to prevent the heating of the sherd, with a tray being placed under the drill to collect the water. The drill speed was set to 580 RPM, which was the slowest speed possible for the drill press. The speed was chosen to reduce the possibility of heating of the sample. Between samples the drill was cleaned by wiping down the base and chuck. The drill bits were submerged in acetone and brushed with a metal wire brush to remove sample from the drill. The drill bits were used in rotation to allow the complete evaporation of the acetone from the drill bit before drilling.

The samples were then cleaned of contaminated surfaces using small burr diamond drill bits and a handheld Dremel. The need to clean only the top and bottom is owing to the use of the core drills in the interior of the sherds (Figure 3.2). The samples were held in place with a small handheld clamp and foam. After cleaning had occurred, each sample was weighed.

## 3.4 Sample preparation

The bulk samples were prepared following standard quartz extraction protocols as described by Aitken (1998), (also see Mahan *et al.*, 2022; Murray and Wintle, 2000;

Porat *et al.*, 2015). The sample preparation involved the collected material undergoing processes to remove the carbonates, organic materials, feldspar, and the alpha contribution. The cases in which the minimum extraction technique (MET) was used, require a different sample preparation (Hood *et al.*, 2019; Hood and Schwenninger, 2015).

### 3.4.1 **Bulk sample preparation**

Once the sample had been extracted, the bulk OSL component was crushed and then subjected to the following chemical treatments, which can be seen in the summary Figure 3.4: To remove any carbonate components, the sample was fully submerged in a 20% solution of hydrochloric acid (HCl) (Dörschner *et al.*, 2012; Sommerville *et al.*, 2007). The submerged sample was stirred and left in a fume cupboard until the reaction had completed. The samples were then washed three times with distilled water. Hydrogen peroxide ($H_2O_2$) (30%) was added until the sample was covered, stirred, and placed within the fume cupboard. The $H_2O_2$ and the sample remained in the fume cupboard until the reaction had ceased. The samples were rinsed with distilled water to remove the residue chemicals and dried in the oven at 80°C. The $H_2O_2$ removed the organic material from the samples (Dörschner *et al.*, 2012; Sommerville *et al.*, 2007).

Once dried, the sample was sieved to a size of 180 – 200 μm using a mechanical shaker and decreasing-sized sieves. The <180 μm and >200 μm portions were archived while the appropriately sized samples were processed further. The quartz grains were separated using liquid sodium polytungstate (SPT), with a density of 2.70 g/cm$^3$, which caused denser minerals to sink and the quartz to float. Quartz has a density of 2.65 g/cm$^3$. The samples were placed in test tubes with the SPT and spun in a centrifuge for 5 minutes. The sample was separated into heavy minerals and the quartz fraction. The separated samples were rinsed with distilled water to remove the residue chemicals. The quartz and heavy mineral fractions were dried in the oven at 80°C, with the quartz fraction processed further and the heavy mineral fraction archived.

To remove feldspar and the alpha contribution, the sample was fully submerged in 40% Hydrofluoric Acid (HF) for 40 minutes. This was done in a Teflon beaker, as the HF etches away at glass beakers. The process does not completely remove all feldspar, although that is considered during the measurements of the samples. The samples were then rinsed with distilled water and dried in the oven, as described previously. The dried samples were sieved again to the appropriate size of 180 – 200 μm using a mechanical shaker and decreasing sized sieves. The need for a second sieve is because HF causes the reduction of grain size through etching. The samples were appropriately stored, labelled, and transferred to the OSL measurement section of the Luminescence laboratory at the University of Witwatersrand.

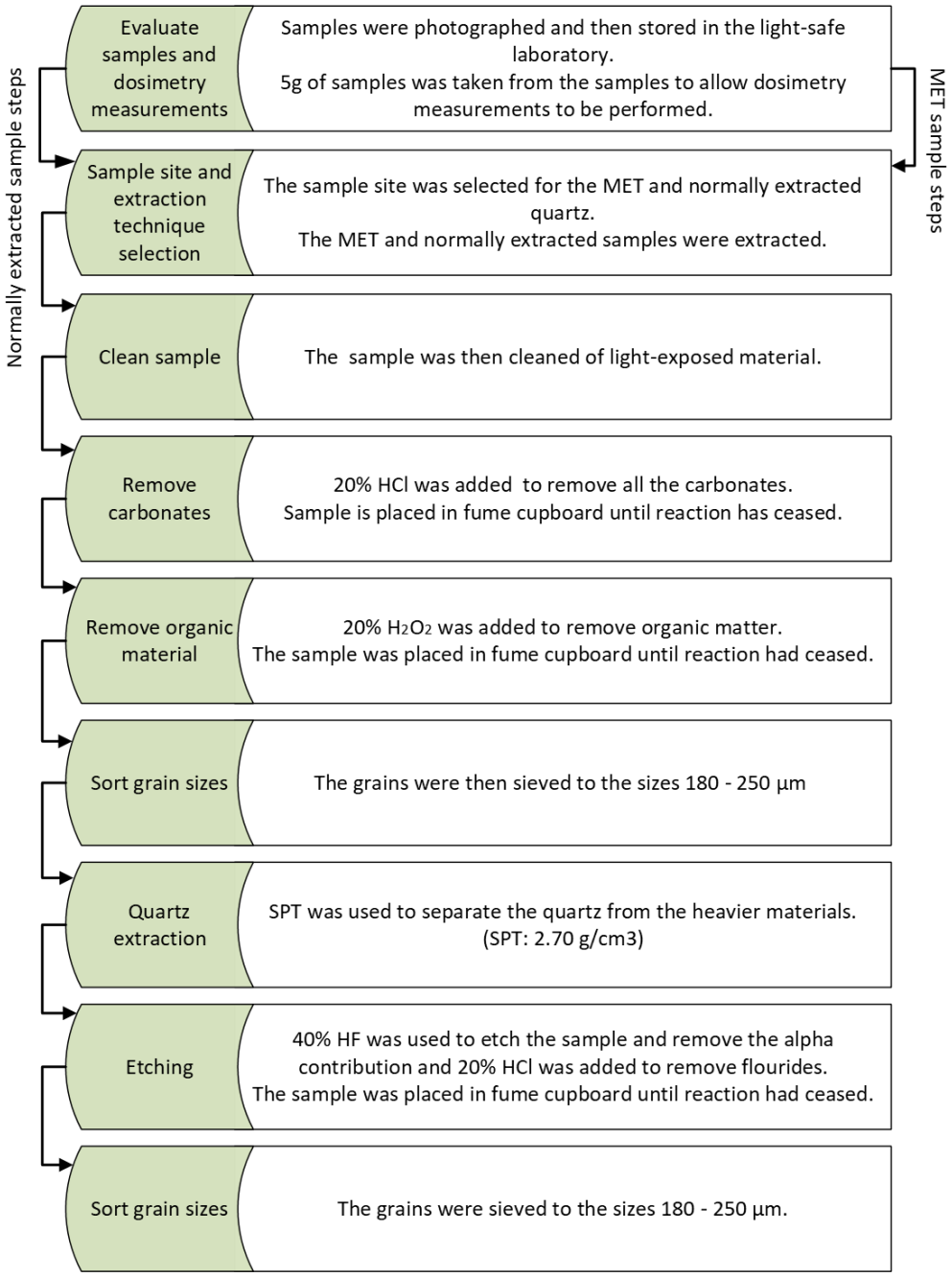


Figure 3.4. Workflow diagram showing the process of $D_e$ sample preparation of the ceramics.

## 3.4.2 **Minimal extraction technique sample preparation**

Although originally intended to do much shorter HF and HCl washes as ascribed by Hood and Schwenninger (2015), the fine grains of the MET sample made

pouring off the chemicals impractical. Techniques were tested with unrelated fine grains, where upon attempting to pour off the chemical and rinse with distilled water, the sample floated to the top and the majority was lost in the process. The result is that the MET samples experienced no further treatment.

### 3.4.3 $D_R$ sample preparation

The concentrations of uranium and thorium were measured using inductively coupled plasma mass spectrometry (ICP-MS) (Mahan *et al.*, 2022). The potassium was measured using X-Ray Fluorescence (XRF) (Pienaar *et al.*, 2008). All sherds had the same $D_R$ sample preparation for ICP-MS and XRF irrespective of the method used for quartz extraction.

The sample site for this aspect of the testing was selected based on the already damaged regions from the ORA analysis. The result was that the sherds were further damaged in already altered regions. The method involved chiselling away the sample to obtain ~5 g of the sample. This was done with a metal chisel and a small hammer. The process requires small increments of sampling, or the sherds shatter or crack. The material is crushed, bagged, and removed from the laboratory as the $D_R$ measurements do not require a light-safe environment. The samples were milled to homogenise and reduce the grain sizes. This was done in a disc mill where grinding barrels were cleaned with methanol to protect against contamination. The samples were bagged, labelled, and sent to EARTHLAB Geochemistry laboratory at the University of Witwatersrand for ICP-MS and XRF determination.

## 3.5 Instrumentation

The luminescence measurements occurred on Risø TL-DA-20 and Risø TL-DA-15 readers (Bøtter-Jensen *et al.*, 2010) in the OSL laboratory at the University of the Witwatersrand. These machines were used to measure OSL data. Each machine contains a carousel that has space for 48 discs. This means that each reader can

contain 48 samples at any given time. The readers were fitted with the Hoya U-340 UV detection filter and an EMI 9235QA photomultiplier tube. Stimulation light sources for both readers were blue LEDs with wavelengths of 470 nm and an output power of 40 mW/cm$^2$ and IR LEDs with wavelengths of 875 nm and an output power of 135 mW/cm$^2$. The blue LED was equipped with a GG-420 green long pass filter.

The readers both had a $^{90}Sr/^{90}Y$ beta source. The calibration for Reader A was 0.158 Gy/s and Reader B was 0.135 Gy/s. The readers were controlled through the Sequence Editor, which was connected to the reader via a computer. The readers then followed the instructions given to perform tasks. The results were saved on the attached computer as a .BIN file and were interpreted through the Analyst software (Duller, 2015).

The aliquots were reviewed individually and were accepted based on the following criteria: a recycling ratio of less than 15%, the max test dose error was less than 15%, recuperation less than 5% and the test dose (Tn) was more than 3σ above the background (see Murray and Wintle, 2000; Hood *et al.*, 2019; Roos *et al.*, 2020). The standard protocols for the acceptance criteria are of 10 % for the recycling ratio and max test dose error (see Duller, 2003), although this was increased owing to the difficulty of measuring the samples with a limited acceptance rate.

## 3.6 Dose recovery and preheat test

The first step was to determine the suitability of the single-aliquot regenerative dose (SAR) protocol (Murray and Wintle, 2000; Carr *et al.*, 2007; Reimann *et al.*, 2011; Dörschner *et al.*, 2012). The SAR protocol is a means in which to determine the equivalent dose ($D_e$). To determine the suitability of the SAR protocol the dose recovery tests are performed, allowing the observation of the closest 1:1 ratio of given and measured doses at different temperatures. The dose recovery measurements involved mounting the samples onto 9 mm stainless steel discs using

a silicone-based spray, producing 0.2 cm single aliquots. Each run involved the twelve discs for each sample and three discs per temperature per sample. The temperatures between 200 ºC and 280 ºC in 20 ºC increments were used for the samples. In the case that a sample had insufficient material to measure both the dose recovery and the equivalent dose, the dose recovery step was skipped.

The dose recovery begins by removing the natural signal. The samples are then given a series of known doses, with a measured dose between each known dose (see Table 3.4). The ratio of the measured dose to the given dose should be consistent with unity if the SAR protocol is appropriate.

Table 3.4 Dose recovery protocol for the OSL samples, including the steps to produce the dose response curve.

| Step | Treatment |
|---|---|
| 1 | OSL stimulation at 205 °C for 40 s at 90 % power (remove signal) |
| 2 | OSL stimulation at 205 °C for 40 s at 90 % power (remove signal) |
| 3 | Beta radiation for 50s |
| 4 | Pre heat samples to test temperatures ** for 10s |
| 5 | OSL stimulation at 175°C IR Diodes for 40s at 90 % power |
| 6 | OSL stimulation at 125 °C for 40 s at 90 % power (Lx) |
| 7 | Test dose Beta radiation 35 s |
| 8 | Cut heat 180 °C |
| 9 | OSL stimulation at 175°C IR Diodes for 40 s at 90 % power |
| 10 | OSL stimulation at 125 °C for 40 s at 90 % power (Tx) |
| 11 | OSL stimulation at 205 °C for 40 s at 90 % power |
| Repeat steps 3-11 for beta doses of 0, 25, 100, 0, 25 s<br>** 200, 220, 240, 260 or 280 °C | |

The dose recovery tests were only performed on a few samples owing to the minimal sample available. The bulk samples LHS02, LHS10, LHS23, LHS29, and

LHS35 contained sufficient material for dose recovery tests. The test results were used as representative of the whole set. Samples can be bleached using the reader (see steps 1 and 2 in Table 3.4) or through exposure to sunlight. In the event that a sample or samples are not providing adequate dose recoveries, this can be seen with too many rejected discs or measured doses being largely different from the given dose, the samples are fully bleached by exposing them to direct sunlight for a minimum of 30 minutes. After which the dose recovery is repeated as ascribed by Table 3.4. Finally, each sample's results were stored on the computer and processed outside the laboratory using Excel. The dose recovery tests determined the suitability of the SAR protocol and the preheat-dose recovery tests allowed the ideal temperature to be determined by identifying a preheat plateau.

## 3.7 Equivalent dose ($D_e$) measurements

The equivalent dose (De) was measured using a SAR protocol optimised for the samples in this study (see Table 3.5) based on the results of the preheat-dose recovery test. The $D_e$ measurements were made on 48, 24 or 12 discs per sample, the number of discs was based on the amount of sample available. For each sample, grains were mounted onto 9 mm stainless steel discs using a silicone-based spray, producing 0.1 cm single aliquots.

Table 3.5. SARs protocol for the OSL samples, including the steps followed for individual samples.

| Step | Treatment |
|---|---|
| 1 | Regeneration dose Beta radiation at ** |

| | |
|---|---|
| 2 | Preheat the sample for 5s at the determined temperature * |
| 3 | OSL stimulation at 175°C IR Diodes for 40s at 90 % power |
| 4 | OSL stimulation at 125 °C for 40 s at 90 % power (Lx) |
| 5 | Test dose Beta radiation 35 s |
| 6 | Cut heat 180 °C |
| 7 | OSL stimulation at 175°C IR Diodes for 40 s at 90 % power |
| 8 | OSL stimulation at 125 °C for 40 s at 90 % power (Tx) |
| 9 | OSL stimulation at 205 °C for 40 s at 90 % power |
| * 220, 240 or 260 °C | |
| ** Dose Response Curve: Repeat steps 1-9 for beta doses of 0, 25, 0, 50, 100, 0, 25 s | |

## 3.8 Dosimetry measurement ($D_R$)

The environmental dose rate ($D_R$) incorporates cosmic radiation, the alpha, beta, and gamma radiation produced by both external radionuclides and internal radionuclides (Prescott and Hutton, 1994). The measurement for $D_R$ was determined with Equation 2, the summation of the alpha (Dα), beta (Dβ), gamma (Dγ), and cosmic (Dc) dose rates. The internal radionuclides are considered negligible in quartz grains (Prescott and Hutton, 1994; Rhodes, 2011; Evans, 2016). As the bulk samples were etched, the alpha dose rate was also considered negligible (see Aitken, 1985).

The calculations of the Dγ and Dβ take into consideration radioactive concentration of U, Th, and K (Zink, 2013; Wang *et al.*, 2022). The uranium and thorium were measured using inductively coupled plasma mass spectrometry (ICP-MS). The potassium was measured using X-Ray Fluorescence (XRF). The tests were done by an outside laboratory, EARTHLAB Geochemistry laboratory at the University of Witwatersrand, and received in tabulated format. The conversion factors used for this dissertation are that of Cresswell *et al.* (2018) for Th, U, and K (Table 3.6).

Table 3.6. Conversion rates for thorium, uranium, and potassium (Cresswell *et al.*, 2018)

| Element | Beta | Gamma | Error |
|---|---|---|---|
| Thorium | 0.028 × Th (ppm) | 0.0489 × Th (ppm) | $Th(\frac{Gy}{ka}) \times \frac{Th_{err}(ppm)}{Th(ppm)}$ |
| Uranium | 0.142 × U (ppm) | 0.112 × U (ppm) | $U(\frac{Gy}{ka}) \times \frac{U_{err}(ppm)}{U(ppm)}$ |
| Potassium | 0.854 × K (ppm) | 0.248 × K (ppm) | $K(\frac{Gy}{ka}) \times \frac{K_{err}(ppm)}{K(ppm)}$ |

The Dβ was then corrected for beta attenuation, which was proportional to grain size (Mejdahl, 1979). The grains were between 180 – 250 µm; thus, the conversion factor was 0.887 ± 0.007 (Mejdahl, 1979). The Dγ and Dβ were corrected for water content using Equation 4 and Equation 5.

The water content is always considered tricky in the context of OSL dating. More so in situations where artefacts were excavated without dosimetry samples being collected from the environment. The region of Mpumalanga has had climate reconstruction and thus the estimates of the water content will be considered based on those observations. Each sample was tested with consideration for a variation of 1 – 5 % of water content. The results were analysed within the range of possible dates and the likelihood of water content variations.

The Dγ and Dβ were corrected for water content using Equation 4 and Equation 5.

The Dc and Dβ are affected by depth of the sample, therefore depth estimations were determined through available environmental factors. The depth of the samples, where possible, was used from the found depth on samples (see Figure 2.5 and Figure 3.1). In the case of the majority of samples the depth was only determinable from the maximum depth of the pits. This meant that the depth was considered in light of multiple variables to determine the variability and likely true age. An example is LHS02, the pit's maximum depth is 82 cm. The depths

considered as possible were on surface level (0 cm), at gamma penetration level (30 cm), two gamma penetration levels (60 cm) and at the maximum depth (82 cm).

The Dc was determined with the above depth and water content as well as geographic location. The site was said by Evers (1982a) to be located at -25 º 06' 20" S; 30º 29' 40" E (2530AB4) (Evers, 1982a). Although when reviewing the present-day location and the maps made by Evers (1982a), these coordinates constitute an error with the site being situated further south and east with site between 25°10' 44" S; 30° 32' 34" E and 25° 8' 40" S; 30° 36' 34" E. In extension to the geographic location, the altitude was not available to a sufficient accuracy in the excavation notes. Thus, the altitude was determined to be between 1600 and 1700 m, using the updated site location and GIS information of the region.

## 3.9 Age calculations

The age models were performed in R and excel. The CAM (Burow, 2023) and ADM (Christophe *et al.*, 2023) functions from the Luminescence R Package (see www.CRAN.R-project.org/package=Luminescence) were used to determine the $D_e$ values. The arithmetic mean $D_e$ was calculated on excel.

Finally, the ages were determined by Equation 1, which involves dividing the average $D_e$ over the $D_R$. The information is processed and interpreted on Excel, which provides the ages in 'ka' from the date the artefact was excavated from the site.

## 3.10 Permission process

In order to date the ceramics, the permission from the South African Heritage Resource Agency needed to be obtained. This involved providing detailed description of how the ceramics would be altered and justifying the destructive nature of the research. The process requires the photographs of all ceramics pre and

post sampling (see Table 3.1, Table 3.2, and Appendix C). The permit for the altering/damaging of the archaeological material was obtained.

## 3.11 Summary

The methodology follows the steps necessary to obtain the ages. The sample preparation involved the quartz extraction for the MET and bulk samples. The bulk samples experienced chemical cleaning for the isolation of the quartz grains. The dose recovery and preheat tests allowed the suitability of the SAR protocol to be established. The subsequent measurements of the equivalent dose and dose rate were described. The dose rate incorporated the unknown environmental measurements of the water content and depth. The equivalents dose were determined with the use of three age models, which allowed comparison and accuracy in the results. The final age was determined using the above measurements.

# CHAPTER 4 - RESULTS

## 4.1 Introduction

In this chapter the results from the methodology described in Chapter 3 are discussed. Firstly, a recalibration was done on the radiocarbon ages from Lydenburg Heads Site (LHS) and sites in the Mashishing region. All pertinent information that was used to produce or interpret the final determined ages for the Kalundu and Urewe ceramics from LHS will be discussed. The sample extraction is shown owing to the use of the MET and bulk techniques. The elements required to determine an age follow with the results from the dose recovery and preheat tests, equivalent dose ($D_e$) and dose rate ($D_R$). The variations to the water content and depths are considered during calculation of the ages. The final ages are shown and expressed graphically.

## 4.2 Radiocarbon ages recalibration

To compare the OSL and radiocarbon ages, I recalibrated these ages using the most recent calibration OxCal SHCal20 curve (www.c14.arch.ox.ac.uk/oxcal; Hogg *et al.*, 2020http:///). The resultant ages for the LHS are 540-684 AD (Pta-328) and 592-769 AD (Pta-1634). For purposes of this project these ages will be considered the radiocarbon ages for the site (Figure 4.1; Appendix figure A.1).

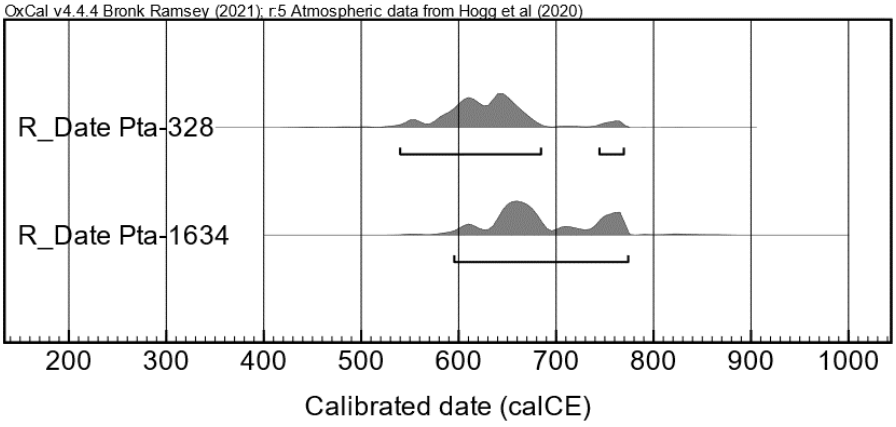


Figure 4.1. Recalibrated radiocarbon results for Pta-328 and Pta-1634.

Similarly, the ages with the sites in the Mashishing region (Figure 2.6), Doornkop and Klingbeil were recalibrated using the most recent curve, (Hogg *et al.*, 2020) for the southern hemisphere. The radiocarbon ages for Klingbeil are: 1019 – 1163 AD (Pta-1747), 876 – 1047 AD (Pta-2160) and 846 – 1022 AD (Pta-1663). The radiocarbon ages for Doornkop are: 672 – 901 AD (Pta-2944), 771 – 993 AD (Pta-2535), and 856 – 1029 AD (Pta-2536). (Figure 4.2; see Appendix A Recalibration of $^{14}C$ for further details on the Mashishing and other sites recalibrated).

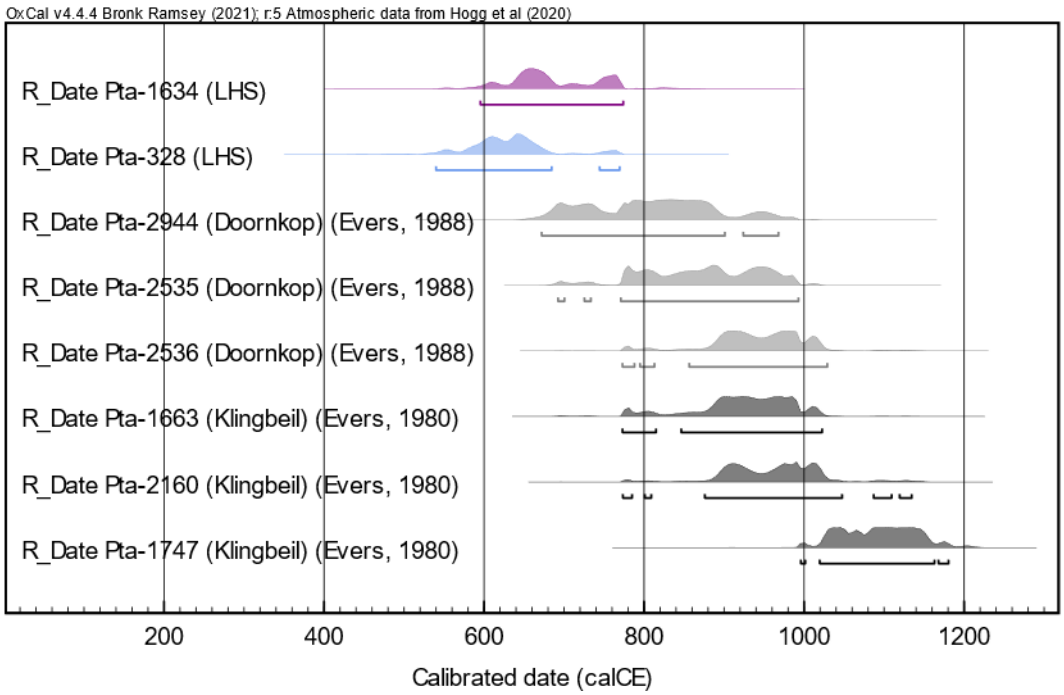


Figure 4.2. Recalibrated radiocarbon results for the sites Lydenburg Heads Site (purple - pit 1, blue – near pit 8), Doornkop (light grey) and Klingbeil (dark grey).

## 4.3 $D_e$ Sample extraction

Samples extracted using MET and bulk techniques were weighed in order to review the differences. The amount of sample holds importance to the quantity of measurements and the subsequent reliability of the ages. The weight of the extracted sample from all samples are shown in Table 4.1. The thickness of the drill location for the MET samples was measured, as the effects of contamination or anomalous heating were considered.

Table 4.1. Weight of extracted sample for MET and bulk sampling, and thickness of location of sampling for MET samples. For the samples LHS40, four samples were extracted and as a result there is no 2nd hole for those MET samples.

| Sample | MET $D_e$ weight | | | Thickness of MET site | | Bulk $D_e$ weight |
|---|---|---|---|---|---|---|
| | 1st hole (g) | 2nd hole (g) | Total (g) | 1st hole (cm) | 2nd hole (cm) | (g) |
| **LHS02** | 0.10 | 0.05 | 0.15 | 0.61 | 0.74 | 1.29 |
| **LHS07** | 0.16 | 0.15 | 0.31 | 1.08 | 0.86 | 0.30 |
| **LHS10** | 0.16 | 0.16 | 0.32 | 0.90 | 0.83 | 0.85 |
| **LHS11** | - | - | - | - | - | 0.74 |
| **LHS12** | - | - | - | - | - | 0.54 |
| **LHS18** | 0.10 | 0.13 | 0.23 | 0.94 | 0.96 | - |
| **LHS23** | - | - | - | - | - | 1.06 |
| **LHS24** | 0.15 | 0.14 | 0.29 | 1.22 | 1.22 | 0.84 |
| **LHS25** | 0.19 | 0.05 | 0.24 | 1.49 | 1.44 | - |
| **LHS29** | 0.12 | 0.14 | 0.26 | 1.27 | 1.25 | 1.08 |
| **LHS35** | 0.07 | 0.14 | 0.21 | 1.52 | 1.54 | 2.88 |
| **LHS40a** | 0.21 | - | 0.21 | 0.98 | - | - |
| **LHS40b** | 0.20 | - | 0.20 | 0.95 | - | - |
| **LHS40c** | 0.20 | - | 0.20 | 0.89 | - | - |
| **LHS40d** | 0.24 | - | 0.24 | 1.39 | - | - |

The sample LHS35 (bulk) shows a much higher weight than the other samples. This is owing to the sample being taken from a broken piece of ceramic when the sample was being handled. The relationship between the thickness of the ceramic and the weight of the extracted MET material is shown in Figure 4.3. This relationship is important because the sample site should be chosen to produce the most accurate ages. Considering the minimal sample extracted, the possibility of thicker sample sites producing more material was considered. In addition, the consequences of partial resetting of the signal through use or production of the ceramic can take into consideration the thickness of a sample.

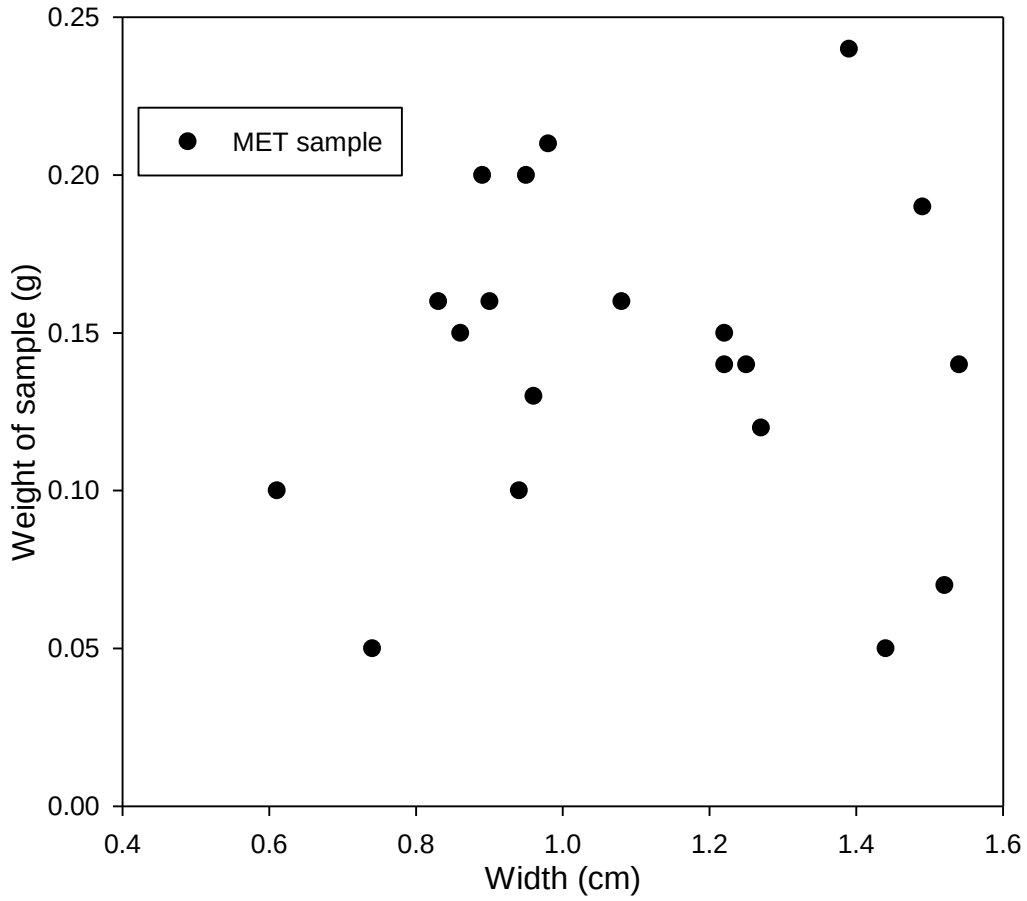


Figure 4.3. Weight of sample extracted using the MET against the thickness of the ceramics at drill site.

The amount of sample obtained through the MET is shown to not be correlated with the thickness of the drilling site. While one must still consider the thickness of the drilling site for being sufficient to obtain uncontaminated material, the sample size seems to be unpredictable.

## 4.4 Dose recovery and preheat temperature tests

The dose recovery graphs show the temperature variations versus the dose recovery. The dose recovery is the ratio of measured to given dose $\left(\frac{Lx}{Tx}\right)$ (see steps 6 and 10 in Table 3.4). The dose recovery is considered viable when within ±10 % of unity (between 0.9 and 1.1).

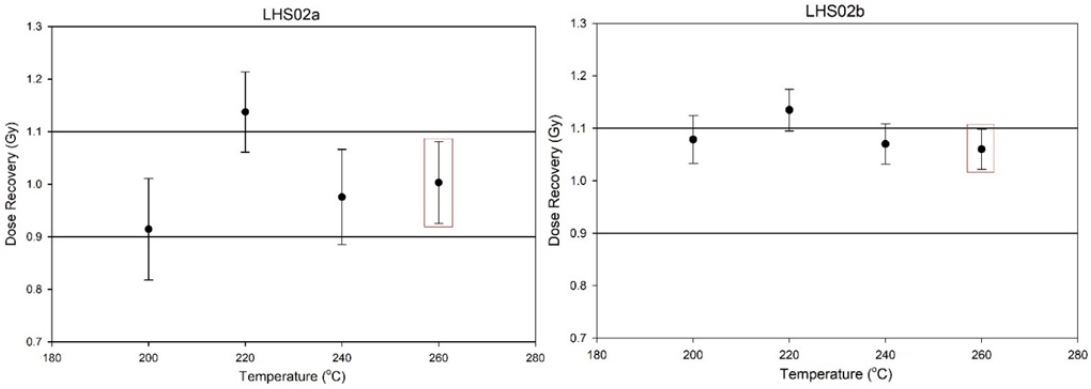
LHS02a
Dose Recovery (Gy)
Temperature (°C)


LHS02b
Dose Recovery (Gy)
Temperature (°C)

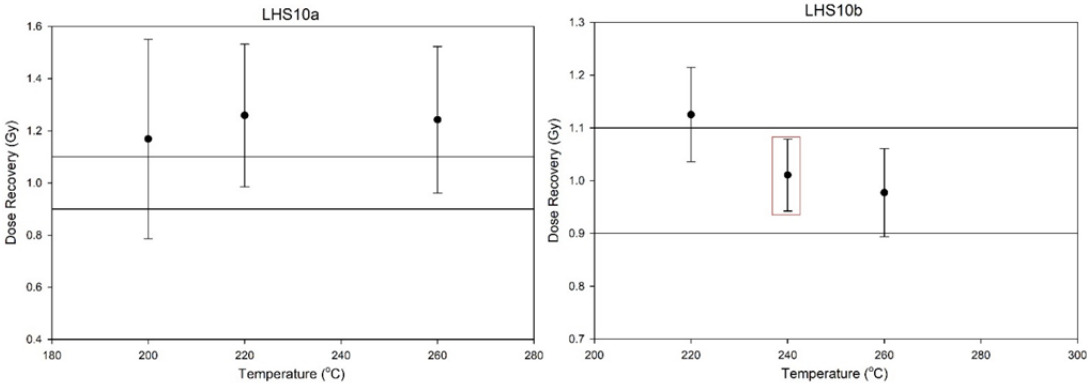
LHS10a
Dose Recovery (Gy)
Temperature (°C)


LHS10b
Dose Recovery (Gy)
Temperature (°C)

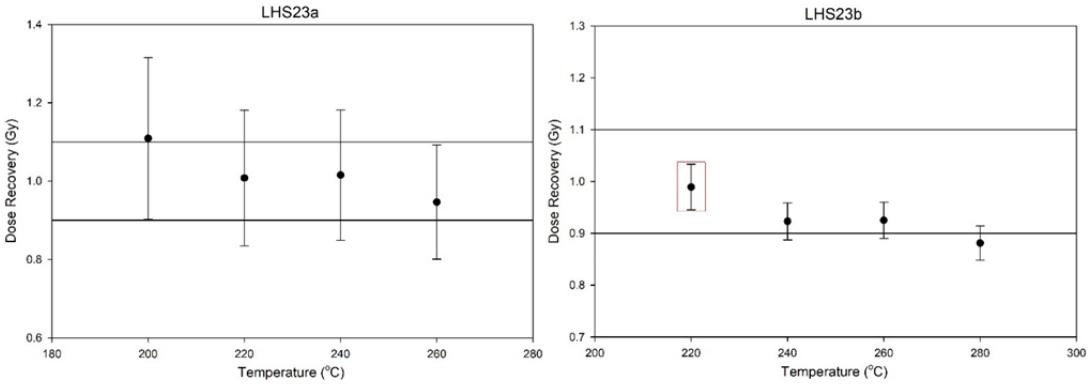
LHS23a
Dose Recovery (Gy)
Temperature (°C)


LHS23b
Dose Recovery (Gy)
Temperature (°C)

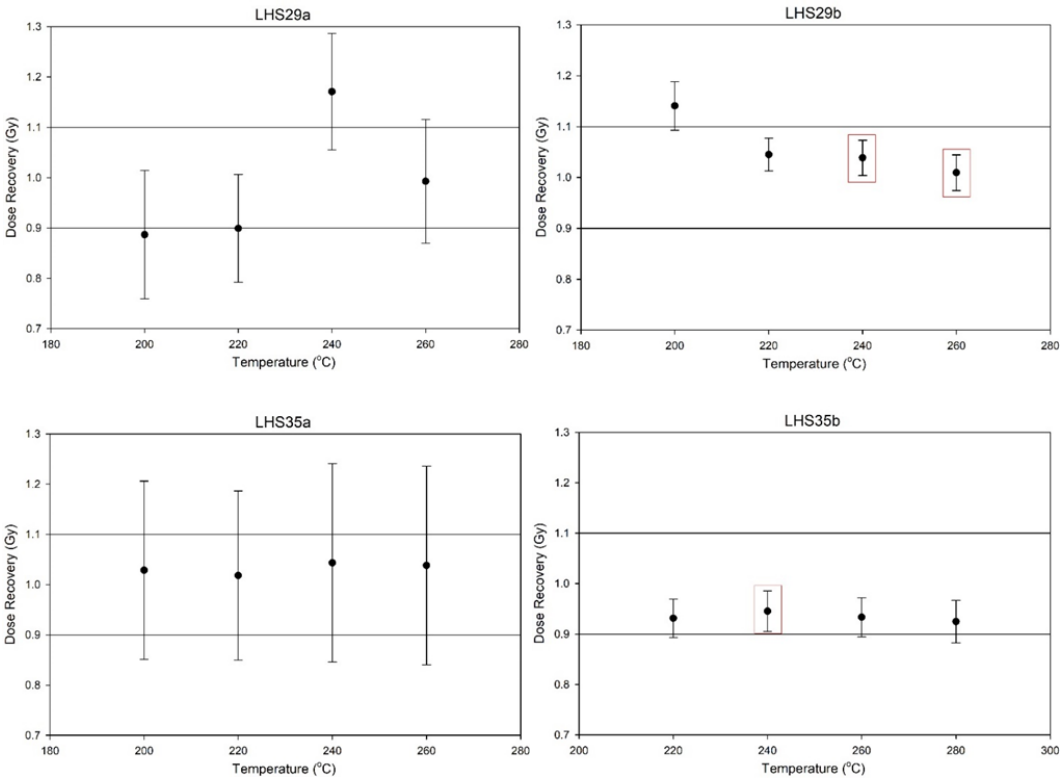


Figure 4.4 Dose recovery vs preheat temperature (a) samples were irradiated in the reader (b) samples were exposed to solar irradiation for 30 minutes. The viable temperatures are outlined in red.

The given dose was recovered within unity at 240 ºC for most of the samples. The dose recovery/preheat test results are shown, with the reader and full sun exposure bleaching (Figure 4.4). All the graphs show that after the full sunlight bleaching, the samples produced temperatures, including error within unity (0.9 - 1.1). The samples with machine bleaching show preheat temperature plateaus (LHS35a), although the large errors cause the readings to be out of the 10 % range. The samples all show a significant reduction in error in the second, solar irradiation tests. The temperatures determined for use in the $D_e$ measurements are shown in Table 4.2.

Table 4.2. Preheat temperatures at which the samples were measured. For samples LHS02 and LHS29, the tests were performed twice and at both temperatures.

| Sample | Preheat Temperatures |
|---|---|
| **LHS02** | 240 ºC / 260 ºC |
| **LHS02MET** | 240 ºC |
| **LHS07** | 240 ºC |
| **LHS07MET** | 240 ºC |
| **LHS10** | 240 ºC |
| **LHS10MET** | 240 ºC |
| **LHS11** | 240 ºC |
| **LHS12** | 240 ºC |
| **LHS18MET** | 240 ºC |
| **LHS23** | 220 ºC |
| **LHS24** | 240 ºC |
| **LHS24MET** | 240 ºC |
| **LHS25MET** | 240 ºC |
| **LHS29** | 240 ºC / 260 ºC |
| **LHS29MET** | 240 ºC |
| **LHS35** | 240 ºC |
| **LHS35MET** | 240 ºC |
| **LHS40a** | 240 ºC |
| **LHS40b** | 240 ºC |
| **LHS40c** | 240 ºC |
| **LHS40d** | 240 ºC |

The use of two temperatures for the samples LHS02 and LHS29 is due to the samples' poor performance at one of the temperatures. Thus, subsequent measurements were done at the alternate temperature. The results from both temperatures were used to produce the final results where the aliquots passed the acceptance criteria.

## 4.5 Equivalent dose ($D_e$) results

The aliquots were reviewed individually and were accepted or rejected based on the criteria previously discussed (3.5 Instrumentation). The resultant rejection rate is shown in Table 4.3.

Table 4.3. Rejection rate, including the total discs tested and rejected per sample.

| Sample | Total discs | Rejected discs | Rejection rate |
|---|---|---|---|
| **LHS02** | 48 | 15 | 31% |
| **LHS02MET** | 24 | 3 | 13% |
| **LHS07** | 36 | 7 | 19% |
| **LHS07MET** | 24 | 2 | 8% |
| **LHS10** | 48 | 6 | 13% |
| **LHS10MET** | 24 | 3 | 13% |
| **LHS11** | 48 | 12 | 25% |
| **LHS12** | 24 | 5 | 21% |
| **LHS18MET** | 24 | 1 | 4% |
| **LHS23** | 36 | 4 | 11% |
| **LHS24** | 12 | 1 | 8% |
| **LHS24MET** | 24 | 0 | 0% |
| **LHS25MET** | 24 | 0 | 0% |
| **LHS29** | 48 | 15 | 31% |
| **LHS29MET** | 24 | 0 | 0% |
| **LHS35** | 48 | 2 | 4% |
| **LHS35MET** | 24 | 0 | 0% |
| **LHS40a** | 24 | 7 | 29% |
| **LHS40b** | 24 | 2 | 8% |
| **LHS40c** | 24 | 6 | 25% |
| **LHS40d** | 24 | 2 | 8% |

The bulk sample ages were considered viable if there was a minimum of 20 discs accepted. To achieve this, a minimum of 36 discs were tested per sample. The exception was LHS24 as there was limited sample material to work with and only 12 discs were measured. The MET samples were originally intended to only have 12 samples owing to the assumed small sample size. When the sample size proved to be more than expected, 24 discs per sample were produced. The samples with the highest rejection rate were LHS02 and LHS29 at 31%, both are bulk samples where the discs were rejected for either having too high an error or no signal was recorded.

The OSL decay curves show the signal released in response to blue light stimulation (Figure 4.5 column 1 and Table 3.5 step 4). The selection of integration channels allows for differentiation of signal and background (Figure 4.5 column 1). The natural signal is interpolated onto the dose response curve allowing the $D_e$ to be determined (Table 3.5; Figure 4.5 column 2). Determining the signal and background is dependent on the amount of noise present in the grains. The background noise needs to be removed in order to isolate the OSL signal (Figure 4.5 C1 and H1). Some samples had minimal noise and well-defined OSL curves (Figure 4.5 E1 and D1). In all samples, the technique of early background was used following the work by Cunningham and Wallinga (2010).

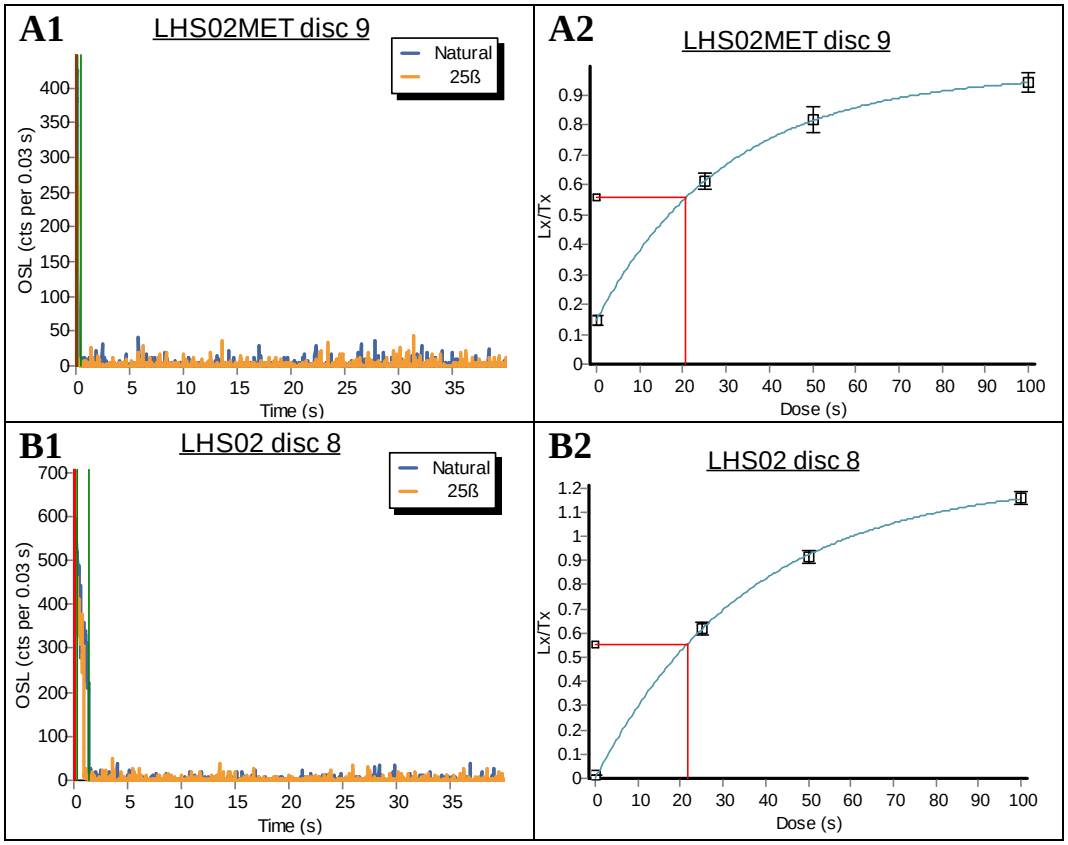

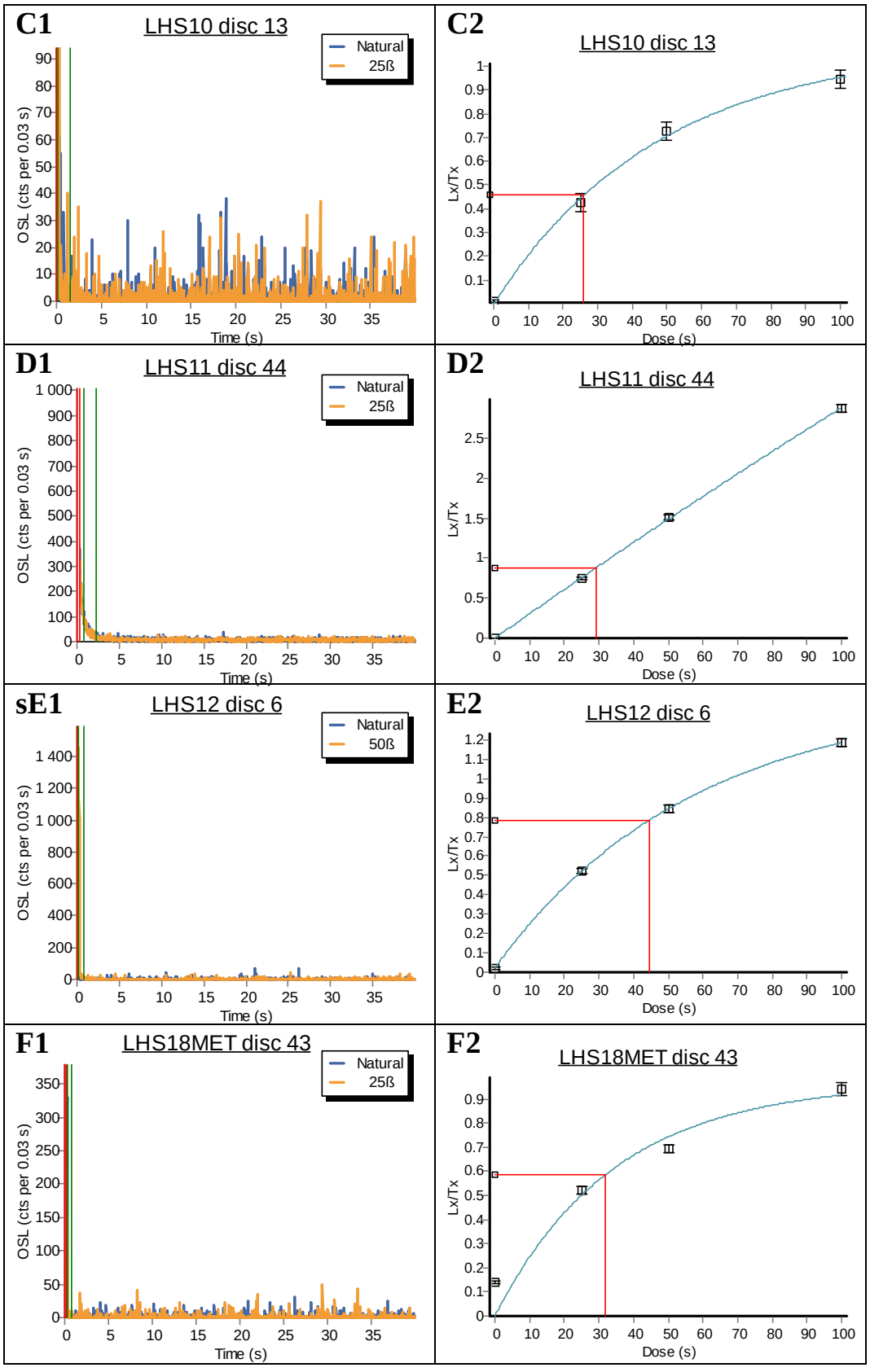
C1
LHS10 disc 13
Natural
25ß
OSL (cts per 0.03 s)
Time (s)
C2
LHS10 disc 13
Lx/Tx
Dose (s)
D1
LHS11 disc 44
Natural
25ß
OSL (cts per 0.03 s)
Time (s)
D2
LHS11 disc 44
Lx/Tx
Dose (s)
sE1
LHS12 disc 6
Natural
50ß
OSL (cts per 0.03 s)
Time (s)
E2
LHS12 disc 6
Lx/Tx
Dose (s)
F1
LHS18MET disc 43
Natural
25ß
OSL (cts per 0.03 s)
Time (s)
F2
LHS18MET disc 43
Lx/Tx
Dose (s)

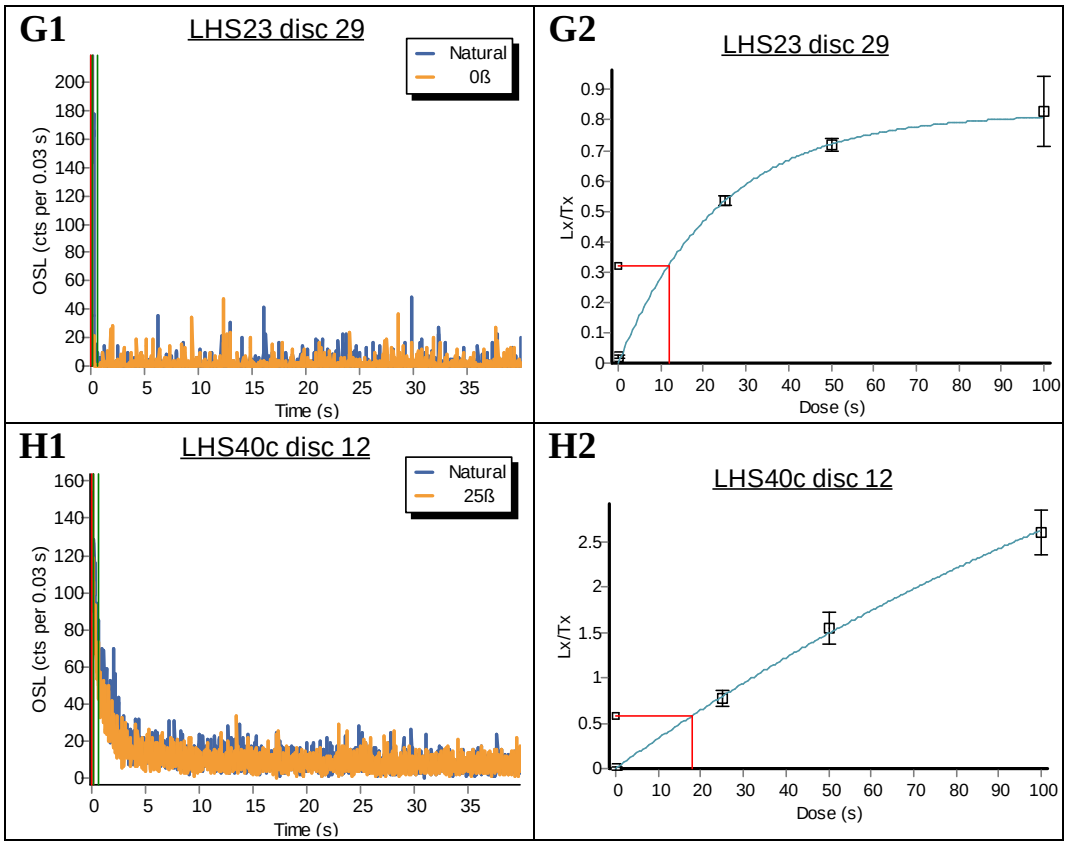


Figure 4.5. OSL curves for selected samples and discs; blue is the signal and yellow is the background (column 1). Dose response curves selected samples and discs; blue is the given and measured known doses and red is the natural OSL signal interpolated onto the dose response curve to determine the $D_e$ (column 2).

Abanico plots are a graphic display of $D_e$ distribution (Dietze *et al.*, 2016) and incorporate the use of a radial plot and kernel density estimate plot into a single plot. Although the $D_e$ is averaged through an age model, the visual display of the variation is important in understanding each sample's flaws and true nature. The plots provide a wealth of information including the relative error, scattering, and dispersion (1 and 2 σ) (see Figure 4.6 and Figure 4.7).

**LHS02**

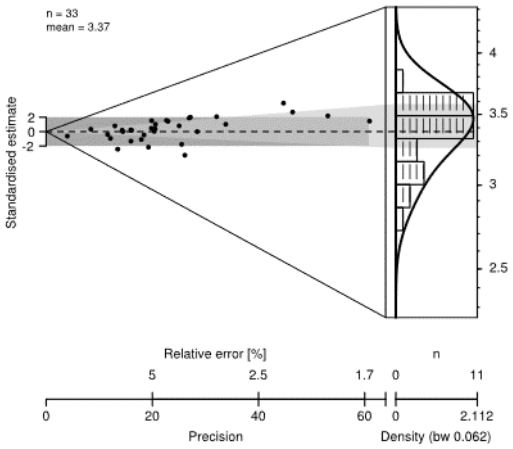


**LHS02MET**

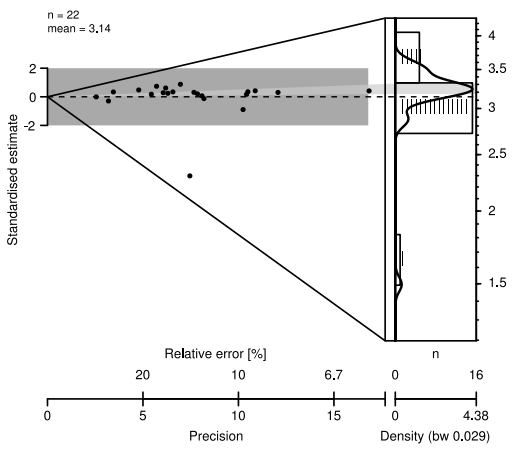


**LHS07**

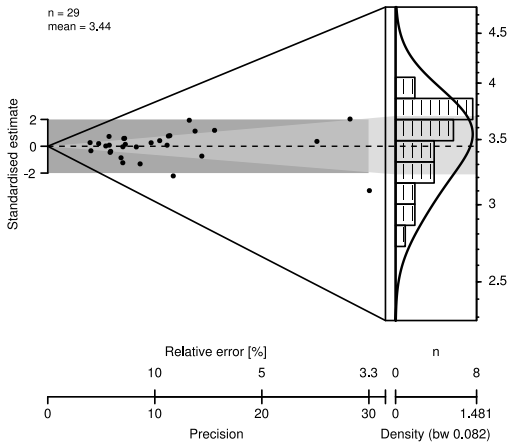


**LHS07MET**

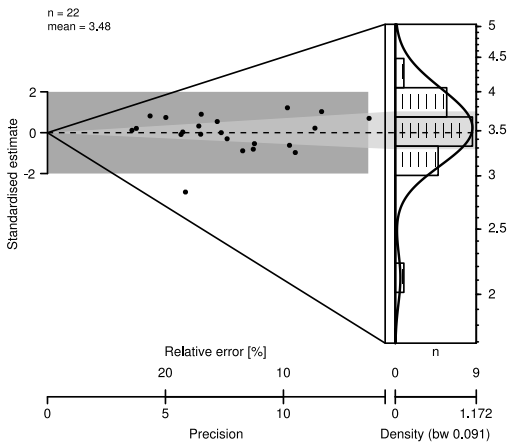


**LHS10**

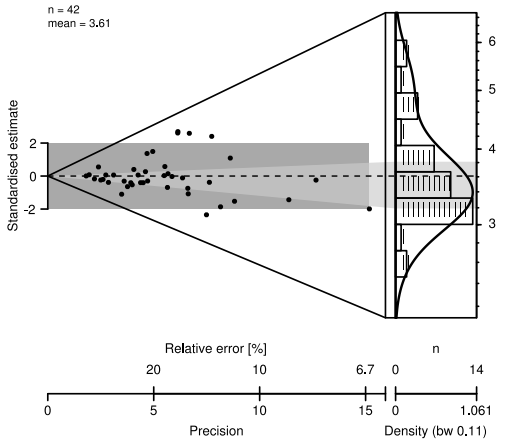


**LHS10MET**

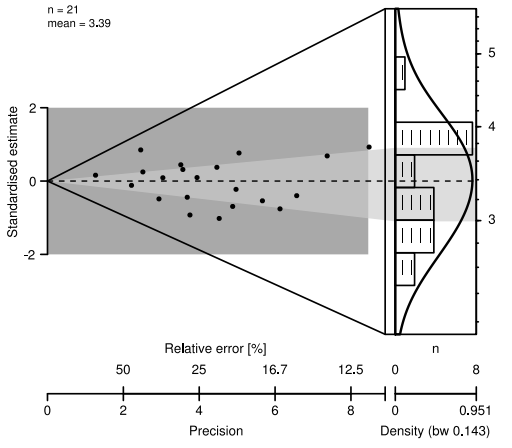

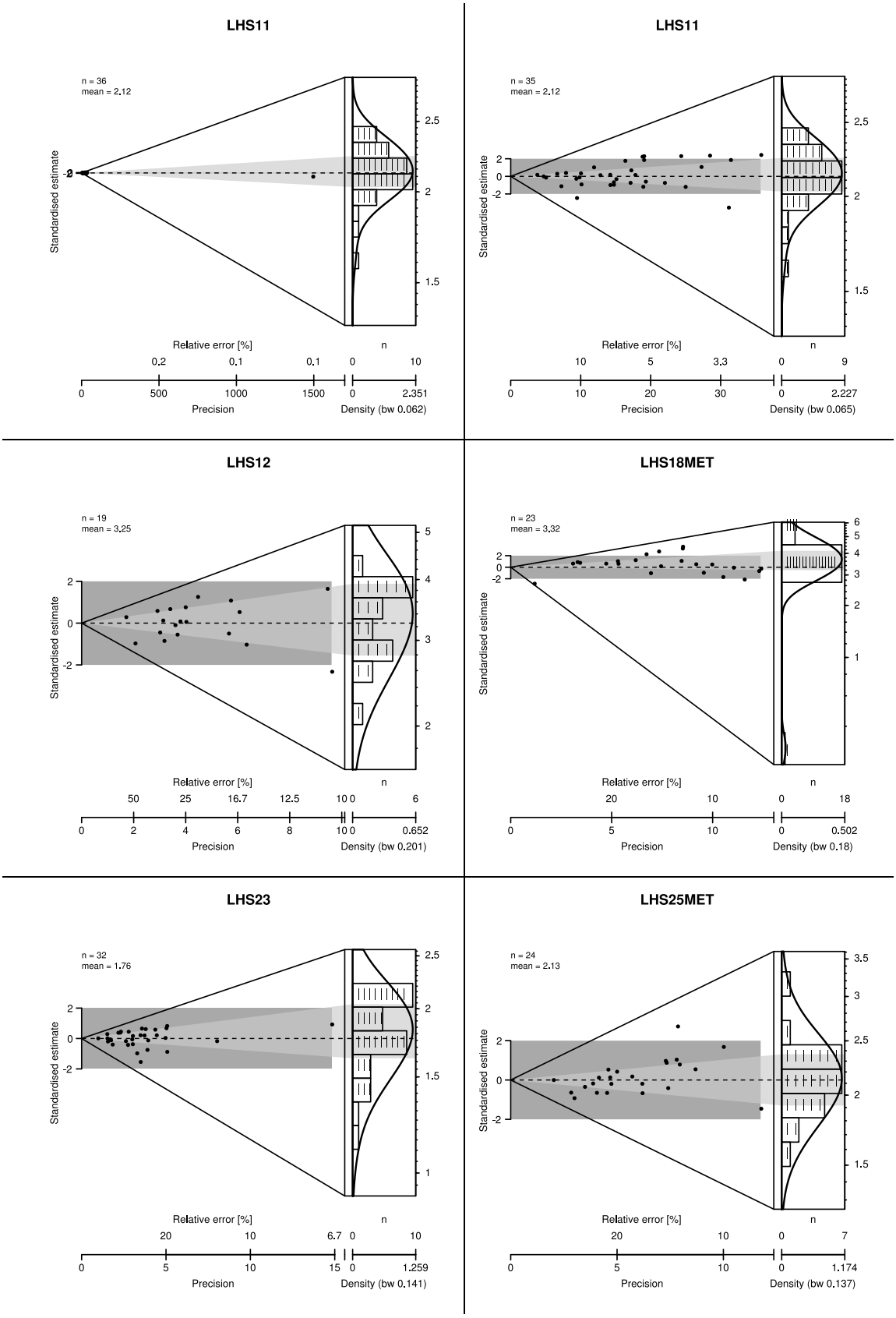
LHS11
n = 36
mean = 2.12
Standardised estimate
Relative error [%]
0.2
0.1
0.1
0
10
0
500
1000
1500
0
2.351
Precision
Density (bw 0.062)
LHS11
n = 35
mean = 2.12
Standardised estimate
Relative error [%]
10
5
3.3
0
9
0
10
20
30
0
2.227
Precision
Density (bw 0.065)
LHS12
n = 19
mean = 3.25
Standardised estimate
Relative error [%]
50
25
16.7
12.5
10
0
6
0
2
4
6
8
10
0
0.652
Precision
Density (bw 0.201)
LHS18MET
n = 23
mean = 3.32
Standardised estimate
Relative error [%]
20
10
0
18
0
5
10
0
0.502
Precision
Density (bw 0.18)
LHS23
n = 32
mean = 1.76
Standardised estimate
Relative error [%]
20
10
6.7
0
10
0
5
10
15
0
1.259
Precision
Density (bw 0.141)
LHS25MET
n = 24
mean = 2.13
Standardised estimate
Relative error [%]
20
10
0
7
0
5
10
0
1.174
Precision
Density (bw 0.137)

**LHS24**

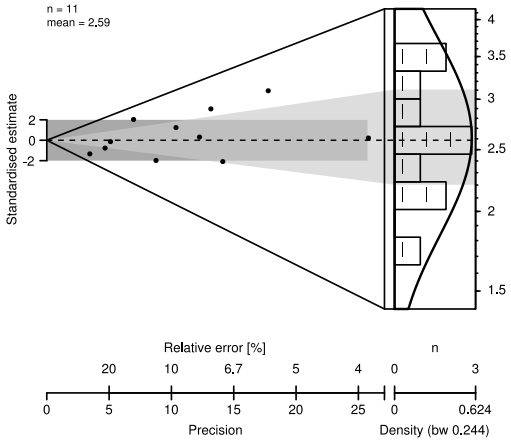


**LHS24MET**

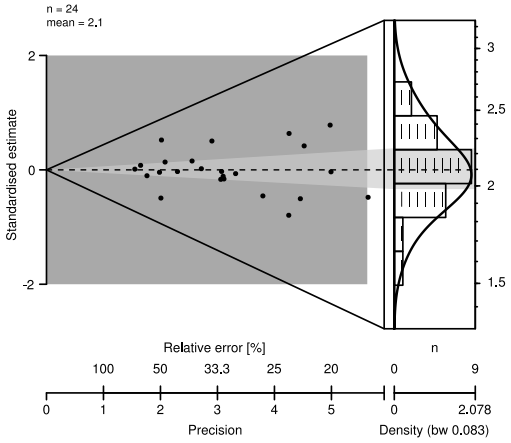


**LHS29**

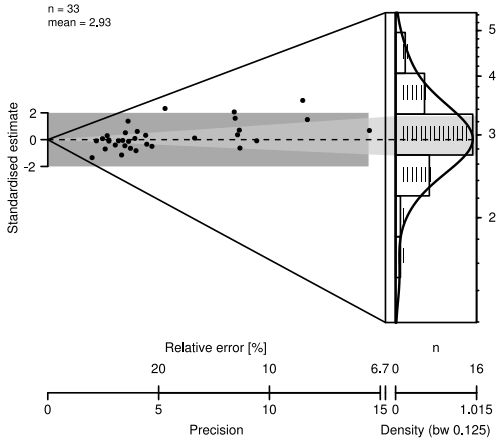


**LHS29MET**

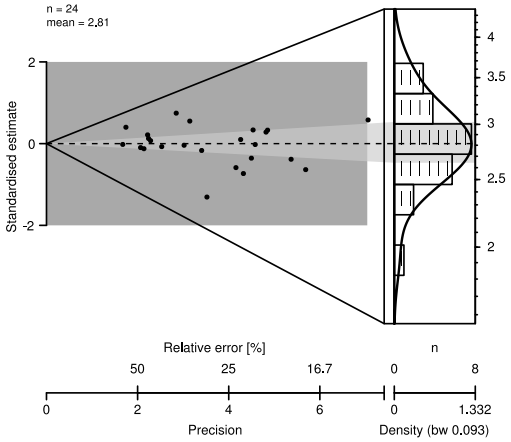


**LHS35**

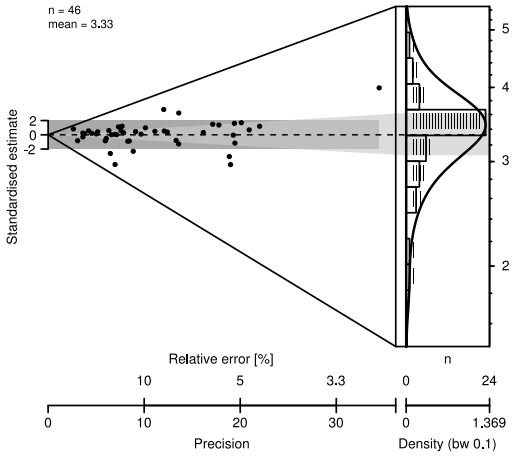


**LHS35MET**

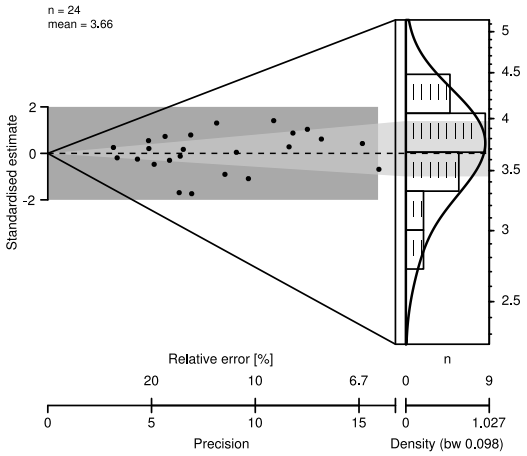

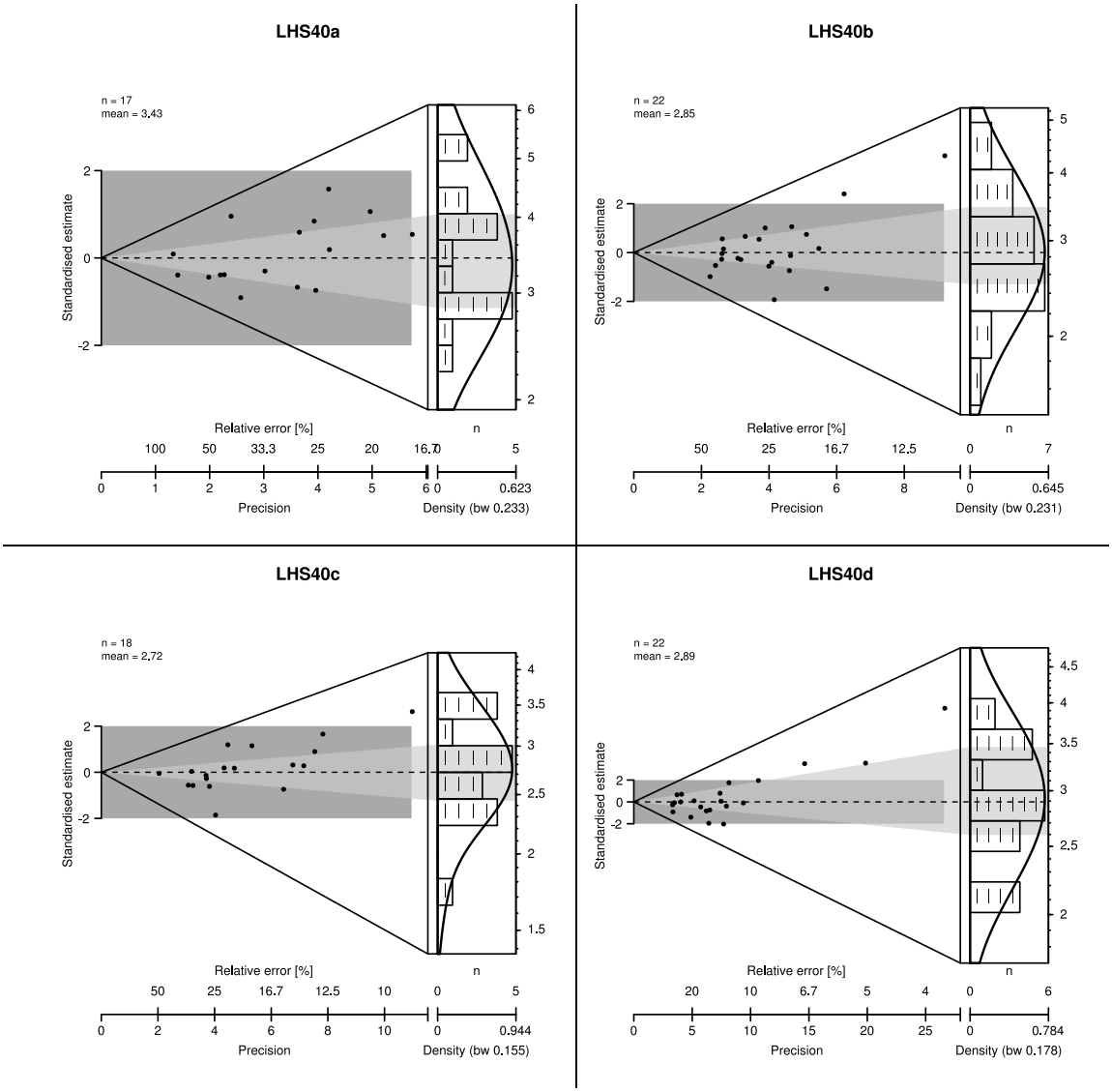


Figure 4.6. Abanico plots for all samples (Plot design by Dietze *et al.*, 2016). The z-axis is equivalent dose (Gy).

In some of the plots, a complete inclusion of all $D_e$ values within 2σ range can be seen (LHS10MET; LHS24MET; LHS23, LHS29MET, LHS35MET; and LHS40a). The result is that these samples show homogenous bleaching. The other samples show a majority of $D_e$ values within 2σ range.

In LHS02MET, except for a single outlier, the measurements are clustered around the mean value with the relative error varying between the $D_e$ values (ranging from

6.7 and 25% relative error). In LHS11, the data seems to be clustered around the mean value. Although when the graph was reproduced excluding the outlier, the $D_e$ is shown to not be clustered and having a higher general relative error. The relative errors of LHS24MET and LHS40a are high, with some exceeding 50% RE. The counterparts to these samples, LHS24 and LHS40b-d, show a lower relative error for the same ceramics.

The multi-sampled pot's (LHS40) samples are best reviewed in comparison to each other. In Figure 4.7 all the possible comparisons for the four locations are shown. In A, B, and C, the samples are all compared to LHS40a. The kernel density estimate plot shows the different peaks in the $D_e$. Although the clustering of the $D_e$ values is within the acceptable range of 2σ, the plots for LHS40a are much less reliable. In comparison, the plots of LHS40b vs LHS40c (Figure 4.7.D), LHS40b vs LHS40d (Figure 4.7.E), and LHS40c vs LHS40d (Figure 4.7.F) show similar characteristics to each other (KDE peak, relative error range and cluster location). The variations are likely caused by uneven heating of the ceramics.

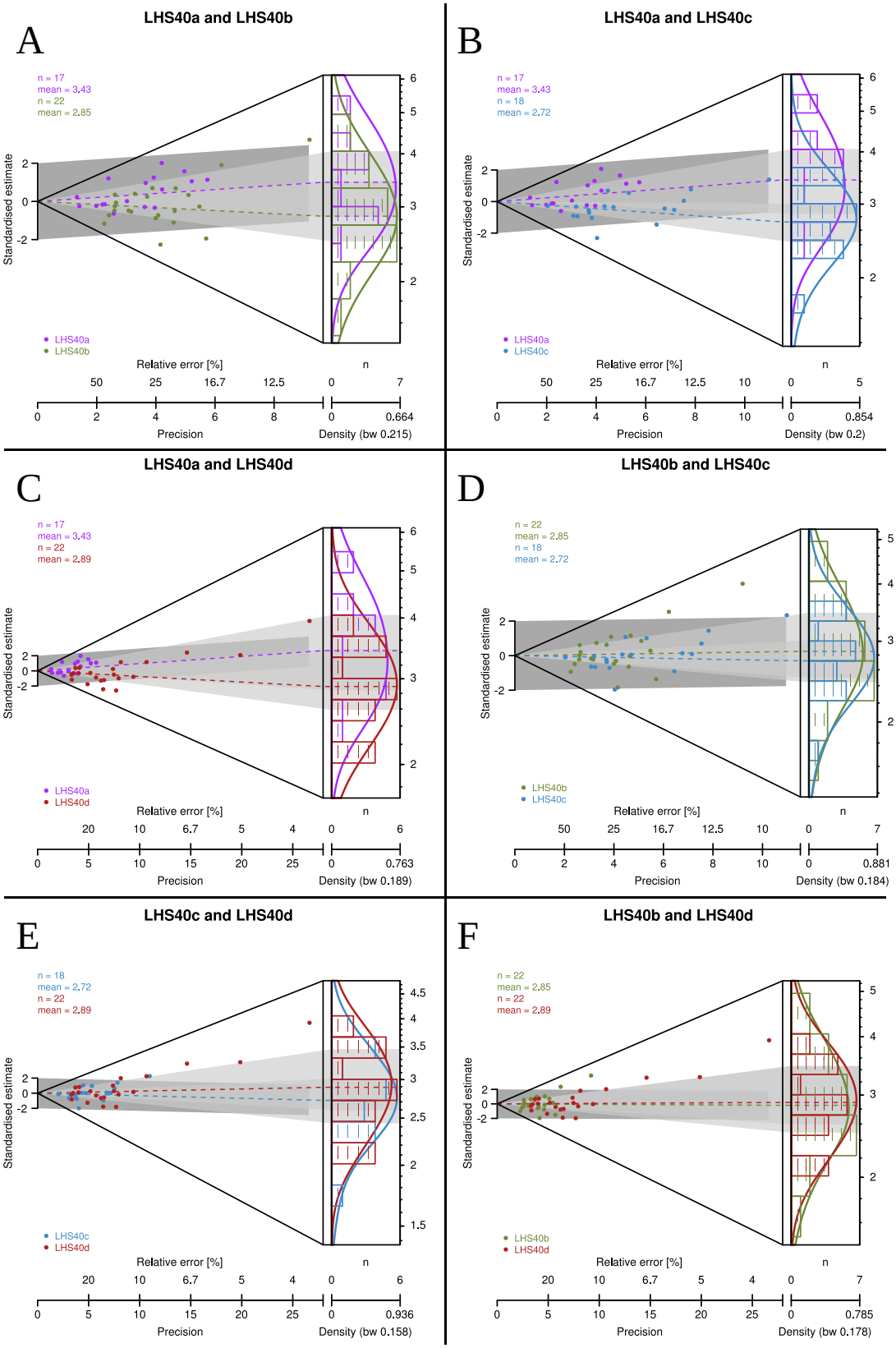


Figure 4.7. Abanico plots showing comparison of LHS40a, LHS40b, LHS40c, and LHS40d.

The $D_e$ result for the central age model (CAM), additive dose model (ADM) and the arithmetic mean (AM) highlight the variations in the $D_e$ determination based on the age model in question. The details of the age models are explained in Sections 2.4.3 and 3.9.

Table 4.4. The $D_e$ determined using the central age model (CAM), additive dose model (ADM) and pure arithmetic mean (AM) and overdispersion (OD)

| **Sample** | **CAM $D_e$ (Gy)** | **ADM $D_e$ (Gy)** | **AM $D_e$ (Gy)** | **OD (%)** |
|---|---|---|---|---|
| LHS02 | 3.42 ± 0.04 | 3.40 ± 0.04 | 3.38 ± 0.19 | 4 ± 0 |
| LHS02MET | 3.13 ± 0.11 | 3.13 ± 0.09 | 3.18 ± 0.51 | 10 ± 1 |
| LHS07 | 3.46 ± 0.07 | 3.46 ± 0.06 | 3.46 ± 0.43 | 5 ± 1 |
| LHS07MET | 3.48 ± 0.09 | 3.46 ± 0.08 | 3.51 ± 0.52 | 0 ± 0 |
| LHS10 | 3.60 ± 0.12 | 3.61 ± 0.14 | 3.67 ± 0.84 | 12 ± 1 |
| LHS10MET | 3.38 ± 0.16 | 3.36 ± 0.11 | 3.42 ± 0.98 | 0 ± 0 |
| LHS11 | 2.14 ± 0.03 | 2.14 ± 0.03 | 2.13 ± 0.17 | 5 ± 0 |
| LHS12 | 3.26 ± 0.18 | 3.27 ± 0.17 | 3.31 ± 0.88 | 9 ± 2 |
| LHS18MET | 3.58 ± 0.15 | 3.60 ± 0.16 | 3.62 ± 0.57 | 14 ± 1 |
| LHS23 | 1.80 ± 0.07 | 1.78 ± 0.05 | 1.78 ± 0.65 | 0 ± 0 |
| LHS24 | 2.69 ± 0.15 | 2.71 ± 0.16 | 2.64 ± 0.31 | 15 ± 2 |
| LHS24MET | 2.09 ± 0.13 | 2.09 ± 0.05 | 2.11 ± 0.77 | 0 ± 0 |
| LHS25MET | 2.22 ± 0.08 | 2.21 ± 0.07 | 2.15 ± 0.42 | 5 ± 2 |
| LHS29 | 3.17 ± 0.09 | 3.12 ± 0.09 | 2.99 ± 0.71 | 1 ± 7 |
| LHS29MET | 2.78 ± 0.15 | 2.78 ± 0.07 | 2.84 ± 0.92 | 0 ± 0 |
| LHS35 | 3.35 ± 0.08 | 3.36 ± 0.08 | 3.37 ± 0.44 | 11 ± 0 |
| LHS35MET | 3.70 ± 0.08 | 3.68 ± 0.08 | 3.68 ± 0.54 | 0 ± 0 |
| LHS40a | 3.67 ± 0.25 | 3.64 ± 0.17 | 3.51 ± 1.21 | 0 ± 0 |
| LHS40b | 2.99 ± 0.19 | 3.01 ± 0.19 | 2.93 ± 0.78 | 16 ± 2 |
| LHS40c | 2.93 ± 0.13 | 2.88 ± 0.12 | 2.76 ± 0.61 | 4 ± 3 |
| LHS40d | 3.01 ± 0.13 | 3.03 ± 0.15 | 2.94 ± 0.48 | 15 ± 1 |

In comparison the age models show similar $D_e$ results, while the noticeable difference is the error in the arithmetic mean. While the error for the CAM and ADM $D_e$ values are acceptable, the AM error is at times over 40% of the measured $D_e$. While all results show similar $D_e$ barring error, the AM is deemed inappropriate for use. Thus, the ages are calculated based on the CAM and ADM values.

## 4.6 Dose rate ($D_R$) results

The environmental dose rate was calculated as the sum of the beta, gamma, and cosmic dose rates (Equation 2). The uranium, thorium, and potassium measurements from the ceramics are used to calculate the environmental dose rate ($D_R$) (Table 4.5).

Table 4.5. Potassium, thorium, and uranium concentrations obtained through XRF and ICP-MS testing.

| Sample | $K_2O$ (%) | Th (ppm) | U (ppm) |
|---|---|---|---|
| **LHS02** | 1.02 ± 0.02 | 8.325 ± 0.15 | 2.181 ± 0.03 |
| **LHS07** | 1.08 ± 0.02 | 10.123 ± 0.15 | 2.495 ± 0.03 |
| **LHS10** | 1.45 ± 0.02 | 11.567 ± 0.15 | 3.131 ± 0.03 |
| **LHS11** | 0.42 ± 0.02 | 5.947 ± 0.15 | 1.431 ± 0.03 |
| **LHS12** | 0.62 ± 0.02 | 8.546 ± 0.15 | 3.099 ± 0.03 |
| **LHS18** | 1.11 ± 0.02 | 10.300 ± 0.15 | 2.663 ± 0.03 |
| **LHS23** | 0.50 ± 0.02 | 6.107 ± 0.15 | 1.403 ± 0.03 |
| **LHS24** | 0.60 ± 0.02 | 8.199 ± 0.15 | 2.112 ± 0.03 |
| **LHS25** | 0.64 ± 0.02 | 4.865 ± 0.15 | 1.419 ± 0.03 |
| **LHS29** | 1.04 ± 0.02 | 9.508 ± 0.15 | 2.303 ± 0.03 |
| **LHS35** | 1.17 ± 0.02 | 8.065 ± 0.15 | 2.624 ± 0.03 |
| **LHS40** | 0.78 ± 0.02 | 8.324 ± 0.15 | 2.625 ± 0.03 |

The depth of the samples combined the use of the pit description and the knowledge of the gamma radiation range of 30 cm. The result was in using the variations of 0.01 cm, 30 cm, 60 cm, and 90 cm increments of reviewing the variations in age owing to the changes in the $D_R$. The maximum depths of the pits were described by Evers (1982a, p. 18) and used to restrict the variations into possible ranges. The exception to the variation is LHS35, as the ceramic had a depth indicated on the pottery. The depth and water content variations and how they affect the age will be reviewed in 4.7.1 (Age calculations). Alterations to the $D_R$ from variations of water content and depth can be seen in full in Appendix D. While the final depths and water content can be seen in Table 4.6, as well as the cosmic, beta, gamma, and annual dose rates. The conversion factors for uranium, thorium, and potassium used are shown in a previous chapter (Table 3.6). The beta attenuation conversion factor use was 0.887 ± 0.007 (Mejdahl, 1979). The water content corrections for beta (Equation 4) and gamma (Equation 5) were also previously shown. An example of the working out of a $D_R$ for LHS02 can be seen in Appendix B.

Table 4.6. Final annual dose rate ($D_R$) for each ceramic, including the depth, water content (WC), and the cosmic (Dc), beta (Dβ) and gamma (Dγ) dose rates.

| Sample | Depth (m) | WC (%) | Dc (Gy/ka) | Dβ (Gy/ka) | Dγ (Gy/ka) | $D_R$ (Gy/ka) |
|---|---|---|---|---|---|---|
| **LHS02** | 0.3 | 1 ± 1 | 0.33 ± 0.02 | 1.24 ± 0.05 | 0.86 ± 0.03 | 2.45 ± 0.06 |
| **LHS07** | 0.3 | 1 ± 1 | 0.33 ± 0.02 | 1.37 ± 0.06 | 0.99 ± 0.04 | 2.71 ± 0.07 |
| **LHS10** | 0.3 | 1 ± 1 | 0.33 ± 0.02 | 1.76 ± 0.07 | 1.21 ± 0.05 | 3.32 ± 0.09 |
| **LHS11** | 0.1 | 1 ± 1 | 0.35 ± 0.02 | 0.64 ± 0.03 | 0.44 ± 0.02 | 1.45 ± 0.04 |
| **LHS12** | 0.1 | 1 ± 1 | 0.36 ± 0.02 | 1.06 ± 0.04 | 0.73 ± 0.03 | 2.17 ± 0.06 |
| **LHS18** | 0.3 | 1 ± 1 | 0.33 ± 0.02 | 1.41 ± 0.06 | 1.02 ± 0.04 | 2.80 ± 0.07 |
| **LHS23** | 0.3 | 1 ± 1 | 0.33 ± 0.02 | 0.70 ± 0.03 | 0.55 ± 0.02 | 1.60 ± 0.04 |
| **LHS24** | 0.3 | 1 ± 1 | 0.33 ± 0.02 | 0.91 ± 0.04 | 0.75 ± 0.03 | 2.01 ± 0.05 |
| **LHS25** | 0.3 | 1 ± 1 | 0.33 ± 0.02 | 0.77 ± 0.03 | 0.53 ± 0.02 | 1.65 ± 0.04 |
| **LHS29** | 0.3 | 1 ± 1 | 0.33 ± 0.02 | 1.30 ± 0.05 | 0.93 ± 0.04 | 2.58 ± 0.07 |
| **LHS35** | 0.3 | 1 ± 1 | 0.33 ± 0.02 | 1.40 ± 0.06 | 0.93 ± 0.04 | 2.68 ± 0.07 |
| **LHS40** | 0.3 | 1 ± 1 | 0.33 ± 0.02 | 1.11 ± 0.05 | 0.85 ± 0.03 | 2.31 ± 0.06 |

## 4.7 Age calculations

The age calculations involved the application of Equation 1, using the results from Table 4.4 and Table 4.6. The age calculations incorporated the $D_e$ values from the CAM and ADM values, with the AM being excluded owing to the extreme error. The ages are given as ka (Kiloannum), which is taken from the time of excavation (i.e., 1978), and the years converted into the BC/BCE or AD/CE format. When interpreting the ages the threshold value for the error was 10% (relative error) or 0.08 ka. The choice for these threshold values were based on the possible ages of ceramics in the EFC. The determined ages are tabulated in Table 4.7 and Table 4.8 for the Urewe and Kalundu ceramics respectively. The ages are shown graphically in Figure 4.8 and Figure 4.9 for the Urewe and Kalundu ceramics respectively.

Table 4.7. Urewe ceramics OSL ages, showing the pit, CAM, and ADM ages.

| Sample | Pit | CAM age (ka) | ADM age (ka) |
|---|---|---|---|
| **LHS02** | 10 | 1.40 ± 0.04 | 1.39 ± 0.04 |
| **LHS02MET** | 10 | 1.28 ± 0.06 | 1.28 ± 0.05 |
| **LHS07** | 9 | 1.28 ± 0.04 | 1.28 ± 0.04 |
| **LHS07MET** | 9 | 1.29 ± 0.05 | 1.28 ± 0.05 |
| **LHS11** | 12 | 1.48 ± 0.05 | 1.47 ± 0.04 |
| **LHS12** | 12 | 1.51 ± 0.09 | 1.51 ± 0.09 |
| **LHS18MET** | 9 | 1.28 ± 0.06 | 1.29 ± 0.07 |
| **LHS25MET** | 10 | 1.34 ± 0.06 | 1.34 ± 0.06 |
| **LHS35** | 10 | 1.25 ± 0.04 | 1.25 ± 0.04 |
| **LHS35MET** | 10 | 1.38 ± 0.05 | 1.38 ± 0.05 |

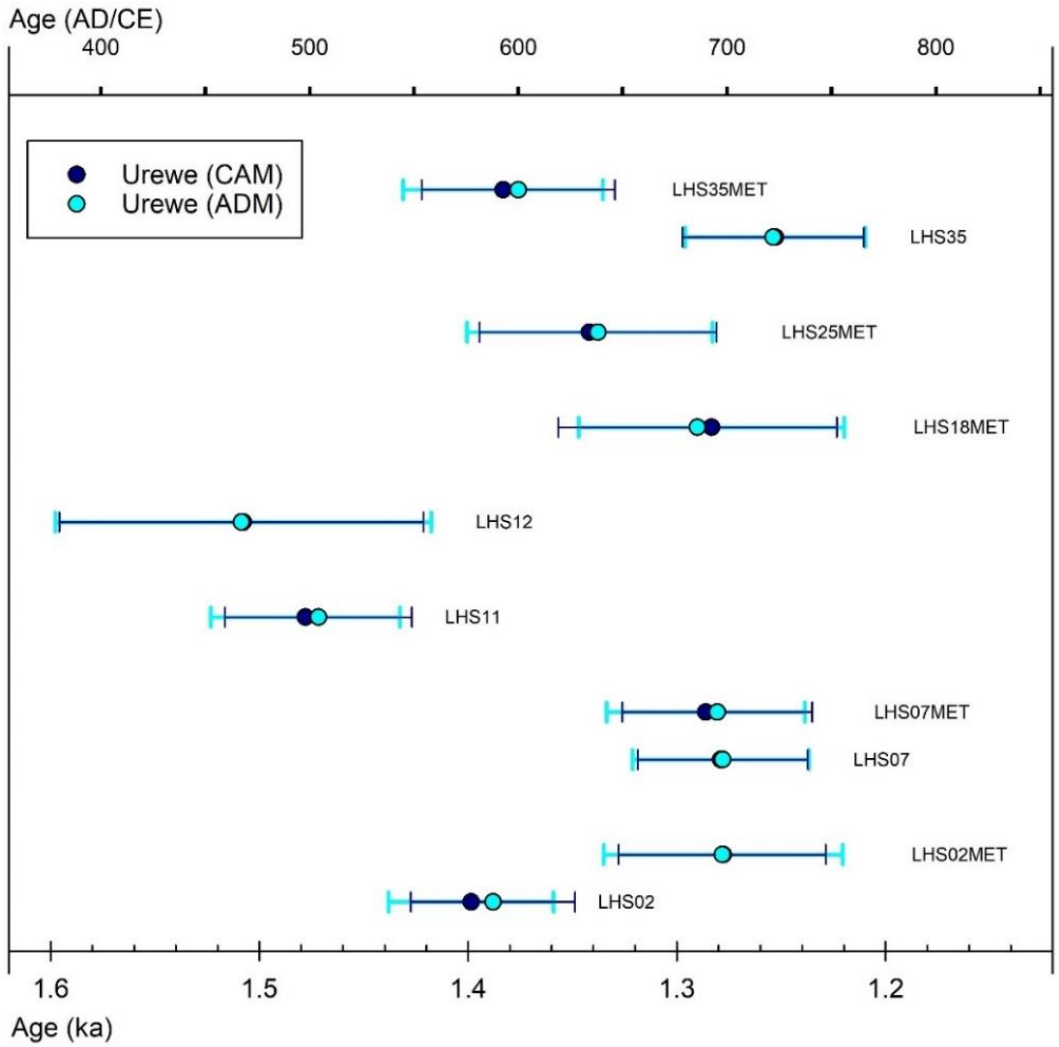


Figure 4.8. Ages for the Urewe samples, including the CAM and ADM determined $D_e$.

The age for LHS02 is 1.40 ± 0.04 ka (577 ± 39 AD) for the CAM and 1.39 ± 0.04 ka (588 ± 39 AD) for the ADM. This age has the lowest relative error, with less than 3 % (~40 years) error for the CAM and ADM. In the case of LHS02MET, the determined ages were 1.28 ± 0.06 ka (698 ± 57 AD) for the CAM and 1.28 ± 0.05 ka (698 ± 50 AD) for the ADM. The two samples are from the same ceramic shard, although they vary in age. The relative error of LHS02MET is ~4 %. The differences in error and ages from the same ceramic hints to the reliability of quartz extraction methods. Within the same location (pit 10), the samples LHS35, LHS35MET and LHS25MET are found. LHS35 and LHS35MET have CAM ages

of 1.25 ± 0.04 ka (723 ± 43 AD) and 1.38 ± 0.05 ka (593 ± 48 AD), and ADM ages of 1.25 ± 0.04 ka (722 ± 43 AD) and 1.38 ± 0.05 ka (600 ± 46 AD), respectively. LHS25MET has an age of 1.34 ± 0.06 ka (634 ± 59 AD) for the CAM and 1.34 ± 0.06 ka (638 ± 57 AD) for the ADM. The ADM and CAM error for LHS25MET, LHS35, and LHS35MET are below the threshold value (between 3 and 5 %). LHS02 and LHS35 show a trend of the bulk sampling displaying different ages than the MET sampling, although LHS35 shows the MET sampling to produce younger ages.

The sample LHS07 is similarly a dual MET and bulk sampling ceramic. The bulk sampling gave CAM ages of 1.28 ± 0.04 ka (697 ± 42 AD) and ADM ages of 1.28 ± 0.04 ka (698 ± 41 AD). While the MET sample gave CAM ages of 1.29 ± 0.05 ka (690 ± 47 AD) and ADM ages of 1.28 ± 0.05 ka (695 ± 45 AD). The bulk and MET samples display little variation between the CAM and ADM ages and errors. Comparative to each other, the samples are remarkably similar with an estimated age of between 1.24 – 1.32 ka, firmly setting the pottery within the late 7$^{th}$ or early 8$^{th}$ century AD. Within the same pit is LHS18MET, with a CAM age of 1.28 ± 0.06 ka (693 ± 64 AD) and ADM age of 1.29 ± 0.07 ka (686 ± 67 AD). Thus, placing all the pottery within this pit within a very similar timeframe.

The oldest Urewe sample is LHS12. It has a CAM age of 1.51 ± 0.09 ka (468 ± 90 AD) and an ADM age of 1.51 ± 0.09 ka (467 ± 87 AD). The relative error of the sample is just under 6 % for the ADM and CAM ages. The ceramic from the same location (pit 12) is LHS11 with an CAM age of 1.48 ± 0.05 ka (498 ± 45 AD) and ADM age of 1.47 ± 0.05 ka (504 ± 45 AD). LHS11 has a low error, particularly in comparison to LHS12. Both ceramics show OD under 10 %, although the higher OD in LHS12 (9% compared to 5% for LHS11) coupled with the larger error shows a trend of the ages being less reliable than that of LHS11.

Table 4.8. Kalundu ceramics OSL ages, showing the pit, CAM and ADM ages.

| Sample | Pit | CAM age (ka) | ADM age (ka) |
|---|---|---|---|
| **LHS10** | 5 | 1.09 ± 0.05 | 1.09 ± 0.05 |
| **LHS10MET** | 5 | 1.02 ± 0.05 | 1.01 ± 0.04 |
| **LHS23** | 3 | 1.13 ± 0.05 | 1.12 ± 0.04 |
| **LHS24** | 5 | 1.34 ± 0.08 | 1.35 ± 0.09 |
| **LHS24MET** | 5 | 1.04 ± 0.07 | 1.04 ± 0.04 |
| **LHS29** | 7 | 1.23 ± 0.05 | 1.21 ± 0.05 |
| **LHS29MET** | 7 | 1.08 ± 0.06 | 1.08 ± 0.04 |
| **LHS40a** | 5 | 1.58 ± 0.12 | 1.58 ± 0.09 |
| **LHS40b** | 5 | 1.29 ± 0.09 | 1.30 ± 0.09 |
| **LHS40c** | 5 | 1.27 ± 0.07 | 1.25 ± 0.06 |
| **LHS40d** | 5 | 1.30 ± 0.07 | 1.31 ± 0.07 |

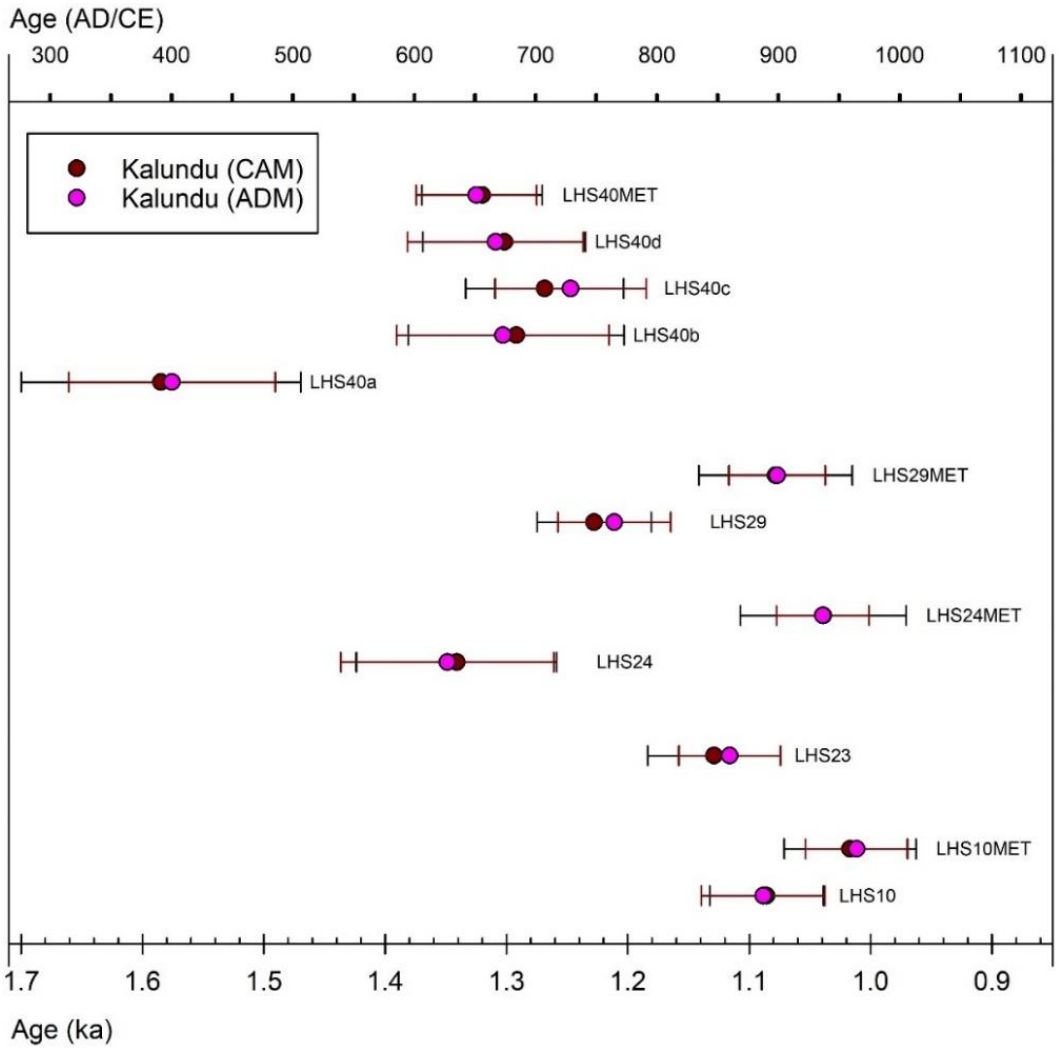


Figure 4.9. Ages for the Kalundu sample, including the CAM and ADM determined $D_e$.

In the case of LHS23, the determined CAM age was 1.13 ± 0.06 ka (847 ± 55 AD), and ADM age was 1.12 ± 0.04 ka (860 ± 42 AD). LHS29 bulk and MET, provided the CAM ages of 1.23 ± 0.05 ka (748 ± 47 AD) and 1.08 ± 0.06 ka (898 ± 63 AD) and the ADM ages of 1.21 ± 0.05 ka (765 ± 46 AD) and 1.08 ± 0.04 ka (899 ± 40 AD), respectively. In comparison, the MET result show younger ages and low error for the ADM age. LHS23 and LHS29 were the sole samples tested from pits 3 and 7. Considering that both LHS23 and LHS29 are of the Kalundu tradition, the age is comparable.

For the samples in pit 5, there is the most amount of data to interpret. That is because there are three ceramic sherds, each with multiple samples from each. The samples of LHS10 and LHS24 each contain a bulk and MET sampling. The following samples had relative errors over 6 %: LHS24 with a CAM age of 1.34 ± 0.08 ka (635 ± 83 AD) and ADM age of 1.35 ± 0.09 ka (627 ± 88 AD); LHS24MET with a CAM age of 1.04 ± 0.07 ka (937 ± 68 AD) and ADM age of 1.04 ± 0.04 ka (937 ± 38 AD). It is important to note that LHS24MET's ADM age has a low error of under 4 % (38 years). For the LHS10 bulk sample, the CAM age of 1.09 ± 0.05 ka (890 ± 47 AD) and ADM age of 1.09 ± 0.05 ka (888 ± 51 AD) was determined. While the MET results are CAM age of 1.02 ± 0.05 ka (959 ± 54 AD) and ADM age of 1.01 ± 0.04 ka (964 ± 42 AD). In the cases of LHS24 and LHS10, the MET and bulk samples are vastly different. The ages are around the 9$^{th}$ to the 10$^{th}$ centuries AD, apart from LHS24.

The sample LHS40 had four points of sampling for an analysis of differences in heating on a single ceramic (see Figure 3.3 drill locations). The samples of LHS40a with a CAM age of 1.59 ± 0.12 ka (391 ± 115 AD) and ADM age of 1.58 ± 0.09 ka (400 ± 85 AD); and LHS40b with a CAM age of 1.29 ± 0.09 ka (684 ± 89 AD) and ADM age of 1.30 ± 0.09 ka (673 ± 87 AD), had errors surpassing the threshold of 0.08 ka. LHS40a provided a much older age than the other three sample drilling sites and all the Kalundu tradition ceramics dated. LHS40c has a CAM age of 1.27 ± 0.07 ka (707 ± 65 AD) and ADM age of 1.25± 0.06 ka (729 ± 62 AD). Similarly, LHS40d has a CAM age of 1.30 ± 0.07 ka (674 ± 67 AD) and ADM age of 1.31 ± 0.07 ka (667 ± 72 AD). The error and ages from LHS40a and LHS40b highlight the issues of differences in heating of ceramics. In general, the trend shows the majority of data giving a 7$^{th}$ century AD age.

The final ages and pertinent details for each sample are shown in Table 4.9, as well as a figure to allow comparison of the Kalundu and Urewe ceramics ages in Figure 4.10.

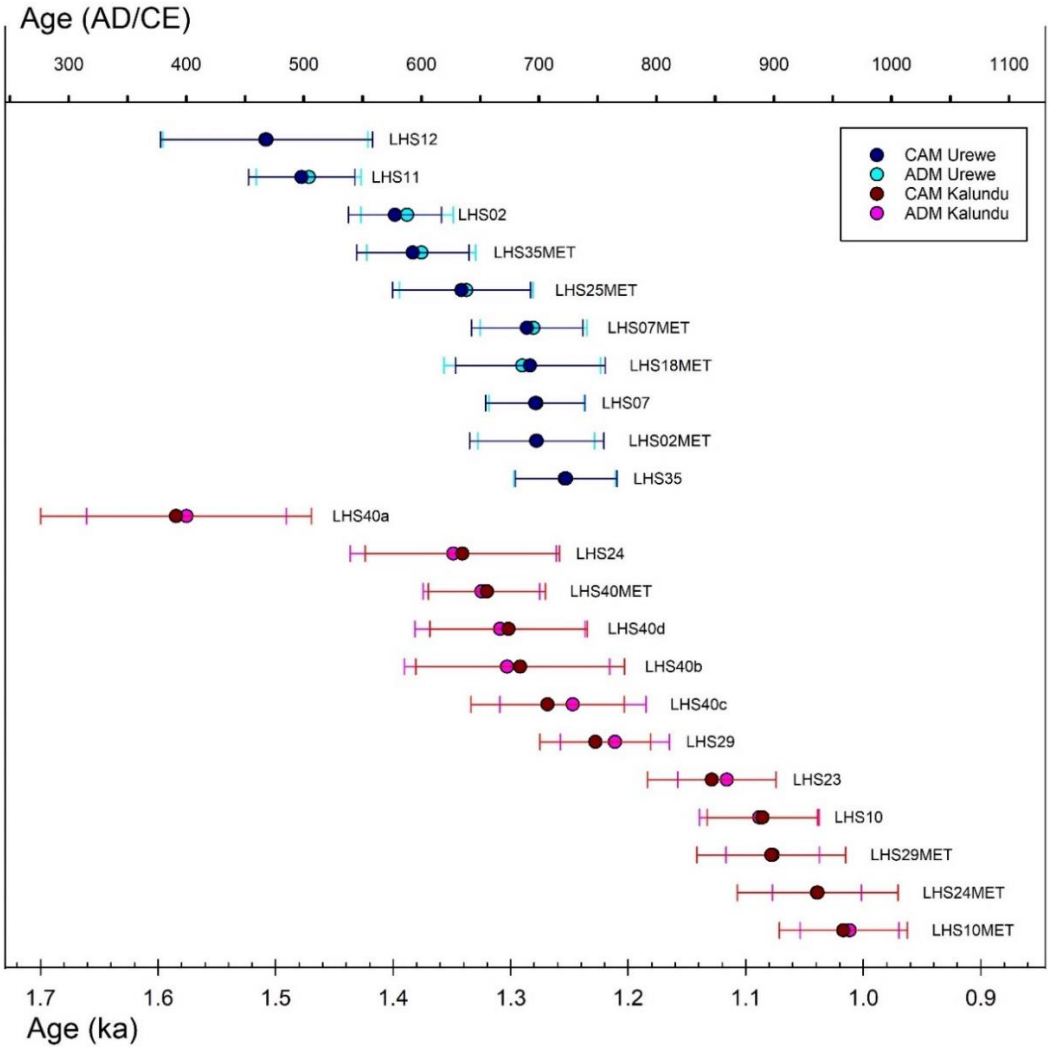


Figure 4.10. All ceramic ages calculated using the CAM and ADM $D_e$.

Table 4.9. Full details of all samples, including: the final depth; thorium, uranium and potassium concentration; water content (WC); cosmic dose rate (Dc); environmental dose rate ($D_R$); the overdispersion (OD) including error; the CAM equivalent dose and age including errors; the ADM equivalent dose and age including errors. The errors that are not shown are uniform and as follows: Th: ± 0.15, U: ± 0.03, K: ± 0.02, WC: ± 1, and Dc: ± 0.02.

| Sample | Pit | Depth | Th | U | K | WC | Dc | $D_R$ | OD | $D_e$ values | CAM $D_e$ | CAM age | ADM $D_e$ | ADM age |
|---|---|---|---|---|---|---|---|---|---|---|---|---|---|---|
| | | (m) | (ppm) | | (%) | | (Gy/ka) | | (%) | (n) | (Gy) | (ka) | (Gy) | (ka) |
| **LHS02** | 10 | 0.3 | 8.33 | 2.18 | 1.02 | 1 | 0.33 | 2.45 ± 0.06 | 4 ± 0 | 33 | 3.42 ± 0.04 | 1.4 ± 0.04 | 3.40 ± 0.04 | 1.39 ± 0.04 |
| **LHS02 MET** | 10 | 0.3 | 8.33 | 2.18 | 1.02 | 1 | 0.33 | 2.45 ± 0.06 | 10 ± 1 | 21 | 3.13 ± 0.11 | 1.28 ± 0.06 | 3.13 ± 0.09 | 1.28 ± 0.05 |
| **LHS07** | 9 | 0.3 | 10.12 | 2.50 | 1.08 | 1 | 0.33 | 2.71 ± 0.07 | 5 ± 1 | 29 | 3.46 ± 0.07 | 1.28 ± 0.04 | 3.46 ± 0.06 | 1.28 ± 0.04 |
| **LHS07 MET** | 9 | 0.3 | 10.12 | 2.50 | 1.08 | 1 | 0.33 | 2.71 ± 0.07 | 0 ± 0 | 22 | 3.48 ± 0.09 | 1.29 ± 0.05 | 3.46 ± 0.08 | 1.28 ± 0.05 |
| **LHS10** | 5 | 0.3 | 11.57 | 3.13 | 1.45 | 1 | 0.33 | 3.32 ± 0.09 | 12 ± 1 | 42 | 3.60 ± 0.12 | 1.09 ± 0.05 | 3.61 ± 0.14 | 1.09 ± 0.05 |
| **LHS10 MET** | 5 | 0.3 | 11.57 | 3.13 | 1.45 | 1 | 0.33 | 3.32 ± 0.09 | 0 ± 0 | 21 | 3.38 ± 0.16 | 1.02 ± 0.05 | 3.36 ± 0.11 | 1.01 ± 0.04 |
| **LHS11** | 12 | 0.1 | 5.95 | 1.43 | 0.42 | 1 | 0.35 | 1.45 ± 0.04 | 5 ± 0 | 36 | 2.14 ± 0.03 | 1.48 ± 0.05 | 2.14 ± 0.03 | 1.47 ± 0.04 |
| **LHS12** | 12 | 0.1 | 8.55 | 3.10 | 0.62 | 1 | 0.36 | 2.17 ± 0.06 | 9 ± 2 | 19 | 3.26 ± 0.18 | 1.51 ± 0.09 | 3.27 ± 0.17 | 1.51 ± 0.09 |
| **LHS18 MET** | 9 | 0.3 | 10.30 | 2.66 | 1.11 | 1 | 0.33 | 2.79 ± 0.07 | 14 ± 1 | 23 | 3.58 ± 0.15 | 1.28 ± 0.06 | 3.60 ± 0.16 | 1.29 ± 0.07 |
| **LHS23** | 3 | 0.3 | 6.11 | 1.40 | 0.50 | 1 | 0.33 | 1.60 ± 0.04 | 0 ± 0 | 32 | 1.80 ± 0.07 | 1.13 ± 0.05 | 1.78 ± 0.05 | 1.12 ± 0.04 |

| Sample | Pit | Depth | Th | U | K | WC | Dc | $D_R$ | OD | $D_e$ values | CAM $D_e$ | CAM age | ADM $D_e$ | ADM age |
|---|---|---|---|---|---|---|---|---|---|---|---|---|---|---|
| | | (m) | (ppm) | | (%) | | (Gy/ka) | | (%) | (n) | (Gy) | (ka) | (n) | (ka) |
| **LHS24** | 5 | 0.3 | 8.20 | 2.11 | 0.60 | 1 | 0.33 | 2.01 ± 0.05 | 15 ± 2 | 11 | 2.69 ± 0.15 | 1.34 ± 0.08 | 2.71 ± 0.16 | 1.35 ± 0.09 |
| **LHS24 MET** | 5 | 0.3 | 8.20 | 2.11 | 0.60 | 1 | 0.33 | 2.01 ± 0.05 | 0 ± 0 | 24 | 2.09 ± 0.13 | 1.04 ± 0.07 | 2.09 ± 0.05 | 1.04 ± 0.04 |
| **LHS25 MET** | 10 | 0.3 | 4.87 | 1.42 | 0.64 | 1 | 0.33 | 1.65 ± 0.04 | 5 ± 2 | 24 | 2.22 ± 0.08 | 1.34 ± 0.06 | 2.21 ± 0.07 | 1.34 ± 0.06 |
| **LHS29** | 7 | 0.3 | 9.51 | 2.30 | 1.04 | 1 | 0.33 | 2.58 ± 0.07 | 1 ± 7 | 33 | 3.17 ± 0.09 | 1.23 ± 0.05 | 3.12 ± 0.09 | 1.21 ± 0.05 |
| **LHS29 MET** | 7 | 0.3 | 9.51 | 2.30 | 1.04 | 1 | 0.33 | 2.58 ± 0.07 | 0 ± 0 | 24 | 2.78 ± 0.15 | 1.08 ± 0.06 | 2.78 ± 0.07 | 1.08 ± 0.04 |
| **LHS35** | 10 | 0.3 | 8.07 | 2.62 | 1.17 | 1 | 0.33 | 2.68 ± 0.07 | 11 ± 0 | 46 | 3.35 ± 0.08 | 1.25 ± 0.04 | 3.36 ± 0.08 | 1.25 ± 0.04 |
| **LHS35 MET** | 10 | 0.3 | 8.07 | 2.62 | 1.17 | 1 | 0.33 | 2.68 ± 0.07 | 0 ± 0 | 24 | 3.70 ± 0.08 | 1.38 ± 0.05 | 3.68 ± 0.08 | 1.38 ± 0.05 |
| **LHS40a** | 5 | 0.3 | 8.32 | 2.63 | 0.78 | 1 | 0.33 | 2.31 ± 0.06 | 0 ± 0 | 17 | 3.67 ± 0.25 | 1.58 ± 0.12 | 3.64 ± 0.17 | 1.58 ± 0.09 |
| **LHS40b** | 5 | 0.3 | 8.32 | 2.63 | 0.78 | 1 | 0.33 | 2.31 ± 0.06 | 16 ± 2 | 22 | 2.99 ± 0.19 | 1.29 ± 0.09 | 3.01 ± 0.19 | 1.3 ± 0.09 |
| **LHS40c** | 5 | 0.3 | 8.32 | 2.63 | 0.78 | 1 | 0.33 | 2.31 ± 0.06 | 4 ± 3 | 18 | 2.93 ± 0.13 | 1.27 ± 0.07 | 2.88 ± 0.12 | 1.25 ± 0.06 |
| **LHS40d** | 5 | 0.3 | 8.32 | 2.63 | 0.78 | 1 | 0.33 | 2.31 ± 0.06 | 15 ± 1 | 22 | 3.01 ± 0.13 | 1.30 ± 0.07 | 3.03 ± 0.15 | 1.31 ± 0.07 |

### 4.7.1 Age variations from depth and water content

The variations in depth show a large change, up to 0.26 ka, in the ages of the samples. The depth of the pits allows the determination of possible maximum depth of the ceramics (Table 4.10). Figure 4.11 and Figure 4.12 show that with the first increment from directly below the surface (0.01 cm depth) to the next possible depth (either 30 cm or maximum depth of the pit) as a large reduction in the sample's age. LHS11 and LHS12 (Figure 4.12) show a sample that did not have many depth variations. The samples have a change of 140 years for LHS11 and 168 years for LHS12, with a change of depth from 1 cm to 10 cm. The age variation through the first step is a maximum of 263 years for LHS40a (Figure 4.11). In general, the increase in depth of the first 30 cm implies a change of around 200 years.

Table 4.10. Estimated depths based on the pit.

| Sample | Pit | Depths (m) |
|---|---|---|
| **LHS02** | 10 | 0 – 0.82 |
| **LHS07** | 9 | 0 – 0.66 |
| **LHS10** | 5 | 0 – 0.70 |
| **LHS11** | 12 | 0 – 0.10 |
| **LHS12** | 12 | 0 – 0.10 |
| **LHS18** | 9 | 0 – 0.66 |
| **LHS23** | 3 | 0 – 0.43 |
| **LHS24** | 5 | 0 – 0.70 |
| **LHS25** | 10 | 0 – 0.82 |
| **LHS29** | 7 | 0 – 0.50 |
| **LHS35** | 10 | 0.30 – 0.35 |
| **LHS40** | 5 | 0 – 0.70 |

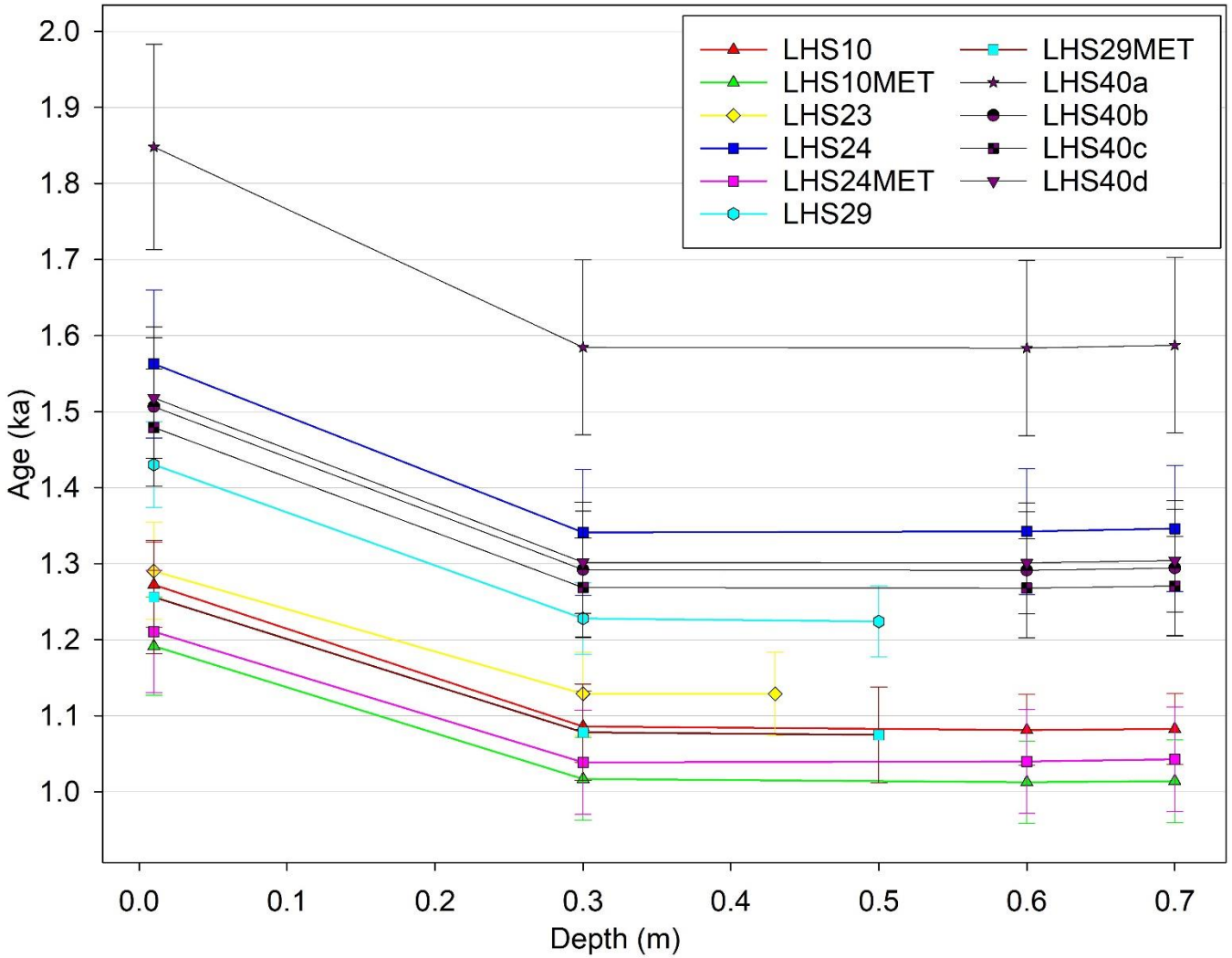


Figure 4.11. Showing the variation in the age with variation in depth for the selected Kalundu ceramics. The deeper the sample, the younger the age; however, at depths below 0.3 m the age experiences slight increases and decreases.

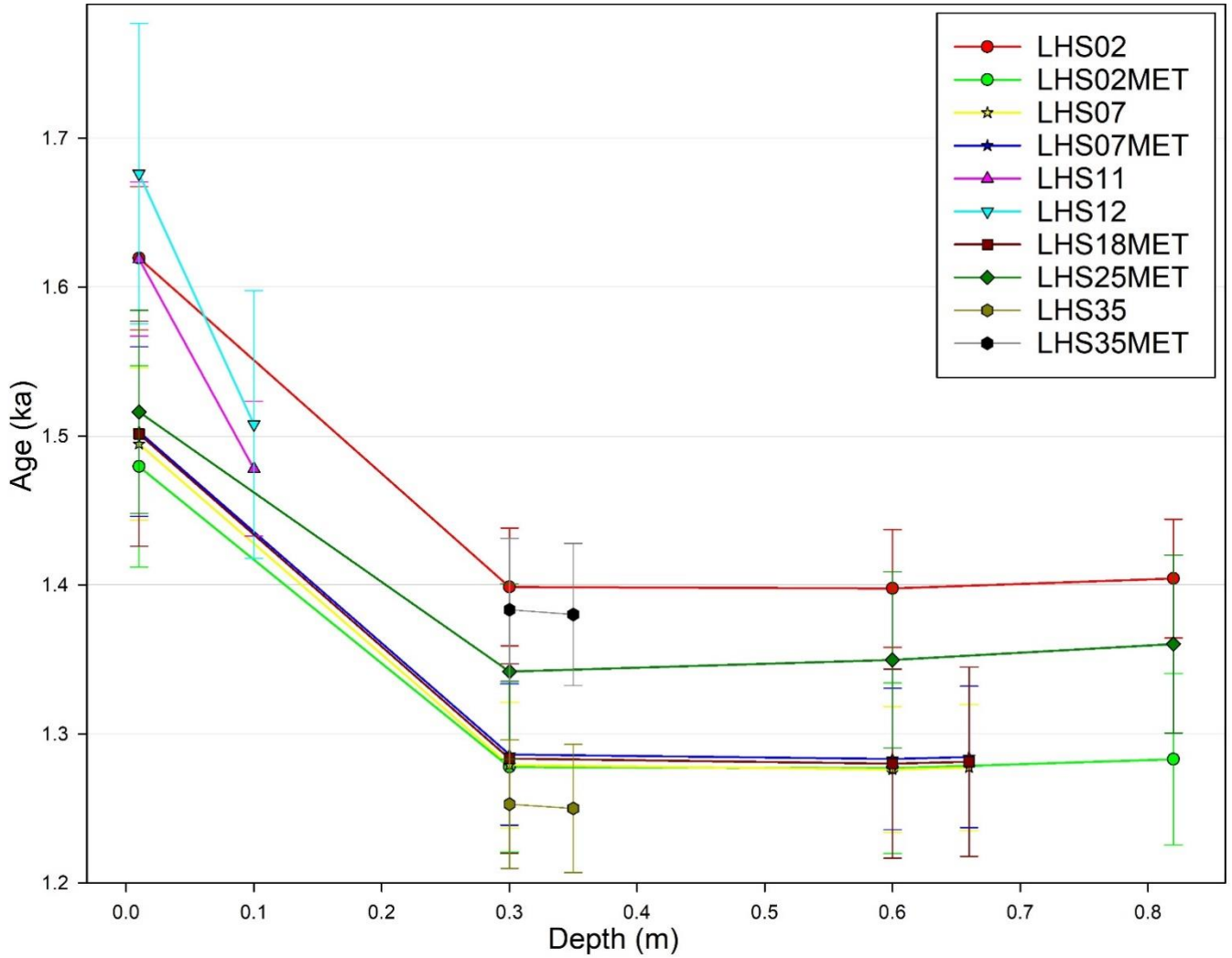


Figure 4.12. Showing the variation in the age with alteration to the depth for the selected Urewe ceramics. The deeper the sample, the younger the age; however, at depths below 0.3 m the age experiences slight increases and decreases.

The samples LHS35 and LHS35MET (Figure 4.12) similarly show a smaller increment of change from 30 cm to 35 cm, with age variations of around three years. In both Figure 4.11 and Figure 4.12 the variation from 30 cm to 60 cm (or maximum depth) is shown. Most of the samples decrease in age by a maximum of five years. The exceptions to this are LHS24, LHS24MET, and LHS25MET which increase in age. LHS24 and LHS24MET increase marginally by a year, while LHS25MET has a larger increase of eight years. The final increment of 60 cm to 90 cm (or the maximum depth) shows a similar increase in age with the increase in depth. The age increase is, on average, two years, with the maximum change being 10 years for sample LHS25MET. The depth that was used to determine the variation of age with changes to the water content are the final depths used and shown in Table 4.9. The final depth for the samples were 0.3 m as that was the point from which most change had occurred with further changes below 0.3 m being nominal and implications of an assumed occupation layer. The exception was the depth of LHS11 and LHS12, of which the pits maximum depth was used (0.1 m).

The water content of the samples was determined without any laboratory measurements owing to the lack of suitable material for measurement. The variations of water content and the resultant change in age are shown below. The water content used increments of 1 % starting at 0 % and ending at 5 % based on regional environmental reconstruction. The water content variations are shown, with the samples being split into three graphs for easier reading. The samples overall show a linear increase in age with the increase in water content. On average, the increase in age per water content percentage increase is 0.013 ka. The result is that the highest water content values are comparable to placing the ceramics into a separate century.

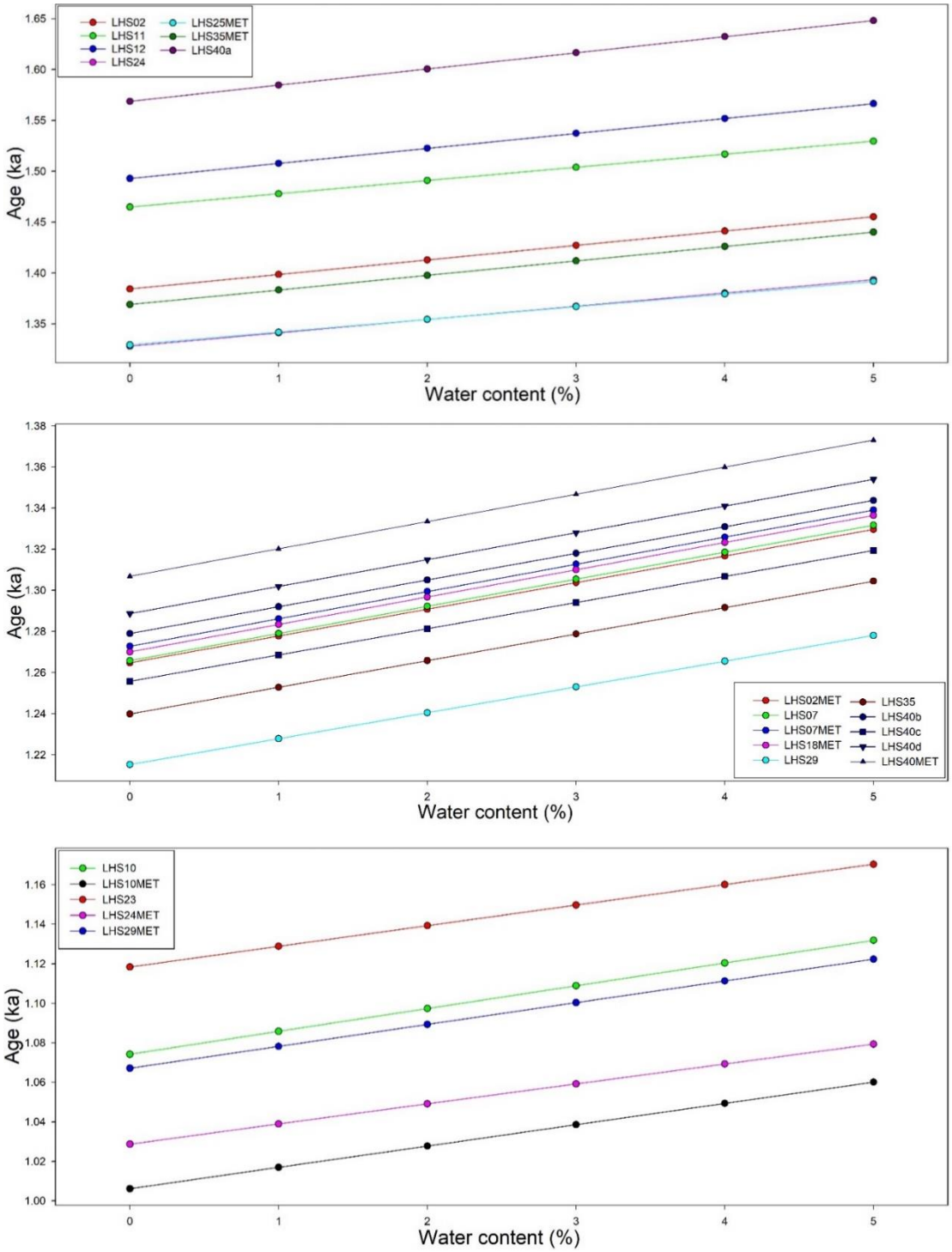


Figure 4.13 Changes in water content and the variations in age of the samples, using a depth of 0.3 m or maximum possible depth.

## 4.8 Summary

The production of a direct age of ceramics using OSL dating incorporates the steps of dose recovery/ preheat tests, equivalent dose, and dose rate. The results of each step have been displayed, allowing a deeper understanding of the process and reliability of the final ages. The ceramics ascribed to the Kalundu and Urewe traditions were successfully dated, providing a chronology in which to understand the LHS's occupation history.

# CHAPTER 5 - DISCUSSION

## 5.1 Introduction

The dating of a selection of ceramics from the Lydenburg Heads Site (LHS), provides an insight into the chronology of the site. The use of the standard quartz extraction and minimal extraction technique (MET), which has unique application in South Africa, allowed a comparative study of the techniques. The complexity of OSL dating ceramics that have been previously excavated, needed to be assessed by reviewing variables such as water content and depth variations. The resultant ages of the ceramics do experience variability, while the relationship between the two occupations is shown.

The Urewe samples displayed ages generally within the $6^{th}$ and $8^{th}$ centuries AD. While the Kalundu samples dated from the $7^{th}$ to $10^{th}$ centuries AD. These occupations present a possible overlap. The OSL dates correlate well with the radiocarbon ages and the relative dates suggested by the ceramic sequence.

## 5.2 Chronology of the ceramic tradition

All the ceramics, originally from LHS, were received within three boxes, with details of tradition and locality. The information available for the ceramic sherds was from Evers' (1982a) paper on the excavation, Whitelaw's (1996) reanalysis of the ceramics and the Organic Residue Analysis (ORA) by Becher (2021). The ceramics were obtained without any in situ field samples and excavated between 1976 and 1978. The excavation of the ceramics was not done with OSL dating in mind, thus there were methodological challenges that required assumptions for the water content and depth measurements. As a result, the Dose Rate ($D_R$) was the element with the highest combination of variables and unknowns. Consideration needs to be made that the dose rate is based entirely on the U, Th and K

concentration measured directly from the ceramics. As a result, there is no means from which to understand the effects of the infinite matrix on the measurements. The issue of water content is common throughout the OSL dating technique.

As mentioned previously, the technique assumes the water content remains consistent throughout the burial period. The water content can be measured through weighing the ceramics prior and post drying. While LHS' difficulty in determining the water content was exacerbated owing to the lack of ability to measure sediment in situ. The estimation of water content has been done previously such as the Bushman Rock Shelter located in the Limpopo province was assigned a water content of 5 ± 3% owing to the sandy environment (Porraz *et al.*, 2018). The estimation of water content from observations of the environment and historic climate reconstruction is not uncommon (see Reimann *et al.*, 2011; Dörschner *et al.*, 2012; Hood and Schwenniger, 2016). The result was that variations of water content were examined. The site has a reasonably drier climate owing to being located within the rain shadow zone. Consideration for lower water content is further viable in the region as the pits are not located within a water source. As stated by Becher (2021), the ceramics from the site exhibit signs of possible water proofing techniques. The post excavation treatment of the ceramics is unknown, with a possibility of washing and air drying. The coupling of the waterproofing and the fact that the samples have been stored ex situ for an extended period makes measuring the actual water content of the samples invalid.

The measuring of the water content at 0% is statistically impossible as with an assumed error the water content could possibly become negative. The increase in water content shows linear increase in the age of the sample. With exclusion of water contents that produce ages outside possible age range, the best water content was determined to be 1 ± 1 % (Figure 4.13). The choice of this water content is founded on the most accurate result for most of the samples is between 0% and 2%, thus making the 1 ± 1% water content viable to cover this range. The climate

reconstruction by Sjöström *et al.* (2017) further supports the choice in water content.

The second variable of interest in the $D_R$ is that of the depth of the samples. Similar to the work by Anderson and Feathers (2019), the information of the depth of ceramics were limited to known depths of pits from the excavation. As shown in Figure 4.11 and Figure 4.12 the variation in depth changes the ages significantly. When the depth is just below the surface, the ages are older. The result is that many of the samples are no longer within the viable range. In the case of the Urewe ceramics, three samples have a reduced depth range. For LHS35, the range is restricted to 0.3-0.35 m, while LHS11 and LHS12 are within a pit with a minimal range. For the case of LHS11 and LHS12, the depth change shows a significant reduction in the age. Although there is the possibility of the samples being located closer to the surface, the chosen depth (0.1m) was based on the assumption that all samples were excavated samples and not surface finds.

The majority of the Urewe samples are within age range at all depths except for LHS11, LHS12 and LHS02. LHS02 was located in the same pit as LHS35 and LHS25, although it is showing a substantially older age even with the depth variations. Using the 0.3 m depth is justified by incorporating the assumed occupation horizon and the data that provides the most viable results. For the case that the depths would unlikely be uniform, it is worth noting that, barring the above-mentioned cases, the depth variations post 0.3 m are within age range and can be considered possible.

The Kalundu samples, show a much higher variation of ages, with three samples maintaining older results than expected, even considering the depth variations. The samples LHS24, LHS29, and LHS40MET should be considered in tandem with the MET counterparts or the sample make-up. For the samples LHS24 and LHS29, the MET counterparts show more promising data with the ages within the acceptable range. Whereas all the samples for LHS40 show a trend towards older dates.

In all samples the early background extraction technique was used, leaning heavily on the writing by Cunningham and Wallinga (2010). The focus on this technique was based on the definite youth of the samples and the subsequent rejection of observations of late background extraction. The assumption that the MET samples, having experienced less sample processing, will have a less defined background and signal component is not true. The distinction between the $D_e$ values for the bulk sampling and the MET sampling is not simply defined and instead the samples each found unique issues of signal identification.

The rejection rate was varied although this can be attributed to the individual assessment of the discs. Regarding samples with minimal accepted discs, the minimum of 20 discs was not achieved for all samples. In the case of LHS12, 19 discs were accepted which is close enough to deem acceptable. LHS24, which had an insufficient sample for more than 12 discs with 11 accepted discs is still being assessed owing to the importance of the comparative nature of LHS24 and its MET counterpart LHS24MET. In the studies by Sánchez *et al.* (2008) and Zou *et al.* (2018), ages were accepted with less than 10 accepted aliquots for ceramic samples. Consideration to the validity of an age has not been made strictly on a threshold criterion but instead by reviewing the data obtained through the measurements of the $D_e$ and sample by sample basis.

For LHS40a and LHS40c, the sampling of the MET method needs to be taken into account. With all other MET sampling, two holes were made for each ceramic and considered a single sample. The aim of the testing of LHS40 was to establish the variations within a pot and see how viable the multiple sampling technique was. The result was that LHS40a-d were single drilled holes per sample and thus the extracted material is essentially halved. Thus, the leeway for these samples and the accepted discs should make the samples viable. In Hood *et al.* (2019), a maximum 18 aliquots per sample were produced using the MET method. While the accepted

aliquots were less than 6, the exception being a single sample that had 11 accepted aliquots (Hood *et al.*, 2019).

The $D_e$ was determined through the use of the central age model (CAM) (Galbraith *et al.*, 1999), arithmetic mean (AM) and additive dose model (ADM) (Guérin *et al.*, 2017). In comparison, the CAM and ADM showed the most promising $D_e$ results. The results are shown in Table 4.4, with the models displaying similar outcomes in terms of the $D_e$. The CAM and ADM $D_e$ show the highest similarity with the AM providing slight variations. The issue arose with the error of the AM results. The AM is unweighted in comparison to the CAM and ADM results. The error in the AM is large enough that when combined with the $D_R$ results, the age spans several centuries. The conclusion is that although the AM is useful in determining the age, the error for these samples makes the model invalid for this research.

The final ages are considered the most important aspect of the project. Although one cannot ignore the importance of the means in which the ages were determined, the final determination of timeframe is the key aim of the project. The graphic in Figure 5.1 shows the information of the OSL ages as well as the ranges of the facies and the radiocarbon ages from LHS. The graphic can be used to allow easier visualisation of data during the discussion of the final ages.

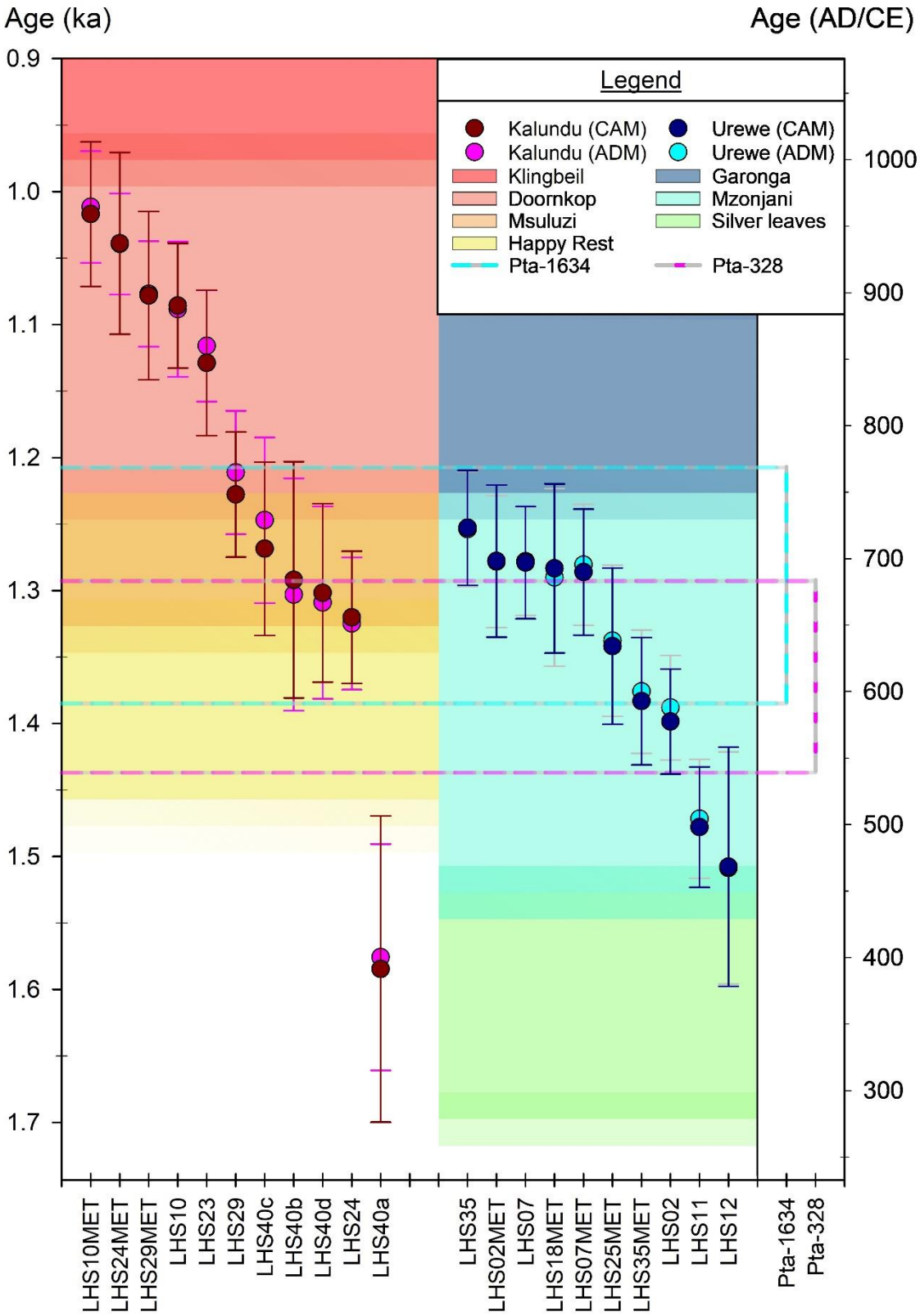


Figure 5.1. All OSL ages including the CAM and ADM ages. Demarcation of the general range of the different facies for the Kalundu and Urewe traditions, and the radiocarbon recalibrated ages for LHS.

The Urewe tradition at Lydenburg Heads is a variation of Mzonjani (Whitelaw 1996), from whom Doornkop was formed through interaction with Happy Rest communities (Huffman and Schoeman, 2011; Schoeman, 2020). Although, based on the similarities of the Mzonjani facies and the other facies within the early Urewe tradition, one can assume a degree of misidentification. The Mzonjani facie has an assumed timeframe of 450 – 750 AD (Mitchell and Whitelaw, 2005; Huffman, 2007; Schoeman, 2020). The OSL ages are similar to this range. It, however, is possible that the assemblage included transitional expressions of this tradition.

The oldest Urewe sample is LHS12, CAM age of 1.51 ± 0.09 ka (468 ± 90 AD) and an ADM age of 1.51 ± 0.09 ka (467 ± 87 AD). The sample is shown to have a relatively large error compared to the other Urewe samples, with an error almost double most other samples in the facie. Its age is in the mid-5$^{th}$ century AD, although the error allows the age to extend from the late 4$^{th}$ to the early 6$^{th}$ century AD. Within the same pit is LHS11, another older Urewe sample. The sample is placed in the late 5$^{th}$ and early 6$^{th}$ century AD. Although the ages of both samples should be considered in the dating of the site, one must consider that LHS12 had a small amount of sample post processing and thus had fewer aliquots to review (with only 19 accepted discs). The ages of the pottery within pit 12 can thus be considered likely between the 5$^{th}$ and 6$^{th}$ centuries AD.

The samples of LHS02, LHS02MET, LHS35, LHS35MET, and LHS25MET are best reviewed together, not only because they all share a location (pit 10) but also because of the observations of the trends within them. Firstly, pit 10 should be noted as the pit furthest from other observed pits (Figure 2.3). Pit 10 is located near the donga and the furthest from the stream. The pit is the closest to the find site of the Lydenburg Heads (located southwest to pit 10). The samples of LHS02 and LHS35MET are the younger samples, with ages that place them in the 6$^{th}$/7$^{th}$ century AD. In comparison the counterparts to these samples (LHS02MET and LHS35) provide 7$^{th}$/8$^{th}$ century AD ages. In interpreting the sample, LHS25MET gives additional information on the possible ages of the pit 10 ceramics.

LHS25MET was dated to the 7th century AD, providing the common age for the pit. Further issues arise within pit 10 owing to the ambiguity of whether the ceramics are truncated or eroded from Kalundu pits. Seeing as not all samples are decorated and were attributed to a ceramic tradition through locality (pit), the issue of vertical displacement and incorrect identification is present.

The samples of LHS07, LHS07MET and LHS18MET are the most uniform in terms of age. All three samples show an age of the late 7th – early 8th century AD. In comparing LHS07 and LHS07MET, one cannot miss that they are the closest MET and bulk sampling pair within the whole project. This raises the question of why these samples displayed a very successful method of producing ages in both methods. The location of drilling was not within the same region of the ceramics, although as a smaller sherd, the movement from one side to the other may not be exactly a different region of the sherd. The overall age of the Urewe pottery technically spans from the 4th to the 8th centuries AD. Although considering trends within the ceramics and devaluing the more dubious data, the OSL ages trend towards the 6th and 8th centuries AD.

The Kalundu ceramics at the LHS have been identified as the Doornkop facies (Whitelaw, 1996; Becher, 2021). Although, similarly to the Urewe samples, the exact facie is difficult to determine owing to stylistic similarities within the Kalundu tradition. The Doornkop facie (previously named the Lydenburg facie) is considered the result of the interactions between Happy Rest and Mzonjani pottery makers (Huffman and Schoeman, 2011; Schoeman, 2020). The dates for the Doornkop facie range from 750 - 1000 AD (Huffman, 2007; Huffman *et al.*, 2020; Schoeman, 2020).

Firstly, one should compare the ages of the multi-sample ceramic. The relationship of the drill sites and the produced ages can be seen in Figure 5.2. In relation to what the sites are showing is that LHS40a shows measurements on the rim of the sherd, LHS40b shows the measurements below the everted rim, LHS40c the body of the

ceramic and LHS40d the base of the pot. The differential heating and the resultant age variations are evident from the results of sample LHS40. The measurements for LHS40a showed the largest error and considered the least likely ages for the Kalundu ceramics. The age placed the pot in the 3rd to 6th century AD, much younger than all other data (OSL, $^{14}C$ and ceramic sequence). The samples of LHS40b-d show more promising results with the addition of centring around a possible age in the 7th and 8th century AD. Based on the ages and the other elements (the OD- see Table 4.9) the most accurate location for the MET method would be the base or more accurately the body of the pot. The results are justifiable owing to the assumption that these pots were used on an open flame and thus experienced post-production anomalous heating.

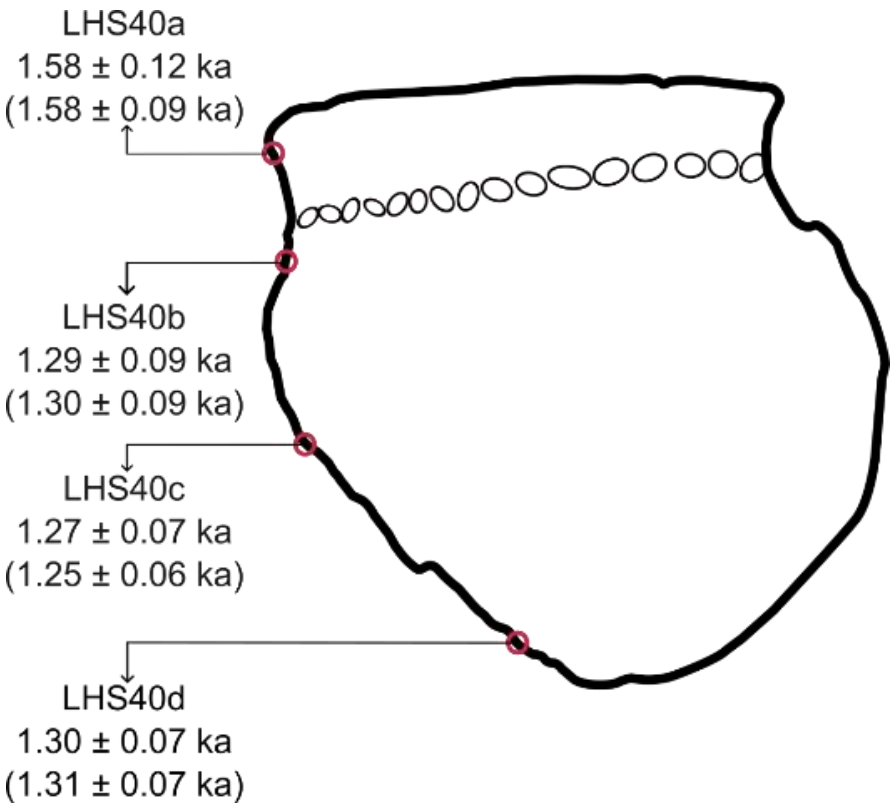


Figure 5.2. LHS40 ages in comparison to location on ceramic. The ages are shown as the CAM age with the ADM age in brackets below.

Within the same pit as the LHS40 samples (pit 5), the samples LHS10, LHS10MET, LHS24 and LHS24MET can be found. The samples of LHS24 first need to be considered similarly inaccurate as LHS40a. LHS24 experienced an extensive reduction of sample in the sample processing and thus was not sufficient to produce more than 12 aliquots. The comparison to the likely age and the MET counterpart displayed a lower error and a more reliable age. The LHS24 age is thus rejected owing to insufficient data but can be considered a comparative data point for the MET and bulk sampling processes. The samples of LHS10 and LHS10MET provided ages in the 9$^{th}$ and 10$^{th}$ centuries, although it is important to note that the error slightly puts LHS10MET into the first 10 years of the second millennium. The combined information of all the samples in pit 5, without analysis, says that the pottery dates from the 3$^{rd}$ to the 11$^{th}$ century AD. However, when removing the rejected and the less reliable samples, the age tends towards the late 7$^{th}$ to 10$^{th}$ centuries.

The final samples are that of LHS23, LHS29, and LHS29MET, which show trends towards the 8$^{th}$ to 10$^{th}$ century AD. A note on the sample LHS29 and the MET counterpart: the ages are surprisingly varied with no overlap in ages. LHS29 had the highest rejection rate of discs (Table 4.3), suggesting that possibly the sampling site was not the most accurate choice for obtaining quartz.

## 5.3 Occupation phases of the ceramic tradition

The Kalundu ceramics showed a higher variability than that of the Urewe samples. However, through a review of the ages, the Kalundu occupation can be placed in the 7$^{th}$ to 10$^{th}$ century AD. Allowing a variation in facies and misidentification, the OSL ages demonstrate that there is a Urewe layer with a subsequent Kalundu layer. While the ages show that there is a possibility that the occupations overlapped.

The Urewe ceramics from the site are dated to the originally assumed dates of the 6$^{th}$ to 8$^{th}$ century AD. The Urewe ages are easily associated with the radiocarbon

results of 592-769 AD (Pta-1634) and 540-684 AD (Pta-328). Although important to date the Urewe and Kalundu ceramics, the issues of OSL dating a complex and ambiguous site does pose risks. In this light the uniform method of dating both the Kalundu and Urewe ceramics in the same manner makes them comparable. In conjunction the similarity of the Urewe ceramics ages with the ceramic sequence and the radiocarbon results provide a more reliable age. The relationship of the LHS chronology produced is compared to other sites or ages of interest in Figure 5.3.

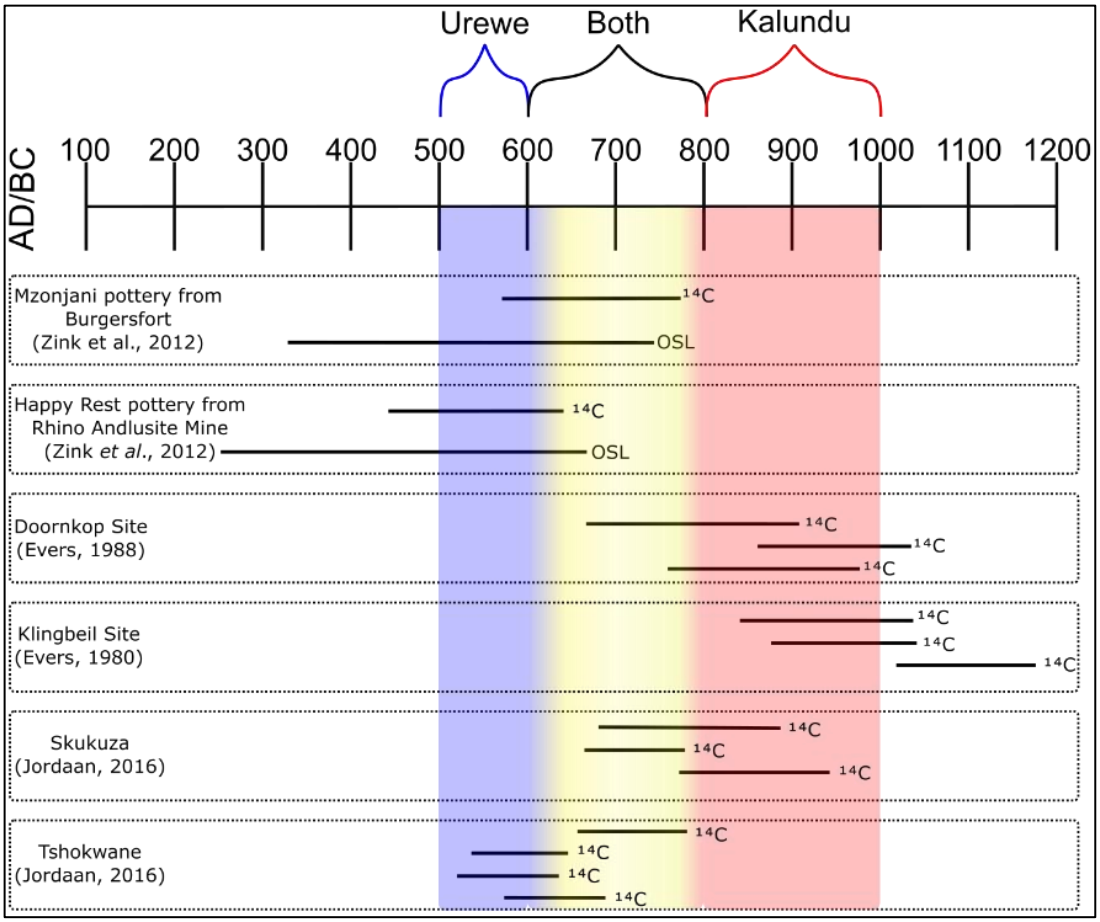


Figure 5.3. Timeline of occupation compared to other OSL ages and $^{14}C$ ages.

The OSL ages produced by Zink *et al.* (2012) for ceramics belonging to the Happy Rest and Mzonjani facies, show an overlap with the Urewe and dual occupation of the LHS. Although these ages display a larger error and thus range as possibly older (Zink *et al.*, 2012).

The radiocarbon dates from the Doornkop and Klingbeil sites (see Figure 2.6 for their locations and Figure 4.2 for recalibration) show possible occupation during a similar time to the LHS dual and Kalundu occupation periods (Figure 5.3). Although the ages from Klingbeil and Doornkop extend to the second millennium, while LHS has no ages to suggest occupation within that period. The Skukuza site, in the Kruger National Park, shows purely first millennium ages that occur at the same time of the dual and Kalundu ages from the LHS. While the other Kruger National Parks site, Tshokwane, has ages similar to the Urewe and dual occupation of LHS.

The importance of understanding the Mpumalanga sequence is that the production of assemblages is not discreet, as a result the creation and deposition of assemblages and artefacts should been seen as continuous and interconnected (spatially and temporally). The existence of the Doornkop facie provides the evidence of interaction between ceramic traditions, although the date or means of which the interaction occurred is unknown. The ages of the ceramics do not prove or disprove the possible facie the ceramic belongs to but instead that the pottery was produced by two groups of peoples that interacted. In regard to the Mpumalanga sequence, the ages of the Kalundu ceramics from LHS provide an interesting context to contemplate the origin of the Doornkop ceramics.

# CHAPTER 6 – CONCLUSIONS

## 6.1 Summary of findings

Dating ceramics with the technique of optically stimulated luminescence dating allows the direct dating of the production of cultural materials. Regarding the process of OSL dating, two methods of sample extraction were employed. The use of the minimal extraction technique (MET) allowed the dating with the reduced destruction of the ceramics (Hood and Schwenninger, 2015; Hood, 2022). The technique incorporates a reduced processing time and allows the dating of museum pieces that require structural integrity to be maintained. The bulk sampling allowed the comparison of the technique with MET, as well as the means to justify the dating of the ceramics at Lydenburg Heads Site.

The overarching aim of the research was to determine whether the Kalundu and Urewe occupations of the Lydenburg Heads Site were sequential or contemporaneous. The methods of which they were determined holds importance to the progression of dating materials that cannot be destroyed, although the technique is the most viable in regions with multiple sampling abilities. The result is the recommendation that the MET be used within a comparison situation to provide the best results.

The ages of the ceramics tended towards the typology and radiocarbon facilitated dates. The OSL ages for the Urewe tradition ceramics closely align with the originally assumed ages of the 6$^{th}$ to 8$^{th}$ century AD. The ages are further shown to be associated with the radiocarbon ages from the site, while the Kalundu tradition ceramics were considerably older than originally hypothesised. The ages of the 7$^{th}$ to 10$^{th}$ century AD are thus shown to have a potential overlapping occupation of the two traditions. The results of the ages show an important juncture in the

Mpumalanga ceramic sequence. The Kalundu and Urewe presence in the Lydenburg Heads Site at the same time provides interest to the beginning of the Doornkop facie. Although considering the site in isolation from the rest of the sequence, observations show that the site was likely occupied for over 400 years. The site and the find of the terracotta heads should be considered important for further research.

There are multiple means to date archaeological sites. The recalibrated radiocarbon ages for the LHS provide ages that correlate well with the ages produced through OSL dating. While radiocarbon and OSL dating give ages for different events, the connection between absolute and relative dating techniques (typology seriation), is important in extending the understanding of the EFCs. The ability to date every ceramic or site using OSL and radiocarbon dating is impossible, while the production of chronologies and the comparative analysis between dating techniques allows broader understanding.

## 6.2 Limitations of study and recommendation for future research

The major limitation to the study was the limited information of the context of the ceramics. The inability to access the site restricted observations that would have allowed increased accuracy to the environmental dose rate. The means for tackling the in-situ context and dosimetry ambiguity, had a site visit been possible, could have entailed the use of high-resolution gamma spectrometry or a thermoluminescence dosimetry (TLD) device that remain in situ for a period of time, measuring the dosimetry.

The ceramics were received in a box, thus there are unknown effects of location of storage or alterations since excavation. The limitations to the assessment of the MET involve the lack of dosimetry measurements from the MET drill site. While each ceramic had direct dosimetry measurements, the testing of the MET applicability to southern Africa's EFC ceramics is limited in that regard.

Considering the work provided the OSL ages for a selection of ceramics within the site, further work would benefit from dating a larger portion of the ceramics to provide a clearer picture of the occupation periods. Consideration should be given to dating the already reviewed ceramics by Becher (2021) and Becher *et al.* (2024) to provide the deeper insight of the site. The result would be the ages of production of ceramics and the possible uses of said ceramics, which allows a complex review of the occupation of the site.

Regarding the MET technique and the application to the EFC of South Africa, the dating of the surrounding area and ceramics could allow an extension of research. The means of being able to date ceramics without destruction allows the range of artefacts to be increased significantly. The terracotta heads found within the site, owing to their significance, could benefit from the MET dating once the technique and method has been refined further. The dating of ceramics opposed to sediment using OSL techniques has proven beneficial to providing direct ages in which to create a chronology. Having done so, the sequence can be reviewed through a particular dating technique and means, possibly allowing the clarification of the entire sequence.

# REFERENCE LIST


Aitken, M.J., 1998. An Introduction to Optical Dating: The Dating of Quaternary Sediments by the Use of Photon-Stimulated Luminescence. Oxford University Press Inc, New York.

Aitken, M.J., 1989. Luminescence dating: a guide for non-specialists. Archaeometry 31, 147–159.

Aitken, M.J. 1985. Thermoluminescence dating. Academic Press, London.

Aitken, M.J. and Xie, J., 1990. Moisture correction for annual gamma dose. Ancient TL 8, 6–9.

al Khasawneh, S., Murray, A., Kafafi, Z. and Petit, L., 2019. Luminescence dating of the Iron Age deposits from Tell Damiyah in the Jordan Valley. Radiocarbon 62, 1–12. https://doi.org/10.1017/RDC.2019.90

Anderson, S.L. and Feathers, J.K., 2019. Applying luminescence dating of ceramics to the problem of dating Arctic archaeological sites. Journal of Archaeological Science 112, 105030. https://doi.org/10.1016/j.jas.2019.105030

Antonites, A., 2016. The organization of salt production in early first millennium CE South Africa. Journal of Anthropological Archaeology 44, 31–42. https://doi.org/10.1016/j.jaa.2016.08.001

Antonites, A., 2013. Archaeological salt production at the Baleni Spring, Northeastern South Africa. South African Archaeological Bulletin 68, 105–118.

Antonites, A., Antonites, A.R., Kruger, N. and Roodt, F., 2014. Report on excavations at Penge, a first-millennium Doornkop settlement. Southern African Humanities 26, 177–192. https://doi.org/10.10520/EJC161786

Arnold, J.R. and Libby, W.F., 1949. Age Determinations by Radiocarbon Content: Checks with Samples of Known Age. Science 110, 678–680.

Arnold, L.J., Demuro, M., Parés, J.M., Pérez-González, A., Arsuaga, J.L., Bermúdez de Castro, J.M. and Carbonell, E., 2015. Evaluating the suitability of extended-range luminescence dating techniques over early and Middle Pleistocene timescales: Published datasets and case studies from Atapuerca, Spain. Quaternary International 389, 167–190. https://doi.org/10.1016/j.quaint.2014.08.010

Ashley, C.Z., 2010. Towards a Socialised Archaeology of Ceramics in Great Lakes Africa. African Archaeological Review 27, 135–163. https://doi.org/10.1007/s10437-010-9074-0

Ashley, C.Z. and Grillo, K.M., 2015. Archaeological ceramics from eastern Africa: Past approaches and future directions. Azania 50, 460–480. https://doi.org/10.1080/0067270X.2015.1102939

Avery, G., Halkett, D., Orton, J., Steele, T., Tusenius, M. and Klein, R.G., 2008. The Ysterfontein 1 Middle Stone Age rock shelter and the evolution of coastal foraging. Goodwin Series 10, 66–89.

Banerjee, D., Murray, A.S., Bøtter-Jensen, L. and Lang, A., 2001. Equivalent dose estimation using a single aliquot of polymineral fine grains. Radiation Measurements 33, 73–94. https://doi.org/10.1016/S1350-4487(00)00101-3

Becher, J., 2021. Reconstructing vessel use at Lydenburg Heads site, South Africa, using GC-MS and GC-c-IRMS (MA Thesis). Universität Tübingen.

Becher, J., Schoeman, A., Whitelaw, G., Buckley, S., Celliers, J.-P., Cafisso, S., Belser, M., Rageot, M. and Spiteri, C., 2024. Multi-purpose pots: Reconstructing early farmer behaviour at Lydenburg Heads site, South Africa, using organic residue analysis. Journal of Archaeological Science 161, 105894. https://doi.org/10.1016/j.jas.2023.105894

Bell, W.T., 1980. Alpha dose attenuation in quartz grains for thermoluminescence dating. Ancient TL 12, 4–8.

Bell, W.T., 1979. Attenuation factors for the absorbed radiation dose in quartz inclusions for thermoluminescence dating. Ancient TL 8, 2–13.

Botha, G. and Porat, N., 2007. Soil chronosequence development in dunes on the southeast African coastal plain, Maputaland, South Africa. Quaternary International 162–163, 111–132. https://doi.org/10.1016/j.quaint.2006.10.028

Bøtter-Jensen, L., Bulur, E., Duller, G.A.T. and Murray, A.S., 2000. Advances in luminescence instrument systems. Radiation Measurements 32, 523–528. https://doi.org/10.1016/S1350-4487(00)00039-1

Bøtter-Jensen, L., Thomsen, K.J., and Jain, M., 2010. Review of optically stimulated luminescence (OSL) instrumental developments for retrospective dosimetry. Radiation Measurements 45, 253–257. https://doi.org/10.1016/j.radmeas.2009.11.030

Bøtter-Jensen, L. and Mejdahl, V., 1988. Assessment of beta dose-rate using a GM multicounter system. International Journal of Radiation Applications and Instrumentation. Part D. Nuclear Tracks and Radiation Measurements 14, 187–191. https://doi.org/10.1016/1359-0189(88)90062-3

Brennan, B.J., 2003. Beta doses to spherical grains. Radiation Measurements 37, 299–303. https://doi.org/10.1016/S1350-4487(03)00011-8

Burow, C., 2023. calc_CentralDose(): Apply the central age model (CAM) after Galbraith *et al.* (1999) to a given De distribution. Function version 1.4.1., in: Luminescence: Comprehensive Luminescence Dating Data Analysis. R Package Version 0.9.23.

Burrett, R.S., 2007. The Garonga ceramic assemblage. Southern African Humanities 19, 153–166. https://doi.org/10.10520/EJC84785

Carr, A.S., Bateman, M.D. and Holmes, P.J., 2007. Developing a 150ka luminescence chronology for the barrier dunes of the southern Cape, South Africa. Quaternary Geochronology 2, 110–116. https://doi.org/10.1016/j.quageo.2006.09.002

Caton-Thompson, G., 1931. The Zimbabwe Culture. Ruins and Reactions. Clarendon Press, Oxford.

Christophe, C., Philippe, A. and Kreutzer, S., 2023. calc_AverageDose(): Calculate the Average Dose and the dose rate dispersion. Function version 0.1.5, in: Luminescence: Comprehensive Luminescence Dating Data Analysis. R Package Version 0.9.23.

Copley, M., Hansel Fabricio A., Sadr Karim, and Evershed Richard P., 2004. Organic residue evidence for the processing of marine animal products in pottery vessels from the pre-colonial archaeological site of Kasteelberg D east, South Africa : research article. South African Journal of Science 100, 279–283. https://doi.org/10.10520/EJC96255

Coutu, A.N., Taurozzi, A.J., Mackie, M., Jensen, T.Z.T., Collins, M.J. and Sealy, J., 2021. Palaeoproteomics confirm earliest domesticated sheep in southern Africa ca. 2000 BP. Scientific Reports 11, 6631. https://doi.org/10.1038/s41598-021-85756-8

Cresswell, A.J., Carter, J. and Sanderson, D.C.W., 2018. Dose rate conversion parameters: Assessment of nuclear data. Radiation Measurements 120, 195–201. https://doi.org/10.1016/j.radmeas.2018.02.007

Cunningham, A.C. and Wallinga, J., 2010. Selection of integration time intervals for quartz OSL decay curves. Quaternary Geochronology 5, 657–666. https://doi.org/10.1016/j.quageo.2010.08.004

Degano, I., Soriano, S., Villa, P., Pollarolo, L., Lucejko, J.J., Jacobs, Z., Douka, K., Vitagliano, S. and Tozzi, C., 2019. Hafting of Middle Paleolithic tools in Latium (central Italy): New data from Fossellone and Sant'Agostino caves. PLOS ONE 14, e0213473. https://doi.org/10.1371/journal.pone.0213473

Denbow, J. and Wilmsen, E.N., 2023. Iron Age sites in northern Botswana's Okavango Delta 1: the southern Delta sites Mat82 and Matlapaneng plus Qogana on the region's eastern margin. Azania 58, 34–73. https://doi.org/10.1080/0067270X.2023.2182563

Dietze, M., Kreutzer, S., Burow, C., Fuchs, M.C., Fischer, M. and Schmidt, C., 2016. The abanico plot: Visualising chronometric data with individual

standard errors. Quaternary Geochronology 31, 12–18. https://doi.org/10.1016/j.quageo.2015.09.003

Dörschner, N., Reimann, T., Wenske, D., Lüthgens, C., Tsukamoto, S., Frechen, M. and Böse, M., 2012. Reconstruction of the Holocene coastal development at Fulong Beach in north-eastern Taiwan using optically stimulated luminescence (OSL) dating. Quaternary International 263, 3–13. https://doi.org/10.1016/j.quaint.2011.12.009

Duller, G.A.T., 2015. The Analyst software package for luminescence data: overview and recent improvements. Ancient TL 33, 35–42.

Duller, G.A.T., 2004. Luminescence dating of quaternary sediments: recent advances. Journal of Quaternary Science 19, 183–192. https://doi.org/10.1002/jqs.809

Duller, G.A.T., 2003. Distinguishing quartz and feldspar in single grain luminescence measurements. Radiation Measurements 37, 161–165. https://doi.org/10.1016/S1350-4487(02)00170-1

Dunne, J., Grillo, K.M., Casanova, E., Whelton, H.L. and Evershed, R.P., 2019. Pastoralist Foodways Recorded in Organic Residues from Pottery Vessels of Modern Communities in Samburu, Kenya. Journal of Archaeological Method and Theory 26, 619–642. https://doi.org/10.1007/s10816-018-9384-0

Evans, M., 2016. The geology, sedimentology, geochronology and palaeo-environmental reconstruction of the Heelbo hillslope deposit, Free State Province, South Africa (PhD). University of the Witwatersrand.

Evers, T.M., 1988. The recognition of groups in the Iron Age of southern Africa (PHD). University of the Witwatersrand.

Evers, T.M., 1982a. Excavations at the Lydenburg Heads Site, Eastern Transvaal, South Africa. The South African Archaeological Bulletin 37, 16–33. https://doi.org/10.2307/3888577

Evers, T.M., 1982b. Two Later Iron Age Sites on Mabete, Hans Merensky Nature Reserve, Letaba District, N. E. Transvaal. The South African Archaeological Bulletin 37, 63–67. https://doi.org/10.2307/3888677

Evers, T.M., 1980. Klingbeil Early Iron Age Sites, Lydenburg, Eastern Transvaal, South Africa. The South African Archaeological Bulletin 35, 46–57. https://doi.org/10.2307/3888725

Evers, T.M., 1977. Recent progress in studies of the early iron age in the Eastern Transvaal, South Africa. South African Journal of Science 73, 78. https://doi.org/10.10520/AJA00382353_6105

Evers, T.M., 1975. Recent Iron Age Research in the Eastern Transvaal, South Africa. The South African Archaeological Bulletin 30, 71–83. https://doi.org/10.2307/3888096

Evers, T.M., 1974. Iron Age Trade in the Eastern Transvaal, South Africa. The South African Archaeological Bulletin 29, 33–37. https://doi.org/10.2307/3887936

Evers, T.M., Huffman, T.N. and Wandibba, S., 1988. On Why Pots Are Decorated the Way They Are. Current Anthropology 29, 739–741.

Evers, T.M. and Vogel, J.C., 1980. Radiocarbon Dates for Iron Age Sites at Lydenburg and White River, Eastern Transvaal. South African Journal of Science 76, 230–231. https://doi.org/10.10520/AJA00382353_1784

Fain, J., Soumana, S., Montret, M., Miallier, D., Pilleyre, T., Sanzelle, S., 1999. Luminescence and ESR dating Beta-dose attenuation for various grain shapes calculated by a Monte-Carlo method. Quaternary Science Reviews 18, 231–234. https://doi.org/10.1016/S0277-3791(98)00056-0

Feathers, J.K., 2003. Use of luminescence dating in archaeology. Measurement Science and Technology 14, 1493. https://doi.org/10.1088/0957-0233/14/9/302

Feathers, J.K., Evans, M., Stratford, D.J. and de la Peña, P., 2020. Exploring complexity in luminescence dating of quartz and feldspars at the Middle

Stone Age site of Mwulu's cave (Limpopo, South Africa). Quaternary Geochronology 59, 101092. https://doi.org/10.1016/j.quageo.2020.101092

Fewlass, H., Mitchell, P.J., Casanova, E. and Cramp, L.J.E., 2020. Chemical evidence of dairying by hunter-gatherers in highland Lesotho in the late first millennium ad. Nature Human Behaviour 4, 791–799. https://doi.org/10.1038/s41562-020-0859-0

Fouché, L., 1937. Mapungubwe, ancient Bantu civilization on the Limpopo; reports on excavations at Mapungubwe (Northern Transvaal) from February 1933 to June 1935. Cambridge University Press, Oxford.

Fowler, K.D., 2006. Classification and collapse: the ethnohistory of Zulu ceramic use. Southern African Humanities 18, 93–117.

Fredriksen, P.D., 2023. Ceramics and Archaeology in Southern Africa. https://doi.org/10.1093/acrefore/9780190277734.013.811

Fuchs, M. and Lang, A., 2009. Luminescence dating of hillslope deposits—A review. Geomorphology 109, 17–26. https://doi.org/10.1016/j.geomorph.2008.08.025

Galbraith, R., Roberts, R.G., Laslett, G.M., Yoshida, H. and Olley, J.M., 1999. Optical dating of single and multiple grains of quartz from Jinmium rock shelter, northern Australia: Part I, experimental design and statistical models. Archaeometry 41, 339–364. https://doi.org/10.1111/j.1475-4754.1999.tb00987.x

Galbraith, R.F., Roberts, R.G. and Yoshida, H., 2005. Error variation in OSL palaeodose estimates from single aliquots of quartz: a factorial experiment. Radiation Measurements 39, 289–307. https://doi.org/10.1016/j.radmeas.2004.03.023

Galbraith, R.F., and Roberts, R.G., 2012. Statistical aspects of equivalent dose and error calculation and display in OSL dating: An overview and some recommendations. Quaternary Geochronology 11, 1–27. https://doi.org/10.1016/j.quageo.2012.04.020

Gardner, G.A., 1963. Mapungubwe. v. 2, Report on excavations at Mapungubwe and Bambandyanalo in Northern Transvaal from 1935 to 1940. Van Schaik, Pretoria.

Grollemund, R., Schoenbrun, D. and Vansina, J., 2023. Moving Histories: Bantu Language Expansions, Eclectic Economies, and Mobilities. The Journal of African History 64, 13–37. https://doi.org/10.1017/S0021853722000780

Grün, R., 1987. Alpha dose attenuation in thin layers. Ancient TL 5, 6–8.

Guérin, G., Mercier, N., Nathan, R., Adamiec, G. and Lefrais, Y., 2017. On the use of the infinite matrix assumption and associated concepts: A critical review. Radiation Measurements, 47, 778-785.

Guérin, G., Christophe, C., Philippe, A., Murray, A.S., Thomsen, K.J., Tribolo, C., Urbanova, P., Jain, M., Guibert, P., Mercier, N., Kreutzer, S. and Lahaye, C., 2017. Absorbed dose, equivalent dose, measured dose rates, and implications for OSL age estimates: Introducing the Average Dose Model. Quaternary Geochronology 41, 163–173. https://doi.org/10.1016/j.quageo.2017.04.002

Hahn, A., Compton, J.S., Meyer-Jacob, C., Kirsten, K.L., Lucasssen, F., Pérez Mayo, M., Schefuß, E. and Zabel, M., 2016. Holocene paleo-climatic record from the South African Namaqualand mudbelt: A source to sink approach. Quaternary International 404, 121–135. https://doi.org/10.1016/j.quaint.2015.10.017

Hall, S., 2015. Talking Heads. Digging stick, 32 (1), 1-4.

Hall, S., 1992. The First South Africans. The Phoenix 5, 11–19.

Han, M., Kim, J.C., Yang, D.Y., Lim, J. and Yi, S., 2021. The main periods and environmental controls of coastal dune development along the west coast of the Korean Peninsula during the mid to late Holocene. Palaeogeography, Palaeoclimatology, Palaeoecology 569, 110345. https://doi.org/10.1016/j.palaeo.2021.110345

Hogg, A.G., Heaton, T.J., Hua, Q., Palmer, J.G., Turney, C.S., Southon, J., Bayliss, A., Blackwell, P.G., Boswijk, G., Bronk Ramsey, C., Pearson, C., Petchey,

F., Reimer, P., Reimer, R. and Wacker, L., 2020. SHCal20 Southern Hemisphere Calibration, 0–55,000 Years cal BP. Radiocarbon 62, 759–778. https://doi.org/10.1017/RDC.2020.59

Hogg, A.G., Hua, Q., Blackwell, P.G., Niu, M., Buck, C.E., Guilderson, T.P., Heaton, T.J., Palmer, J.G., Reimer, P.J., Reimer, R.W., Turney, C.S.M. and Zimmerman, S.R.H., 2013. SHCal13 Southern Hemisphere Calibration, 0–50,000 Years cal BP. Radiocarbon 55, 1889–1903. https://doi.org/10.2458/azu_js_rc.55.16783

Hood, A.G.E., 2022. Methods Note: The extended minimum extraction technique: an update on sampling protocols. Ancient TL 40, 8–10.

Hood, A.G.E., Köhler, E.C., Highcock, E.G. and Schwenniger, J.-L., 2019. Luminescence as a Relative Dating Tool: Part B – Application. Ancient TL 37, 14–20.

Hood, A.G.E. and Schwenniger, J.-L., 2016. Optically stimulated luminescence (OSL) dating and its application to ancient Egyptian ceramics in the 21st Century. Vienna II: Ancient Egyptian Ceramics in the 21st Century, pp. 287–298.

Hood, A.G.E. and Schwenninger, J.-L., 2015. The minimum extraction technique: A new sampling methodology for optically stimulated luminescence dating of museum ceramics. Quaternary Geochronology 30, 381–385. https://doi.org/10.1016/j.quageo.2015.06.007

Huffman, T.N., 2021. Bambata Pottery and Western Bantu: re-interpreting the Early Iron Age in southern Africa. Southern African Humanities 34, 1-1–17.

Huffman, T.N., 2007. Handbook to the Iron Age: The Archaeology of Pre-Colonial Farming Societies in Southern Africa. University of KwaZulu-Natal Press, Scottsville, South Africa.

Huffman, T.N., 1989. Ceramics, Settlements and Late Iron Age Migrations. The African Archaeological Review 7, 155–182.

Huffman, T.N., 1982. Archaeology and Ethnohistory of the African Iron Age. Annual Review of Anthropology 11, 133–150.

Huffman, T.N., 1970. The Early Iron Age and the Spread of the Bantu. The South African Archaeological Bulletin 25, 3–21. https://doi.org/10.2307/3888762

Huffman, T.N. and Schoeman, M.H., 2011. Lebalelo: Early Iron Age Pits near Burgersfort, South Africa. The South African Archaeological Bulletin 66, 161–166.

Huffman, T.N., Whitelaw, G., Tarduno, J.A., Watkeys, M.K. and Woodborne, S., 2020. The Rhino Early Iron Age site, Thabazimbi, South Africa. Azania: Archaeological Research in Africa 55, 360–388. https://doi.org/10.1080/0067270X.2020.1792196

Hua, Q., 2009. Radiocarbon: A chronological tool for the recent past. Quaternary Geochronology 4, 378–390. https://doi.org/10.1016/j.quageo.2009.03.006

Inskeep, R.R., 1971. Letters to the editor. South African Journal of Science 67, 492–493. https://doi.org/10.10520/AJA00382353_9729

Inskeep, R.R. and Maggs, T., 1975. Unique Art Objects in the Iron Age of the Transvaal, South Africa. The South African Archaeological Bulletin 30, 114–138. https://doi.org/10.2307/3888099

Jacobs, Z., 2010. An OSL chronology for the sedimentary deposits from Pinnacle Point Cave 13B—A punctuated presence. Journal of Human Evolution 59, 289–305. https://doi.org/10.1016/j.jhevol.2010.07.010

Jordaan, G., 2016. An archaeological study of two Early Farming sites in the Kruger National Park, South Africa (MA Thesis). University of Pretoria.

Kigoshi, K., Tomikura, Y. and Endo, K., 1962. Gakushuin Natural Radiocarbon Measurements I. Radiocarbon 4, 84–94. https://doi.org/10.1017/S0033822200036547

Klatzow, S., 2010. Interaction between Hunter-Gatherers and Bantu-Speaking Farmers in the Eastern Free State: A Case Study from De Hoop Cave. South

African Historical Journal 62, 229–251. https://doi.org/10.1080/02582473.2010.493000

Kuper, A., 1980. Symbolic Dimensions of the Southern Bantu Homestead. Africa: Journal of the International African Institute 50, 8–23. https://doi.org/10.2307/1158639

Lamothe, M., 2016. Luminescence dating of interglacial coastal depositional systems: Recent developments and future avenues of research. Quaternary Science Reviews 146, 1–27. https://doi.org/10.1016/j.quascirev.2016.05.005

Lamothe, M., Forget Brisson, L. and Hardy, F., 2018. Dose recovery performance in double IRSL/pIRIR SAR protocols. Radiation Measurements 120, 120–123. https://doi.org/10.1016/j.radmeas.2018.05.003

Lander, F. and Russell, T., 2020. A southern African archaeological database of organic containers and materials, 800 cal BC to cal AD 1500: Possible implications for the transition from foraging to livestock-keeping. PLOS ONE 15, e0235226. https://doi.org/10.1371/journal.pone.0235226

Lander, F. and Russell, T., 2018. The archaeological evidence for the appearance of pastoralism and farming in southern Africa. PLOS ONE 13, e0198941. https://doi.org/10.1371/journal.pone.0198941

Lian, O.B. and Roberts, R.G., 2006. Dating the Quaternary: progress in luminescence dating of sediments. Quaternary Science Reviews 25, 2449–2468. https://doi.org/10.1016/j.quascirev.2005.11.013

Loftus, E., Mitchell, P.J. and Bronk Ramsey, C., 2019. An archaeological radiocarbon database for southern Africa. Antiquity 93, 870–885. https://doi.org/10.15184/aqy.2019.75

Loubser, J.H.N., 1993. Ndondondwane: the significance of features and finds from a ninth-century site on the lower Thukela River, Natal. Natal Mus. J. Humanities 5, 109–151.

Maggs, T., 1993. Three Decades of Iron Age Research in South Africa: Some Personal Reflections. The South African Archaeological Bulletin 48, 70–76. https://doi.org/10.2307/3888944

Maggs, T., 1992. Name Calling in the Iron Age. The South African Archaeological Bulletin 47, 131–131. https://doi.org/10.2307/3889212

Maggs, T., 1980. Msuluzi Confluence: a seventh century Early Iron Age site on the Tugela River. Southern African Humanities 24, 111–145.

Maggs, T. and Davison, P., 1981. The Lydenburg Heads. African Arts 14, 28–88. https://doi.org/10.2307/3335725

Mahan, S.A., Rittenour, T.M., Nelson, M.S., Ataee, N., Brown, N., DeWitt, R., Durcan, J., Evans, M., Feathers, J., Frouin, M., Guérin, G., Heydari, M., Huot, S., Jain, M., Keen-Zebert, A., Li, B., López, G.I., Neudorf, C., Porat, N., Rodrigues, K., Sawakuchi, A.O., Spencer, J.Q.G. and Thomsen, K., 2022. Guide for interpreting and reporting luminescence dating results. GSA Bulletin. https://doi.org/10.1130/B36404.1

Marker, M.E. and Evers, T.M., 1976. Iron Age Settlement and Soil Erosion in the Eastern Transvaal, South Africa. The South African Archaeological Bulletin 31, 153–165. https://doi.org/10.2307/3887737

Mason, R.J., 1986. Origins of black people of Johannesburg and the southern western central Transvaal, AD 350-1880, Occasional Paper No.16 of the Archaeological Research Unit. Cambridge University Press, Johannesburg, Witwatersrand.

Mason, R.J., 1981. Early Iron Age settlement at Broederstroom 24/73, Transvaal, South Africa. South African Journal of Science 77, 401–416. https://doi.org/10.10520/AJA00382353_1554

Mason, R.J., 1954. A Burial Site at Driekopseiland. The South African Archaeological Bulletin 9, 134–134. https://doi.org/10.2307/3886823

Mason, R.J., 1952. South African Iron Age Pottery from the Southern Transvaal. The South African Archaeological Bulletin 7, 70–79. https://doi.org/10.2307/3887449

Mason, R.J., 1951. The Excavations of Four Caves near Johannesburg. The South African Archaeological Bulletin 6, 71–79. https://doi.org/10.2307/3886752

Mejdahl, V., 1979. Thermoluminescence Dating: Beta-Dose Attenuation in Quartz Grains. Archaeometry 21, 61–72. https://doi.org/10.1111/j.1475-4754.1979.tb00241.x

Miller, D., 1991. Materials Analysis of Archaeological Ceramics in Southern Africa. The South African Archaeological Bulletin 46, 12–18. https://doi.org/10.2307/3889008

Mitchell, P., 2013. Early Farming Communities of Southern and South-Central Africa, in: Mitchell, P., Lane, P.J. (Eds.), The Oxford Handbook of African Archaeology. Oxford University Press, p. 0. https://doi.org/10.1093/oxfordhb/9780199569885.013.0045

Mitchell, P. and Whitelaw, G., 2005. The Archaeology of Southernmost Africa from C. 2000 B.P. to the Early 1800s: A Review of Recent Research. Journal of African History 46, 209–241.

Moska, P., Bluszcz, A., Poręba, G., Tudyka, K., Adamiec, G., Szymak, A. and Przybyła, A., 2021. Luminescence Dating Procedures at the Gliwice Luminescence Dating Laboratory. Geochronometria 48, 1–15. https://doi.org/10.2478/geochr-2021-0001

Mucina, L., Hoare, D.B., Lötter, M.C., Preez, J., Rutherford, M.C., Scott-Shaw, C.R., Bredenkamp, G.J., Powrie, L., Scott, L., Camp, K.G.T., Cilliers, S.S., Bezuidenhout, H., Mostert, T.H., Siebert, S., Winter, P., Burrows, J.E., Dobson, L., Ward, R.A., Stalmans, M., Oliver, E.G.H., Siebert, F., Schmidt, E., Kobisi, K. and Kose, L., 2006. Grassland biome, in: Mucina, L., Rutherford, M.C. (Eds.), The Vegetation of South Africa, Lesotho and Swaziland, Strelitzia 19. South African National Biodiversity Institute, Pretoria, pp. 348–437.

Murray, A., Arnold, L.J., Buylaert, J.-P., Guérin, G., Qin, J., Singhvi, A.K., Smedley, R., and Thomsen, K.J., 2021. Optically stimulated luminescence

dating using quartz. Nature Reviews Methods Primers 1, 72. https://doi.org/10.1038/s43586-021-00068-5

Murray, A.S. and Wintle, A.G., 2000. Luminescence dating of quartz using an improved single-aliquot regenerative-dose protocol. Radiation Measurements 32, 57–73. https://doi.org/10.1016/S1350-4487(99)00253-X

Olatoyan, J.O., Neumann, F.H., Orijemie, E.A., Sievers, C., Evans, M., Hattingh, T. and Schoeman, M.H., 2023. Modern pollen- and phytolith-vegetation relationships at a wetland in northeastern South Africa. South African Journal of Botany 161, 780–796. https://doi.org/10.1016/j.sajb.2023.08.025

Olley, J.M., Pietsch, T. and Roberts, R.G., 2004. Optical dating of Holocene sediments from a variety of geomorphic settings using single grains of quartz. Geomorphology 60, 337–358. https://doi.org/10.1016/j.geomorph.2003.09.020

Pacompia, Y., Supo-Ramos, J.G., Gonzales-Lorenzo, C.D., Callo-Escobar, D.J., Rocca, R.R., Pastrana, E.C., Gomes, M.B., Silva-Carrera, B.N., Watanabe, S., Ayca-Gallegos, O. and Ayala-Arenas, J.S., 2023. Luminescence dating and firing temperature determination of ancient ceramics fragments from the Tunata-hill site in the Churajon archaeological complex in Arequipa, Peru. Radiation Physics and Chemistry 204, 110725. https://doi.org/10.1016/j.radphyschem.2022.110725

Pienaar, M., Woodborne, S. and Wadley, L., 2008. Optically stimulated luminescence dating at Rose Cottage Cave. South African Journal of Science 104, 65–70.

Porat, N., Faershtein, G., Medialdea, A. and Murray, A.S., 2015. Re-examination of common extraction and purification methods of quartz and feldspar for luminescence dating. Ancient TL 33, 22–30.

Porraz, G., Val, A., Tribolo, C., Mercier, N., de la peña, P., Haaland, M.M., Igreja, M., Miller, C.E. and Schmid, V.C., 2018. The MIS5 Pietersburg at “28” Bushman Rock Shelter, Limpopo Province, South Africa. PLOS ONE 13, e0202853. https://doi.org/10.1371/journal.pone.0202853

Prehistoric Ceramics Research Group, 2010. The Study of Prehistoric Pottery: General Policies and Guidelines for Analysis and Publication, 3rd ed. Occasional Paper No1 and No 2. Online research available at : https://www.prehistoricpottery.org/_files/ugd/93ae8c_49ff5068d62241f0a662881502173bc9.pdf

Prescott, J.R. and Clay, R.W., 2000. Cosmic ray dose rates for luminescence and ESR dating: measured with a scintillation counter. Ancient TL 18, 11–14.

Prescott, J.R. and Hutton, J.T., 1994. Cosmic ray contributions to dose rates for luminescence and ESR dating: Large depths and long-term time variations. Radiation Measurements 23, 497–500. https://doi.org/10.1016/1350-4487(94)90086-8

Preusser, F., 1999. Bleaching characteristics of some optically stimulated luminescence signals. Ancient TL 17, 11–14.

Preusser, F., Degering, D., Fuchs, M., Hilgers, A., Kadereit, A., Klasen, N., Krbetschek, M., Richter, D. and Spencer, J.Q.G., 2008. Luminescence dating: basics, methods and applications. E&G Quaternary Science Journal 57, 95–149. https://doi.org/10.3285/eg.57.1-2.5

Randall-Maciver, D., 1906. The Rhodesia Ruins: Their Probable Origin and Significance. The Geographical Journal 27, 325–336. https://doi.org/10.2307/1776233

Reimann, T., Tsukamoto, S., Harff, J., Osadczuk, K. and Frechen, M., 2011. Reconstruction of Holocene coastal foredune progradation using luminescence dating — An example from the Świna barrier (southern Baltic Sea, NW Poland). Geomorphology 132, 1–16. https://doi.org/10.1016/j.geomorph.2011.04.017

Rhodes, E.J., 2011. Optically Stimulated Luminescence Dating of Sediments over the Past 200,000 Years. Annu. Rev. Earth Planet. Sci. 39, 461–488. https://doi.org/10.1146/annurev-earth-040610-133425

Roos, C.I., Rittenour, T.M., Swetnam, T.W., Loehman, R.A., Hollenback, K.L., Liebmann, M.J. and Rosenstein, D.D., 2020. Fire Suppression Impacts on

Fuels and Fire Intensity in the Western U.S.: Insights from Archaeological Luminescence Dating in Northern New Mexico. Fire 3. https://doi.org/10.3390/fire3030032

Sadr, K., 2008. An Ageless View of First Millennium AD Southern African Ceramics. Journal of African Archaeology 6, 103–129.

Sadr, K. and Sampson, C.G., 2006. Through Thick and Thin: Early Pottery in Southern Africa. Journal of African Archaeology 4, 235–252.

Sánchez, J., Mosquera, D. and Montero Fenollós, J., 2008. TL and OSL Dating of Sediment and Pottery from Two Syrian Archaeological Sites. Geochronometria 31, 21–29. https://doi.org/10.2478/v10003-008-0017-6

Schoeman, A., 2020. Archaeology of Farming Communities in Mpumalanga Province and the Adjacent Lowveld in Northeastern South Africa. https://doi.org/10.1093/acrefore/9780190277734.013.767

Schoeman, M.H., Aub, B., Burrows, J., Hall, G. and Woodborne, S., 2019. Past Climatic Conditions for Bokoni at Buffelskloof, Mpumalanga, Using $\delta$13C Analysis of Prunus africana and Pittosporum viridiflorum Tree Rings. Journal of African Archaeology 17, 150–160.

Sealy, J. and Yates, R., 1994. The chronology of the introduction of pastoralism to the Cape, South Africa. Antiquity 68, 58–67. https://doi.org/10.1017/S0003598X00046196

Sherwood, J., Barbetti, M., Ditchburn, R., Kimber, R.W.L., McCabe, W., Murray-Wallace, C.V., Prescott, J.R. and Whitehead, N., 1994. A comparative study of Quaternary dating techniques applied to sedimentary deposits in southwest Victoria, Australia. Quaternary Science Reviews 13, 95–110. https://doi.org/10.1016/0277-3791(94)90035-3

Shirar, S., 2011. Late Holocene Chronology of the Noatak and Kobuk Rivers. Alaska Journal of Anthropology 9, 1–16.

Sjöström, J., Norström, E., Risberg, J. and Schoeman, M.H., 2017. Late Holocene palaeoenvironmental reconstruction from Mpumalanga Province (South Africa) inferred from geochemical and biogenic proxies. Review of

Palaeobotany and Palynology 246, 264–277. https://doi.org/10.1016/j.revpalbo.2017.06.011

Sommerville, A.A., Hansom, J.D., Housley, R.A. and Sanderson, D.C.W., 2007. Optically stimulated luminescence (OSL) dating of coastal aeolian sand accumulation in Sanday, Orkney Islands, Scotland. The Holocene 17, 627–637. https://doi.org/10.1177/0959683607078987

Strunk, A., Olsen, J., Sanei, H., Rudra, A., and Larsen, N.K., 2020. Improving the reliability of bulk sediment radiocarbon dating. Quaternary Science Reviews 242, 106442. https://doi.org/10.1016/j.quascirev.2020.106442

Talma, A.S. and Vogel, J.C., 1993. A Simplified Approach to Calibrating 14C Dates. Radiocarbon 35, 317–322. https://doi.org/10.1017/S0033822200065000

Taylor, R.E., 2018. Radiocarbon Dating in Archaeology, in: Smith, C. (Ed.), Encyclopedia of Global Archaeology. Springer International Publishing, Cham, pp. 1–11. https://doi.org/10.1007/978-3-319-51726-1_325-2

Thebe, P.C. and Sadr, K., 2017. Forming and Shaping Pottery Boundaries in Contemporary South-Eastern Botswana. African Archaeological Review 34, 75–92. https://doi.org/10.1007/s10437-016-9238-7

Tribolo, C., Mercier, N., Dumottay, C., Cantin, N., Banks, W.E., Stratford, D., de la peña, P., Backwell, L., Wadley, L. and Francesco, d'Errico, 2022a. Luminescence dating at Border Cave: attempts, questions, and new results. Quaternary Science Reviews 296, 107787. https://doi.org/10.1016/j.quascirev.2022.107787

Tribolo, C., Mercier, N., Martin, L., Taffin, N., Miller, C.E., Will, M. and Conard, N., 2022b. Luminescence dating estimates for the coastal MSA sequence of Hoedjiespunt 1 (South Africa). Journal of Archaeological Science: Reports 41, 103320. https://doi.org/10.1016/j.jasrep.2021.103320

Truc, L., Chevalier, M., Favier, C., Cheddadi, R., Meadows, M.E., Scott, L., Carr, A.S., Smith, G.F. and Chase, B.M., 2013. Quantification of climate change for the last 20,000years from Wonderkrater, South Africa: Implications for

the long-term dynamics of the Intertropical Convergence Zone. Palaeogeography, Palaeoclimatology, Palaeoecology 386, 575–587. https://doi.org/10.1016/j.palaeo.2013.06.024

von Bezing, K.L. and Inskeep, R.R., 1966. Modelled Terracotta Heads from Lydenburg, South Africa. Man 1, 102–102. https://doi.org/10.2307/2795907

Wallinga, J., 2002. Optically stimulated luminescence dating of fluvial deposits: a review. Boreas 31, 303–322. https://doi.org/10.1111/j.1502-3885.2002.tb01076.x

Wang, X., Qiu, F., Nian, X., Liu, R. and Zhang, W., 2022. Testing the applicability of standardised growth curves (SGCs) for OSL signals of quartz grains from the Yangtze Delta, China. Quaternary Geochronology 72, 101348. https://doi.org/10.1016/j.quageo.2022.101348

Whitelaw, G., 2012. Anthropology and History in the Southern African Iron Age. African Studies 71, 127–144. https://doi.org/10.1080/00020184.2012.668297

Whitelaw, G., 1996. Lydenburg Revisited: Another Look at the Mpumalanga Early Iron Age Sequence. The South African Archaeological Bulletin 51, 75–83. https://doi.org/10.2307/3888842

Whitelaw, G., 1994. KwaGandaganda: settlement patterns in the Natal Early Iron Age. Natal Museum Journal of Humanities 6, 1–64.

Whitelaw, G., 1993. Customs and settlement patterns in the first millennium AD: evidence from Nanda, an Early Iron Age in the Mngeni Valley, Natal. Natal Museum Journal of Humanities = Natal Museum Tydskrif vir Geesteswetenskappe 5, 47–81.

Whitelaw, G. and Moon, M.A., 1996. The ceramics and distribution of pioneer agriculturists in KwaZulu-Natal. Natal Museum Journal of Humanities = Natal Museum Tydskrif vir Geesteswetenskappe 8, 53–79.

Whitelaw, G. and van Rensburg, S.J., 2020. Lake Sibaya and the Beginning of the Iron Age in KwaZulu-Natal. The Digging Stick, 37 (2), 1-4.

Wintle, A.G. and Murray, A.S., 2006. A review of quartz optically stimulated luminescence characteristics and their relevance in single-aliquot regeneration dating protocols. Radiation Measurements 41, 369–391. https://doi.org/10.1016/j.radmeas.2005.11.001

Zimmerman, D.W., 1971. Thermoluminescent Dating Using Fine Grains from Pottery*. Archaeometry 13, 29–52. https://doi.org/10.1111/j.1475-4754.1971.tb00028.x

Zink, A., 2013. A coarse Bayesian approach to evaluate luminescence ages. Geochronometria 40, 90–100. https://doi.org/10.2478/s13386-013-0105-x

Zink, A.J.C., Susino, G.J., Porto, E. and Huffman, T.N., 2012. Direct OSL dating of Iron Age pottery from South Africa – Preliminary dosimetry investigations. Quaternary Geochronology 8, 1–9. https://doi.org/10.1016/j.quageo.2011.11.008

Zou, G.-N., Shelach, G., Li, X.-Q., Zhao, C., Rui, X., Zhou, L.-P. and Zhang, J.-F., 2018. Geochronology and paleoenvironment of the Taoshan site, northeastern China, and archaeological implications. Quaternary International 463, 6–17. https://doi.org/10.1016/j.quaint.2017.06.073

# CHAPTER 7 - APPENDIX

## Appendix A Recalibration of $^{14}C$

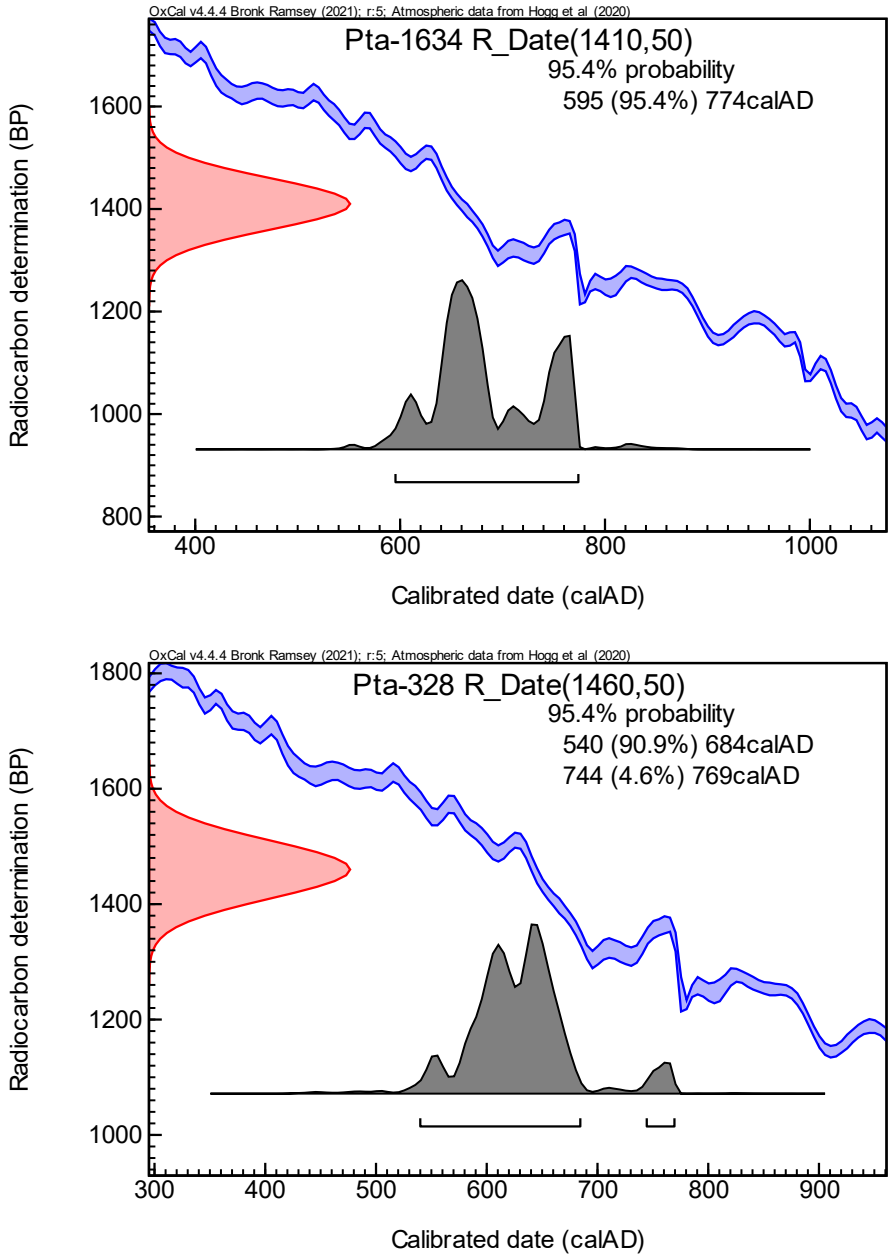


Appendix figure A.1. OxCal calibration of Pta-1634 and Pta-328 using Hogg *et al.* (2020) calibration curve. The samples are from the Lydenburg Heads Site (Inskeep, 1971; Evers, 1982a)

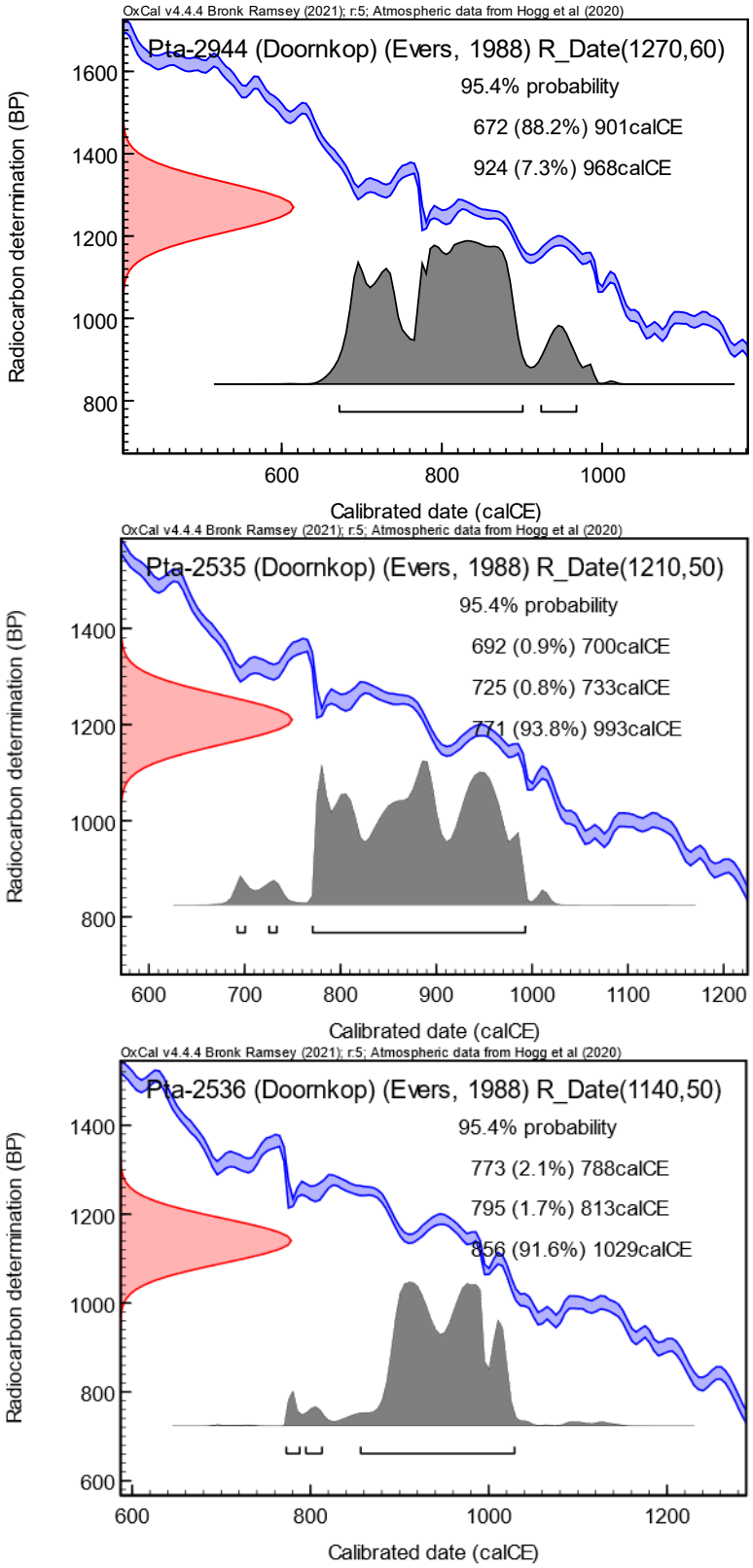


Appendix figure A.2. OxCal calibration of Pta-2944, Pta-2535, and Pta-2536 using Hogg *et al.* (2020) calibration curve. The samples are from the Doornkop site in the Mashishing region (Evers, 1988).

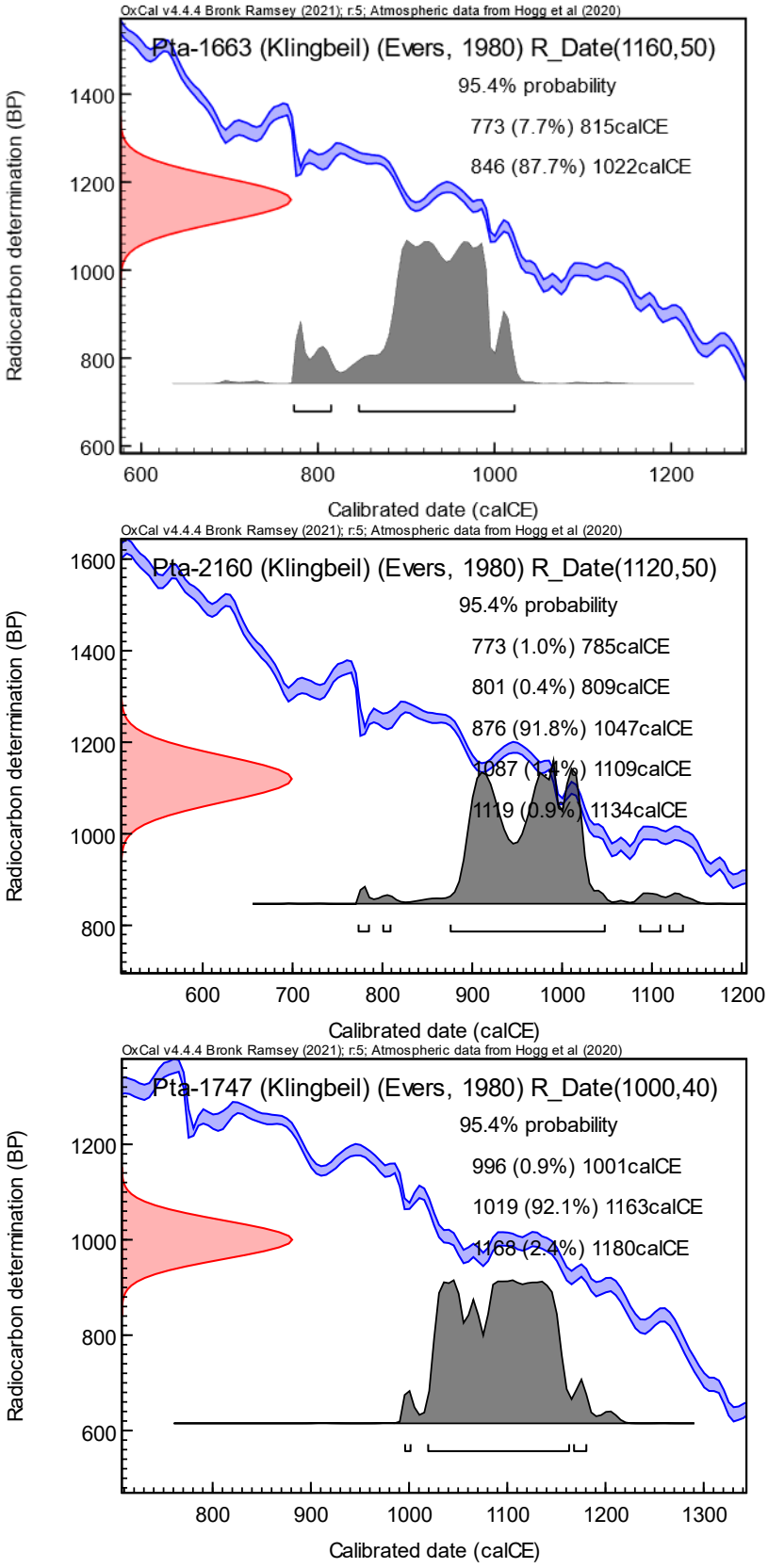


Appendix figure A.3. OxCal calibration of Pta-1663, Pta-2160, and Pta-1747 using Hogg *et al.* (2020) calibration curve. The samples are from the Klingbeil site in the Mashishing region (Evers, 1980).

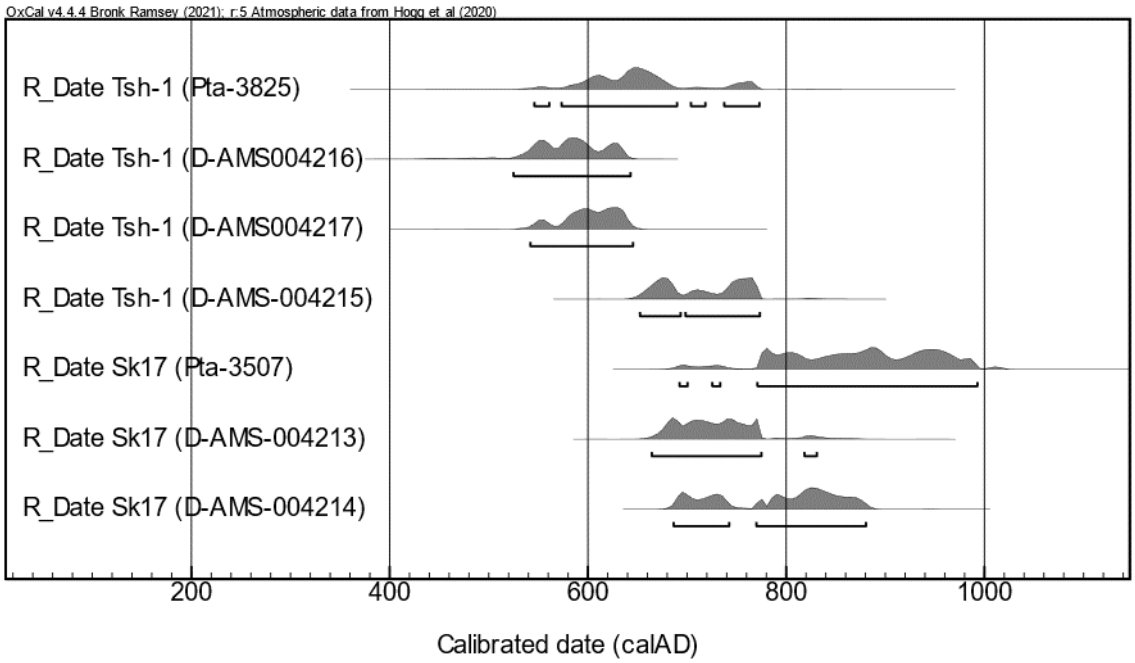


Appendix figure A.4. OxCal calibration of radiocarbon samples from Tshokwane (TSH1) and Skukuza (SK17) (Jordaan, 2016).

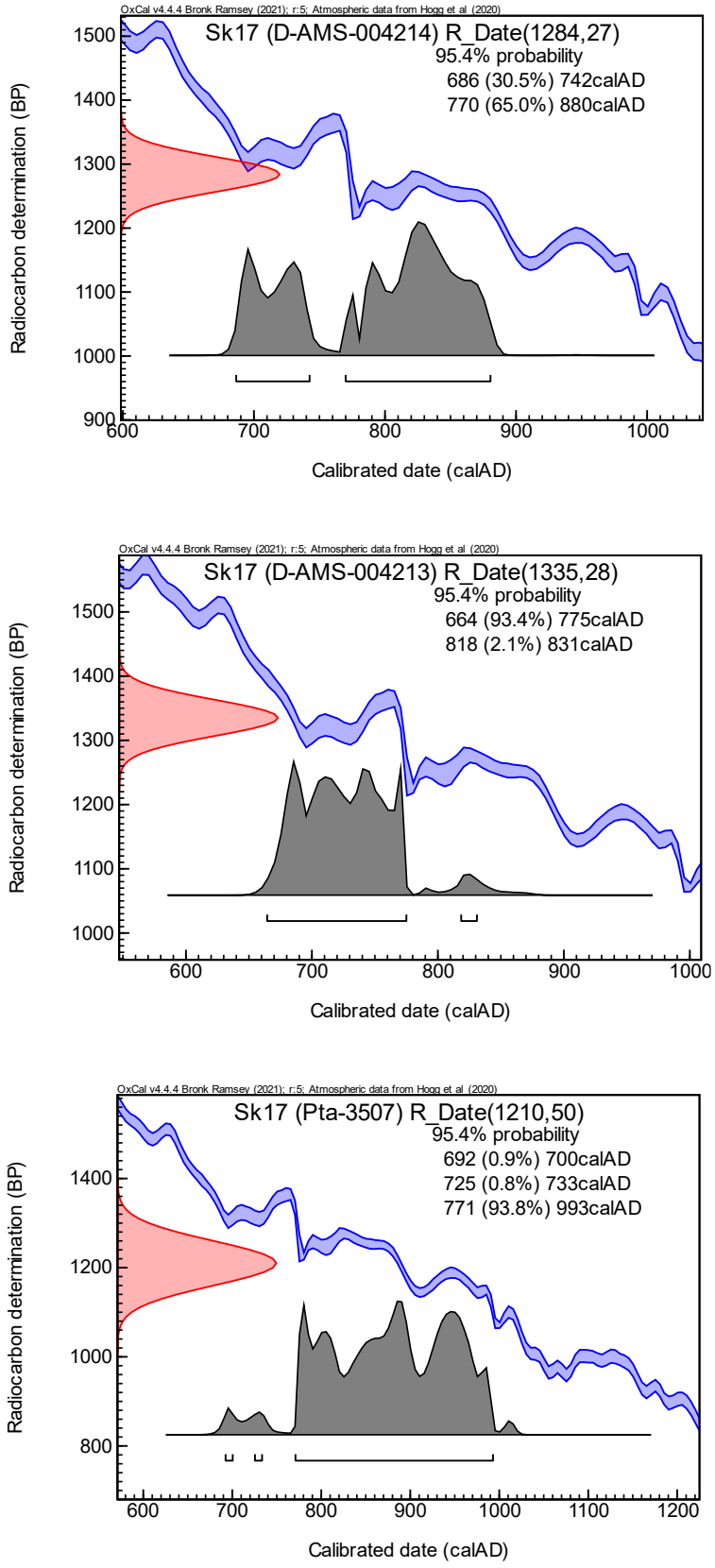


Appendix figure A.5. OxCal calibration curve of radiocarbon samples from Skukuza (SK17) (Jordaan, 2016).

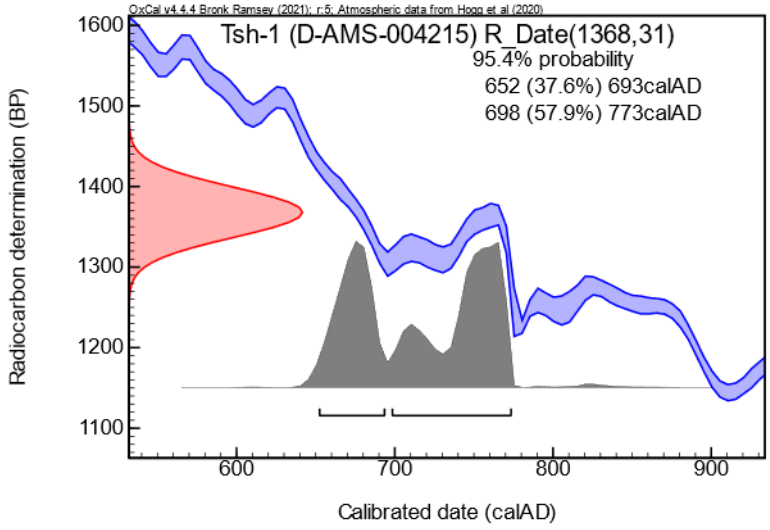
OxCal v4.4.4 Bronk Ramsey (2021); r:5; Atmospheric data from Hogg et al (2020)
Tsh-1 (D-AMS-004215) R_Date(1368,31)
95.4% probability
652 (37.6%) 693calAD
698 (57.9%) 773calAD
Radiocarbon determination (BP)
1600
1500
1400
1300
1200
1100
600
700
800
900
Calibrated date (calAD)

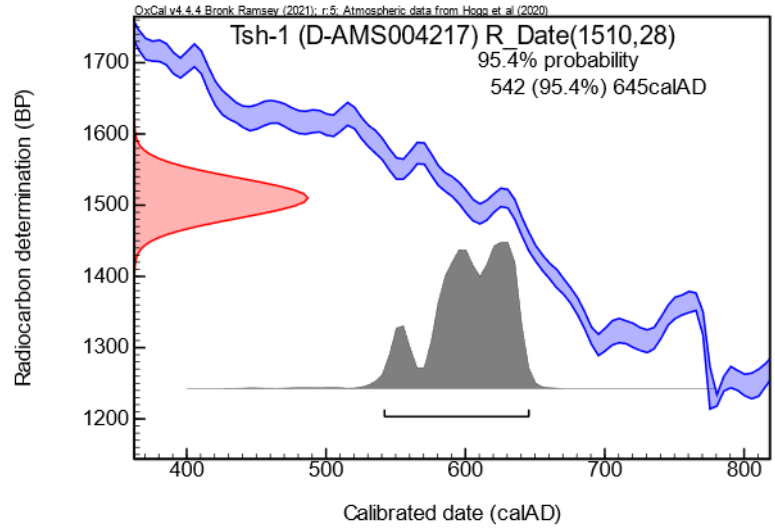
OxCal v4.4.4 Bronk Ramsey (2021); r:5; Atmospheric data from Hogg et al (2020)
Tsh-1 (D-AMS004217) R_Date(1510,28)
95.4% probability
542 (95.4%) 645calAD
Radiocarbon determination (BP)
1700
1600
1500
1400
1300
1200
400
500
600
700
800
Calibrated date (calAD)

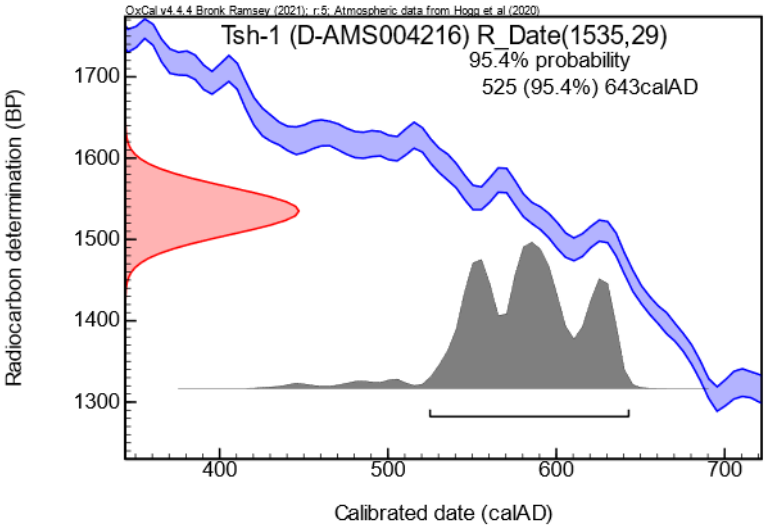
OxCal v4.4.4 Bronk Ramsey (2021); r:5; Atmospheric data from Hogg et al (2020)
Tsh-1 (D-AMS004216) R_Date(1535,29)
95.4% probability
525 (95.4%) 643calAD
Radiocarbon determination (BP)
1700
1600
1500
1400
1300
400
500
600
700
Calibrated date (calAD)

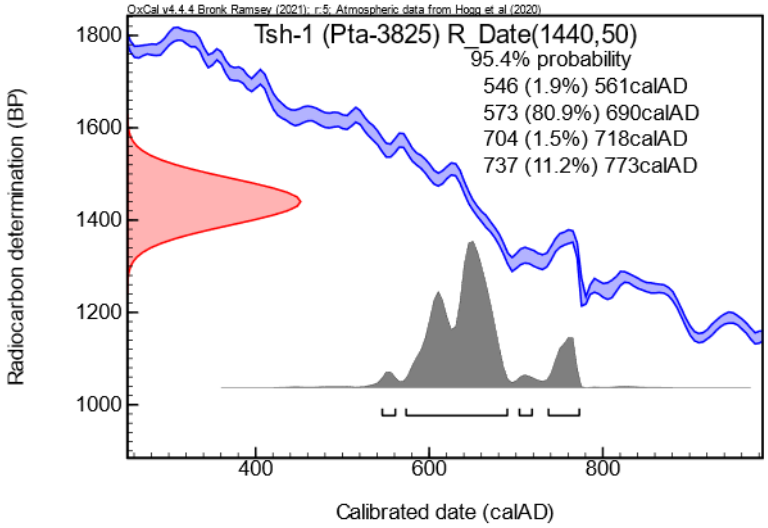


Appendix figure A.6. OxCal calibration curve of radiocarbon samples from Tshokwane (TSH1) (Jordaan, 2016).

# Appendix B Calculations of Dose Rate

## Calculating the beta and gamma dose rates

An example of the calculations of the dose rate for beta ($D_\beta$) and gamma ($D_\gamma$); for LHS02 and the respective Th, U and K values.

| Sample | Th (ppm) | U (ppm) | K (%) | WC |
|---|---|---|---|---|
| LHS02 | 8.325 ± 0.15 | 2.181 ± 0.03 | 1.02 ± 0.02 | 1% |

$$D_R = D_\alpha + D_\beta + D_\gamma + D_c$$

### Calculating the beta dose rate

Beta dose rate for thorium including error:

$$D_\beta \ from\ Th: \ 0.028 \times 8.325 = 0.2331$$

$$D_\beta \ error \ from\ Th: \ 0.2331 \times \frac{0.15}{8.325} = 0.0042$$

$$D_\beta Th \left(\frac{Gy}{ka}\right) = 0.2331 \pm 0.0042$$

Beta dose rate for uranium including error:

$$D_\beta \ from\ U: \ 0.142 \times 2.181 = 0.309702$$

$$D_\beta \ error \ from\ U: \ 0.3097 \times \frac{0.03}{2.181} = 0.00426$$

$$D_\beta U \left(\frac{Gy}{ka}\right) = 0.3097 \pm 0.0043$$

Beta dose rate for potassium including error:

$$D_\beta \ from\ K: \ 0.854 \times 1.02 = 0.8711$$

$$D_\beta \ error \ from\ K: \ 0.8711 \times \frac{0.02}{1.02} = 0.0171$$

$$D_\beta K \left(\frac{Gy}{ka}\right) = 0.8711 \pm 0.0167$$

Total beta dose rate including error (excluding water and grain attenuation)

$$D_\beta = D_\beta Th + D_\beta U + D_\beta K$$

$$D_\beta = 0.2331 + 0.3097 + 0.8711 = 1.4139$$

$$D_\beta error = \sqrt{0.0042^2 + 0.0043^2 + 0.0171^2} = 0.0181$$

$$D_\beta = 1.4139 \pm 0.0181$$

Total beta dose rate including error and considering grain attenuation

$$D_{\beta dry} = D_\beta \times \ 0.887$$

$$D_{\beta dry} = 1.4139 \times \ 0.887 = 1.2541$$

$$D_{\beta dry} \ error = 1.2541 \times \sqrt{\left(\left(\frac{0.0181}{1.4139}\right)^2 + \left(\frac{0.007}{0.887}\right)^2\right)} = 0.0189$$

$$D_{\beta dry} = 1.2541 \pm 0.0189$$

Total beta dose including error and water attenuation

$$D_{\beta\ wet} = \frac{D_{\beta\ dry}}{1 + (1.25 \times WC)}$$

$$D_{\beta\ wet} = \frac{1.2541}{1 + \left(1.25 \times \frac{1}{100}\right)} = 1.2386$$

$$D_{\beta\ wet} error = 1.2386 \times \sqrt{\left(\left(\frac{0.012}{0.988}\right)^2 + \left(\frac{0.0189}{1.2369}\right)^2\right)} = 0.0242 *$$

$$D_{\beta wet} = 1.2386 \pm 0.0242$$

$$\underline{\boldsymbol{D_{\beta} = 1.2386 + 0.0242}}$$

**Calculating the gamma dose**

Gamma dose rate for thorium including error:

$$\underline{D_{\beta} = 1.2386 \pm 0.0242 D_{\gamma}\ from\ Th:\ 0.0489 \times 8.325 = 0.4071}$$

$$D_{\gamma}\ error\ from\ Th:\ 0.4071 \times \frac{0.15}{8.325} = 0.0073$$

$$D_{\gamma} Th\ \left(\frac{Gy}{ka}\right) = 0.4071 \pm 0.0073$$

Gamma dose rate for uranium including error:

$$D_\gamma\ from\ U:\ 0.112 \times 2.181 = 0.2443$$

$$D_\gamma\ error\ from\ U:\ 0.2443 \times \frac{0.03}{2.181} = 0.0034$$

$$D_\gamma U\ \left(\frac{Gy}{ka}\right) = 0.2443 \pm 0.0034$$

Gamma dose rate for potassium including error:

$$D_\gamma\ from\ K:\ 0.248 \times 1.02 = 0.2530$$

$$D_\gamma\ error\ from\ K:\ 0.2530 \times \frac{0.02}{1.02} = 0.0050$$

$$D_\gamma K\ \left(\frac{Gy}{ka}\right) = 0.2530 \pm 0.0050$$

Total gamma dose rate including error (excluding water and grain attenuation):

$$D_\gamma = Depth\ correction(D_\gamma Th + D_\gamma U + D_\gamma K)$$

$$D_\gamma = 0.9611(0.4071 + 0.2443 + 0.2530) = 0.8692$$

$$D_\gamma error = \sqrt{0.0073^2 + 0.0034^2 + 0.0050^2} = 0.0095$$

$$D_\gamma = 0.8692 \pm 0.0095$$

Total gamma dose rate including error and considering water attenuation:

$$D_{\gamma wet} = \frac{D_{\gamma dry}}{1 + (1.25 \times WC)}$$

$$D_{\gamma wet} = \frac{0.8692}{1 + \left(1.25 \times \frac{1}{100}\right)} = 0.8584$$

$$D_{\gamma} wet\ error = 0.8584 \times \sqrt{\left(\left(\frac{0.0113}{0.9887}\right)^2 + \left(\frac{0.0095}{0.8692}\right)^2\right)} = 0.0135 *$$

$$D_{\gamma} wet = 0.8584 \pm 0.0135$$

$$\underline{\boldsymbol{D_{\gamma} total = 0.8584 \pm 0.0135}}$$

*The error calculations include the terms $\left(\frac{0.0113}{0.9887}\right) and \left(\frac{0.0123}{0.9877}\right)$, which are derived from the propagation of the error of water content through the applied equation.

**Cosmic dose rate**

The cosmic dose rate was calculated within the software (on excel) in relation to Prescott and Hutton (1994). Taking into consideration longitude, latitude, and overburden.

$$D_c = 0.329 \pm 0.016$$

$$\underline{\boldsymbol{D_R}\ \mathbf{LHS02}\ = 2.43 \pm 0.0537}$$

The slight difference in the $D_R$ in Table 4.6 and $D_R$LHS02 is owing to the calculation errors from the rounding of numbers

# Appendix C Post analysis photographs

Appendix table C.1. Post analysis photographs Kalundu ceramics.

| Sample | Box | Bag | Pit | Code |
|---|---|---|---|---|
| LHS10 | 3 | 6 | 5 | LIX / k2 / pit 5 |
|  | | | | |
| LHS23 | 1 | 9 | 3 | LIX / n15 |
|  | | | | |

| Sample | Box | Bag | Pit | Code |
|---|---|---|---|---|
| LHS24 | 3 | 6 | 5 | LIX / k2 / pit 5 |

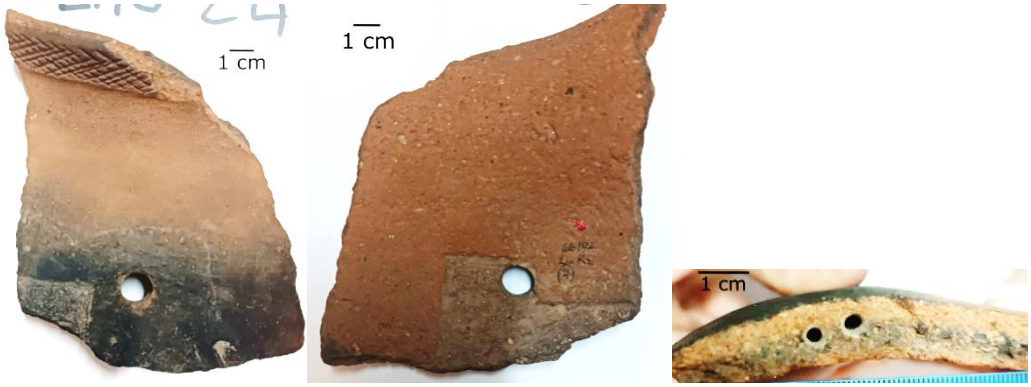


| LHS29 | 3 | 5 | 7 | MVII / o12 / ii |
|---|---|---|---|---|




| LHS40 | 3 | 6 | 5 | LIX / k2 / pit 5 |
|---|---|---|---|---|



Appendix table C.2 Post analysis photographs Urewe ceramics.

| Sample | Box | Bag | Pit | Code |
|---|---|---|---|---|
| LHS02 | 1 | 8 | 10 | JVII / m3 |
| 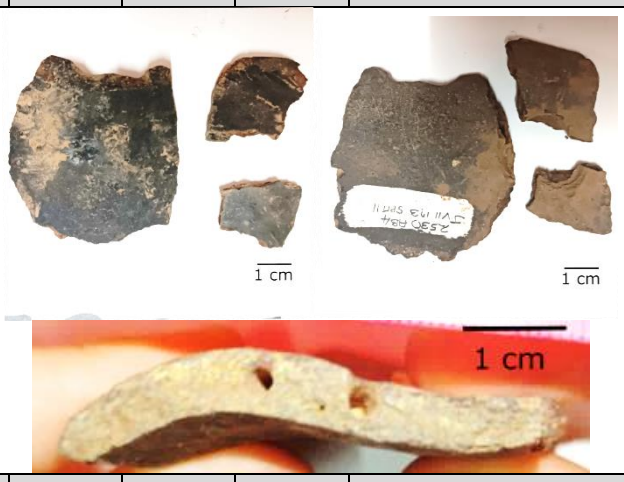  | | | | |
| LHS07 | 2 | 1 | 9 | MVII / f2 / g2 |
|   | | | | |
| LHS11 | 2 | 2 | 12 | LIX / f12 / g12 / f13 / g13 |
|   | | | | |

| Sample | Box | Bag | Pit | Code |
|---|---|---|---|---|
| LHS12 | 2 | 2 | 12 | LIX / f12 / g12 / f13 / g13 |
| 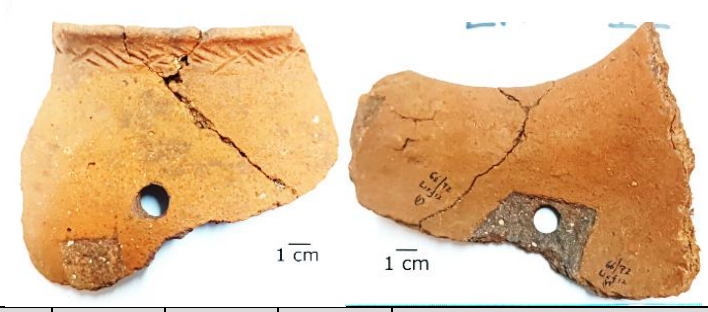 | | | | |
| LHS18 | 2 | 1 | 9 | MVII / f2 / g2 |
| 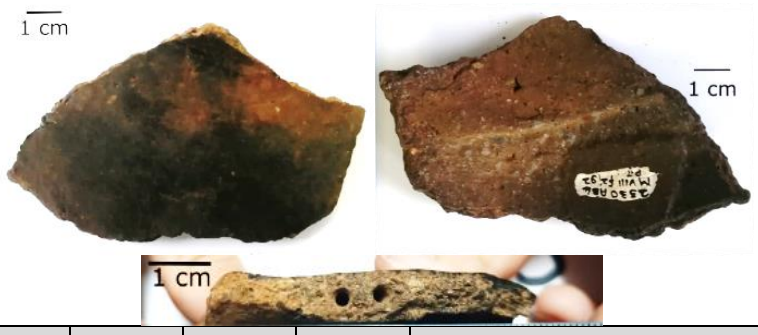 | | | | |
| LHS25 | 1 | 8 | 10 | JVII / m3 |
|  | | | | |
| LHS35 | 1 | 8 | 10 | JVII / m3 / 30-35 |
|  | | | | |

# Appendix D Dose rates for variations in water content and depth

Appendix table D.1. Dose rates for all samples with changes to water content and depth.

| | Sample | Water content (%) | | | | | |
|---|---|---|---|---|---|---|---|
| Depth (m) | **LHS02** | **0 ± 1** | **1 ± 1** | **2 ± 1** | **3 ± 1** | **4 ± 1** | **5 ± 1** |
| | **0.01** | 2.13 ± 0.06 | 2.11 ± 0.06 | 2.09 ± 0.06 | 2.07 ± 0.06 | 2.05 ± 0.06 | 2.03 ± 0.06 |
| | **0.3** | 2.47 ± 0.06 | 2.45 ± 0.06 | 2.42 ± 0.06 | 2.40 ± 0.06 | 2.37 ± 0.06 | 2.35 ± 0.06 |
| | **0.6** | 2.47 ± 0.06 | 2.45 ± 0.06 | 2.42 ± 0.06 | 2.40 ± 0.06 | 2.38 ± 0.06 | 2.35 ± 0.06 |
| | **0.82** | 2.46 ± 0.06 | 2.44 ± 0.06 | 2.41 ± 0.06 | 2.39 ± 0.06 | 2.36 ± 0.06 | 2.34 ± 0.06 |
| | **LHS07** | **0 ± 1** | **1 ± 1** | **2 ± 1** | **3 ± 1** | **4 ± 1** | **5 ± 1** |
| | **0.01** | 2.34 ± 0.06 | 2.32 ± 0.06 | 2.29 ± 0.06 | 2.27 ± 0.06 | 2.25 ± 0.06 | 2.23 ± 0.06 |
| | **0.3** | 2.73 ± 0.07 | 2.71 ± 0.07 | 2.68 ± 0.07 | 2.65 ± 0.07 | 2.62 ± 0.07 | 2.6 ± 0.07 |
| | **0.6** | 2.74 ± 0.07 | 2.71 ± 0.07 | 2.68 ± 0.07 | 2.66 ± 0.07 | 2.63 ± 0.07 | 2.6 ± 0.07 |
| | **0.66** | 2.74 ± 0.07 | 2.71 ± 0.07 | 2.68 ± 0.07 | 2.65 ± 0.07 | 2.63 ± 0.07 | 2.6 ± 0.07 |
| | **LHS10** | **0 ± 1** | **1 ± 1** | **2 ± 1** | **3 ± 1** | **4 ± 1** | **5 ± 1** |
| | **0.01** | 2.86 ± 0.08 | 2.83 ± 0.08 | 2.80 ± 0.08 | 2.77 ± 0.08 | 2.75 ± 0.08 | 2.72 ± 0.07 |
| | **0.3** | 3.35 ± 0.09 | 3.32 ± 0.09 | 3.28 ± 0.09 | 3.25 ± 0.08 | 3.22 ± 0.08 | 3.18 ± 0.08 |
| | **0.6** | 3.37 ± 0.09 | 3.33 ± 0.09 | 3.30 ± 0.09 | 3.26 ± 0.08 | 3.23 ± 0.08 | 3.2 ± 0.08 |
| | **0.7** | 3.36 ± 0.09 | 3.33 ± 0.09 | 3.29 ± 0.09 | 3.26 ± 0.08 | 3.22 ± 0.08 | 3.19 ± 0.08 |
| | **LHS11** | **0 ± 1** | **1 ± 1** | **2 ± 1** | **3 ± 1** | **4 ± 1** | **5 ± 1** |
| | **0.01** | 1.34 ± 0.04 | 1.32 ± 0.04 | 1.31 ± 0.04 | 1.3 ± 0.04 | 1.29 ± 0.04 | 1.28 ± 0.04 |
| | **0.1** | 1.46 ± 0.04 | 1.45 ± 0.04 | 1.44 ± 0.04 | 1.43 ± 0.04 | 1.41 ± 0.04 | 1.4 ± 0.04 |
| | **LHS12** | **0 ± 1** | **1 ± 1** | **2 ± 1** | **3 ± 1** | **4 ± 1** | **5 ± 1** |
| | **0.01** | 1.97 ± 0.05 | 1.95 ± 0.05 | 1.93 ± 0.05 | 1.91 ± 0.05 | 1.89 ± 0.05 | 1.88 ± 0.05 |
| | **0.1** | 2.19 ± 0.06 | 2.17 ± 0.06 | 2.14 ± 0.06 | 2.12 ± 0.05 | 2.1 ± 0.05 | 2.08 ± 0.05 |
| | **LHS18** | **0 ± 1** | **1 ± 1** | **2 ± 1** | **3 ± 1** | **4 ± 1** | **5 ± 1** |
| | **0.01** | 2.41 ± 0.07 | 2.38 ± 0.07 | 2.36 ± 0.06 | 2.33 ± 0.06 | 2.31 ± 0.06 | 2.29 ± 0.06 |
| | **0.3** | 2.82 ± 0.07 | 2.79 ± 0.07 | 2.76 ± 0.07 | 2.73 ± 0.07 | 2.7 ± 0.07 | 2.68 ± 0.07 |
| | **0.6** | 2.82 ± 0.07 | 2.79 ± 0.07 | 2.76 ± 0.07 | 2.74 ± 0.07 | 2.71 ± 0.07 | 2.68 ± 0.07 |
| | **0.66** | 2.82 ± 0.07 | 2.79 ± 0.07 | 2.76 ± 0.07 | 2.73 ± 0.07 | 2.71 ± 0.07 | 2.68 ± 0.07 |

| | Sample | Water content (%) | | | | | |
|---|---|---|---|---|---|---|---|
| Depth (m) | **LHS23** | **0 ± 1** | **1 ± 1** | **2 ± 1** | **3 ± 1** | **4 ± 1** | **5 ± 1** |
| | **0.01** | 1.41 ± 0.04 | 1.4 ± 0.04 | 1.39 ± 0.04 | 1.37 ± 0.04 | 1.36 ± 0.04 | 1.35 ± 0.04 |
| | **0.3** | 1.61 ± 0.04 | 1.6 ± 0.04 | 1.58 ± 0.04 | 1.57 ± 0.04 | 1.56 ± 0.04 | 1.54 ± 0.04 |
| | **0.43** | 1.61 ± 0.04 | 1.6 ± 0.04 | 1.58 ± 0.04 | 1.57 ± 0.04 | 1.55 ± 0.04 | 1.54 ± 0.04 |
| | **LHS24** | **0 ± 1** | **1 ± 1** | **2 ± 1** | **3 ± 1** | **4 ± 1** | **5 ± 1** |
| | **0.01** | 1.74 ± 0.05 | 1.72 ± 0.05 | 1.71 ± 0.05 | 1.69 ± 0.05 | 1.68 ± 0.05 | 1.66 ± 0.05 |
| | **0.3** | 2.03 ± 0.05 | 2.01 ± 0.05 | 1.99 ± 0.05 | 1.97 ± 0.05 | 1.95 ± 0.05 | 1.93 ± 0.05 |
| | **0.6** | 2.03 ± 0.05 | 2.01 ± 0.05 | 1.99 ± 0.05 | 1.97 ± 0.05 | 1.95 ± 0.05 | 1.93 ± 0.05 |
| | **0.7** | 2.02 ± 0.05 | 2 ± 0.05 | 1.98 ± 0.05 | 1.96 ± 0.05 | 1.94 ± 0.05 | 1.92 ± 0.05 |
| | **LHS25** | **0 ± 1** | **1 ± 1** | **2 ± 1** | **3 ± 1** | **4 ± 1** | **5 ± 1** |
| | **0.01** | 1.47 ± 0.04 | 1.46 ± 0.04 | 1.45 ± 0.04 | 1.44 ± 0.04 | 1.42 ± 0.04 | 1.41 ± 0.04 |
| | **0.3** | 1.67 ± 0.05 | 1.65 ± 0.04 | 1.64 ± 0.04 | 1.62 ± 0.04 | 1.61 ± 0.04 | 1.59 ± 0.04 |
| | **0.6** | 1.66 ± 0.04 | 1.64 ± 0.04 | 1.63 ± 0.04 | 1.61 ± 0.04 | 1.6 ± 0.04 | 1.58 ± 0.04 |
| | **0.82** | 1.64 ± 0.04 | 1.63 ± 0.04 | 1.61 ± 0.04 | 1.6 ± 0.04 | 1.58 ± 0.04 | 1.57 ± 0.04 |
| | **LHS29** | **0 ± 1** | **1 ± 1** | **2 ± 1** | **3 ± 1** | **4 ± 1** | **5 ± 1** |
| | **0.01** | 2.24 ± 0.06 | 2.21 ± 0.06 | 2.19 ± 0.06 | 2.17 ± 0.06 | 2.15 ± 0.06 | 2.13 ± 0.06 |
| | **0.3** | 2.61 ± 0.07 | 2.58 ± 0.07 | 2.55 ± 0.07 | 2.53 ± 0.06 | 2.5 ± 0.06 | 2.48 ± 0.06 |
| | **0.5** | 2.61 ± 0.07 | 2.59 ± 0.07 | 2.56 ± 0.07 | 2.53 ± 0.07 | 2.51 ± 0.06 | 2.48 ± 0.06 |
| | **LHS35** | **0 ± 1** | **1 ± 1** | **2 ± 1** | **3 ± 1** | **4 ± 1** | **5 ± 1** |
| | **0.3** | 2.71 ± 0.07 | 2.68 ± 0.07 | 2.65 ± 0.07 | 2.62 ± 0.07 | 2.6 ± 0.07 | 2.57 ± 0.07 |
| | **0.35** | 2.71 ± 0.07 | 2.68 ± 0.07 | 2.66 ± 0.07 | 2.63 ± 0.07 | 2.6 ± 0.07 | 2.58 ± 0.07 |
| | **LHS40** | **0 ± 1** | **1 ± 1** | **2 ± 1** | **3 ± 1** | **4 ± 1** | **5 ± 1** |
| | **0.01** | 2 ± 0.05 | 1.98 ± 0.05 | 1.96 ± 0.05 | 1.95 ± 0.05 | 1.93 ± 0.05 | 1.91 ± 0.05 |
| | **0.3** | 2.34 ± 0.06 | 2.31 ± 0.06 | 2.29 ± 0.06 | 2.27 ± 0.06 | 2.25 ± 0.06 | 2.22 ± 0.06 |
| | **0.6** | 2.34 ± 0.06 | 2.31 ± 0.06 | 2.29 ± 0.06 | 2.27 ± 0.06 | 2.25 ± 0.06 | 2.22 ± 0.06 |
| | **0.7** | 2.33 ± 0.06 | 2.31 ± 0.06 | 2.29 ± 0.06 | 2.26 ± 0.06 | 2.24 ± 0.06 | 2.22 ± 0.06 |